

EXPERIMENTAL INVESTIGATION OF OPTIMAL PARTICULATE SENSOR LOCATION  
IN AN AIRCRAFT CABIN

by

MAHER F. SHEHADI

B.E., Beirut Arab University  
Lebanon, 2007

A THESIS

Submitted in partial fulfillment of the requirements for the degree

MASTER OF SCIENCE

Department of Mechanical and Nuclear Engineering  
College of Engineering

KANSAS STATE UNIVERSITY  
Manhattan, Kansas

2010

Approved by:

Major Professor  
M. H. Hosni

# **Copyright**

MAHER F. SHEHADI

2010

## **Abstract**

Each year millions of people travel by commercial aircrafts. The Bureau of Transportation Statistics indicates that about 600 million passengers fly each year in the United States and, of those, roughly 350,000 are international travelers. This number of travelers leaves commercial airliners potentially vulnerable to biological contamination and makes the transmission of diseases a serious threat. The spread of SARS (Severe Acute Respiratory Syndrome) and H1N1 (swine flu) are examples of documented cases. Consequently, considerable research has been and continues to be conducted to study and understand particulate transport mechanisms and dispersion behavior inside aircraft cabins to develop means for detecting, controlling, and removing contaminants from aircraft cabins and to find methods for preventing the aircraft from being used for intentional contaminant deployment.

In order to develop means to monitor and control air quality, infectious disease transmission, and particulate transport inside aircraft cabins, an experimental study was conducted to determine the best sensor placement locations for detection and to identify the number of sensors needed to accurately track air quality incidents within a cabin. An 11-row mockup, intended to be representative of a typical wide-body aircraft, was used for the research. The mockup interior is based on the actual dimensions of the Boeing 767 aircraft cabin. Inside the mockup cabin, actual aircraft equipment including seats and air diffusers were used. Each row has seven passenger seats.

Particulates were released from different locations in the second row of the mockup cabin. The transported particles were then collected at six different locations in the lateral direction. The best location to place a sensor was defined as the location having the strongest signal (maximum number of particles collected) or the fastest detection time. After determining the best location in the lateral direction, particles were collected at the same location, but in different rows to estimate the differences between the signal strength and the delay time in detecting the signal from row to row. For the later investigation, the particulates were released in Row 2 and in Row 6 as well.

For the six locations examined, it was found that the best location for the placement of a sensor in the 11-row mockup in the lateral direction is on the centerline near the cabin floor. Longitudinally, it was found that a sensor may be used for detecting particulates in the same row as the release and a row in front and in back of the release location. For the mockup cabin, a total of 4 sensors was recommended to monitor particulate releases in the 11 row mockup cabin, each of these sensors separated by two rows.

# Table of Contents

List of Figures .....	viii
List of Tables .....	xii
Acknowledgements.....	xiv
Dedication.....	xv
CHAPTER 1 - Introduction .....	1
CHAPTER 2 - Literature Review .....	3
2.1 Overview.....	3
2.2 Aircraft Cabin Air Quality Factors .....	4
2.2.1 Temperature .....	4
2.2.2 Relative Humidity .....	4
2.2.3 Pressure .....	5
2.2.4 Ventilation.....	6
2.2.5 Air Contaminants .....	6
2.2.5.1 Physical and Chemical Air Contaminants .....	7
2.2.5.2 Biological Air Contaminants .....	8
CHAPTER 3 - Experimental Setup .....	9
3.1 Cabin.....	9
3.1.1 Cabin Geometry .....	11
3.1.2 Seat Locations .....	12
3.1.3 Seat Geometry.....	15
3.2 Air Supply System.....	18
3.2.1 Heating and Cooling Supply System .....	18
3.2.2 Supply Air Instrumentation and Control.....	25
3.2.3 Air Distribution System .....	27
3.2.3.1 Main Supply Duct Geometry .....	27
3.2.3.2 Diffuser Geometry .....	29
3.3 Powder Measurement .....	35
3.3.1 Powder Injection System .....	35

3.3.2 Powder Measurement Device .....	36
3.4 Experimental Methodology .....	38
CHAPTER 4 - Results .....	43
4.1 Normalization Procedures.....	43
4.1.1 Experimental Determination of the Total Number of Particles at the Source .....	44
4.2 Detection Times and Normalized Particle Counts in the Lateral Direction of Row 2: .....	46
4.3 Detection Times and Normalized Particle Counts in the Longitudinal Direction:.....	53
4.3.1 Longitudinal Investigation – Injection in Row 2 .....	53
4.3.2 Longitudinal Investigation – Injection in Row 6 .....	56
CHAPTER 5 - Data Analysis .....	58
5.1 Analysis of the Data Collected in the Lateral Direction of Row 2 .....	58
5.2 Analysis of the Data Collected in the Longitudinal Direction of the Cabin.....	61
5.2.1 Injection in Row 2.....	62
5.2.2 Injection in Row 6.....	62
5.2.3 Comparing the longitudinal results when injecting in Row 2 and in Row 6: .....	63
5.3 Uncertainty Analysis.....	66
5.3.1 Uncertainty Analysis of the Results Collected in the Lateral Locations (Row 2).....	67
5.3.2 Uncertainty Analysis of the Results Collected in the Longitudinal Locations .....	71
5.3.2.1 Injection in Row 2.....	71
5.3.2.2 Injection in Row 6.....	72
5.3.3 Uncertainty of the Powder Samples Used in the Tests .....	73
5.3.4 Total Relative Uncertainty .....	74
CHAPTER 6 - Instruments and Cabin Verification .....	77
6.1 APS Verification.....	77
6.2 Powder Injection System Verification.....	86
6.3 Mockup Cabin Verification .....	91
6.3.1 Mockup Cabin Verification using Powder .....	92
6.3.2 Mockup Cabin Verification using Smoke.....	94
CHAPTER 7 - Summary .....	97
CHAPTER 8 - Recommendations .....	99
References.....	100

Appendix A - Supply Air Temperature Control System .....	103
Appendix B - Controlling the Powder Injection System .....	106
Appendix C - Aerodynamic Particle Sizer Control System.....	107
Appendix D - Effect of the Air Injection Nozzle Tilting Angle for Seat G Injection .....	110
Appendix E - Powder Particles Settling Velocity.....	113

## List of Figures

Figure 3-1 Cabin Chamber Overall Dimensions .....	9
Figure 3-2 Cabin Cross-Sectional View .....	10
Figure 3-3 Cabin Profile of the West Portion .....	12
Figure 3-4 First Row Location inside the Cabin.....	13
Figure 3-5 Reference Mounting Point .....	14
Figure 3-6 Front View Dimensions of the Side Seats.....	15
Figure 3-7 Front View Dimensions of the Centered Seats .....	16
Figure 3-8 Side View Dimensions of the Seats .....	17
Figure 3-9 Heating and Cooling System Details .....	19
Figure 3-10 A View of the Air Supply Heating & Cooling System Installation.....	20
Figure 3-11 Air flow parts and the components in the supply air heating and cooling system....	22
Figure 3-12 Primary Water Loop.....	23
Figure 3-13 Primary Water Loop Installation.....	23
Figure 3-14 Heating Water Loop.....	25
Figure 3-15 Cabin Outer Surface Temperature Control Loop.....	25
Figure 3-16 Control System.....	26
Figure 3-17 Air Supply Ducting Layout.....	27
Figure 3-18 Air Supply Duct Details .....	28
Figure 3-19 Diffuser Location in the Cabin.....	30
Figure 3-20 Diffuser Assembly Mounting.....	30
Figure 3-21 Installation of the Diffuser Assemblies in the Cabin .....	31
Figure 3-22 Diffuser Joint Locations.....	32
Figure 3-23 Dimensions of the Air Supply Connections to the Diffuser Plenum .....	32
Figure 3-24 Dimensions of the Diffusers.....	33
Figure 3-25 Dimensions of the Connections .....	34
Figure 3-26 Diffuser Assembly .....	35
Figure 3-27 Powder Cups .....	36

Figure 3-28 Aerodynamic Particle Sizer (APS).....	37
Figure 3-29 Different Detection Locations in the Lateral Direction .....	39
Figure 3-30 Schematic Diagram of the Mockup Cabin.....	40
Figure 3-31 Air Flow Distribution in the Lateral Direction .....	41
Figure 4-1 APS Alignment during Particle Determination at the Source.....	44
Figure 4-2 Powder Particles Collected at the Release Point with Different Release Quantities ..	46
Figure 4-3 Detection Times at Location I - Row 2 (Injection in Row 2) .....	47
Figure 4-4 Normalized Counts - Location I - Row 2 (Injection in Row 2) .....	47
Figure 4-5 Detection Times at Location II - Row 2 (Injection in Row 2).....	48
Figure 4-6 Normalized Counts at Location II - Row 2 (Injection in Row 2) .....	48
Figure 4-7 Detection Times at Location III - Row 2 (Injection in Row 2).....	49
Figure 4-8 Normalized Counts at Location III - Row 2 (Injection in Row 2).....	49
Figure 4-9 Detection Times at Location IV - Row 2 (Injection in Row 2) .....	50
Figure 4-10 Normalized Counts at Location IV - Row 2 (Injection in Row 2).....	50
Figure 4-11 Detection Times at Location V - Row 2 (Injection in Row 2).....	51
Figure 4-12 Normalized Counts at Location V - Row 2 (Injection in Row 2).....	51
Figure 4-13 Detection Times at Location VI - Row 2 (Injection in Row 2) .....	52
Figure 4-14 Normalized Counts at Location VI - Row 2 (Injection in Row 2).....	52
Figure 4-15 Longitudinal Data Collection Locations when Injecting in Row 2.....	54
Figure 4-16 Detection Times at Location II in Different Longitudinal Locations ( Injection in Row 2 ) .....	55
Figure 4-17 Normalized Particle Counts at Location II in Different Longitudinal Locations (Injection in Row 2).....	55
Figure 4-18 Longitudinal Data Collection Locations (Injecting in Row 6).....	56
Figure 4-19 Detection Times at Loc. II in Different Longitudinal Locations (Injection in Row 6).....	57
Figure 4-20 Normalized Counts at Loc. II in Different Longitudinal Locations (Injection in Row 6).....	57
Figure 5-1 Detection Times of the Data Collected in the Lateral Direction of Row 2 (Injection in Row 2) .....	59

Figure 5-2 Normalized Counts of the Data Collected in the Lateral Direction of Row 2 (Injection in Row 2) .....	59
Figure 5-3 Detection Times in Different Longitudinal Locations (Injecting in Row 2 & Row 6) .....	63
Figure 5-4 Normalized Counts at Different Longitudinal Locations (Injection in Row 2 & Row 6) .....	64
Figure 5-5 Sketch of the Assumed Swirl in the Front part of the Cabin .....	66
Figure 6-1 Comparison Tests Setup inside the Cabin.....	78
Figure 6-2 APS Units Alignment in the Cabin Mockup.....	78
Figure 6-3 APS Comparison Results - Location 1 and Location 2.....	80
Figure 6-4 APS Comparison Results - Location 2 only .....	81
Figure 6-5 APS Comparison Results - $d < 0.5 \mu\text{m}$ .....	82
Figure 6-6 APS Comparison Results - $0.5\mu\text{m} < d < 1\mu\text{m}$ .....	82
Figure 6-7 APS Comparison Results - $1\mu\text{m} < d < 5\mu\text{m}$ .....	83
Figure 6-8 Total Particle Counts Collected by the Two APS Units after Cleaning the Nozzles ( $0.5 - 5 \mu\text{m}$ ).....	85
Figure 6-9 Schematic Diagram of the Powder Injection System.....	86
Figure 6-10 Details of the Injection System .....	87
Figure 6-11 Powder Cloud Height.....	88
Figure 6-12 Powder Injection System Verification - Data Collection Location .....	89
Figure 6-13 Powder Injection Verification - Collected Data.....	89
Figure 6-14 Schematic of the Mockup Cabin Verification using Powder.....	92
Figure 6-15 Exhaust Fans of the Cabin.....	93
Figure 6-16 Mockup Cabin Verification Results using Powder.....	93
Figure 6-17 Smoke Injection Setup for Cabin Verification.....	94
Figure 6-18 Smoke System Setup.....	95
Figure 6-19 Cabin Verification – Smoke Results .....	96
Figure A-1 Supply Air Temperature Lab View Control Software .....	104
Figure A-2 Controlling Keys & Supply Temperature Plot.....	104
Figure A-3 Chiller Flow Meter.....	105
Figure B-1 Lab View Main Window Controlling the Powder Injection System .....	106

Figure C-1 AIM Software Windows.....	108
Figure C-2 Transient Particle Distribution Example .....	109
Figure D-1 Injection Air Nozzle Tilting Angles Considered.....	110
Figure D-2 Comparison Between the Results Collected in Location II and in Location III with Different Powder Release Angles (Detection Time Results).....	111
Figure D-3 Comparison Between the Results Collected in Location II and in Location III with Different Powder Release Angles ( Normalized Particle Counts Results ).....	112
Figure E-1 Settling Velocity vs. Powder Particle Diameter .....	114

## List of Tables

Table 3-1 Cabin Interior Profile Mathematical Equations.....	11
Table 3-2 Powder Samples Weight.....	36
Table 3-3 Particulate Detection Locations' Co-ordinates in the Lateral Direction of Row 2.....	38
Table 5-1 Relative uncertainties of the detection times in the lateral direction of row 2 (In seconds).....	68
Table 5-2 Relative uncertainties of the normalized particle count results collected in the lateral direction of row 2.....	69
Table 5-3 Total Standard Errors and Total Relative Uncertainties of the Detection Time Results Collected in the Lateral Direction (seconds).....	70
Table 5-4 Total Standard Errors and Total Relative Uncertainties of the Normalized Counts Results Collected in the Lateral Direction.....	70
Table 5-5 Total Standard Errors and Total Relative Uncertainties of the Detection Time Results Collected in the Longitudinal Locations (Injection in Row 2) (seconds).....	71
Table 5-6 Total Standard Errors and Total Relative Uncertainties of the Normalized Counts Results Collected in the Longitudinal Locations (Injection in Row 2).....	72
Table 5-7 Total Standard Errors and Total Relative Uncertainties of the Detection Time Results Collected in the Longitudinal Locations (Injection in Row 6) (seconds).....	72
Table 5-8 Total Standard Errors and Total Relative Uncertain of the Normalized Counts Results Collected in the Longitudinal Locations (Injection in Row 6).....	73
Table 5-9 Total Relative Uncertainties of the Data Collected in the Lateral Locations (Row 2).	75
Table 5-10 Combined Total Uncertainties of the Data Collected in the Lateral Direction (Row 2).....	75
Table 5-11 Combined Total Relative Uncertainties of the Data Collected in the Longitudinal Locations (Injection in Row 2).....	75
Table 5-12 Combined Total Uncertainties of the Data Collected in Longitudinal Locations (Injection in Row 6).....	76
Table 6-1 Flow Rate ( l/min ) Comparison between the Two APS Units.....	84

Table 6-2 Total Particle Counts – APS Verification # 2 .....	85
Table E-1 Talcum Powder Samlpe Properties .....	113
Table E-2 Settling Velocity versus Particle Diameter .....	114

## **Acknowledgements**

I would like to express my gratitude to Dr. M. Hosni and Dr. B. Jones for their guidance and support in all aspects of my research and thesis. I would also like to thank Dr. Beck for being one of the committee members, for reviewing my thesis, and providing useful suggestions.

Also, I would like to thank the Department of Mechanical and Nuclear Engineering at Kansas State University for giving me the opportunity to pursue my graduate studies.

It should be noted that the results presented are from research funded, in part, by the U.S. Federal Aviation Administration (FAA) Office of Aerospace Medicine through the National Air Transportation Center of Excellence for Research in the Intermodal Transport Environment under Cooperative Agreement 07-C-RITE-KSU. Although the FAA has sponsored this project, it neither endorses nor rejects the findings of this research. The presentation of this information is in the interest of invoking technical community comment on the results and conclusions of the research. The research was also funded by the Kansas State University Targeted Excellence Program.

Finally, I would like to thank my parents and the rest of my family and friends for their continued encouragements and support.

## Dedication

*To my lovely Parents, To all members of my Family, and  
To Reem*

## CHAPTER 1 - Introduction

Aircraft cabin environmental health is clearly an important national need. In 2002, the National Research Council (NRC) included issues in its report, "The Airliner Cabin Environment and the Health of Passengers and Crew", related to the effects of low humidity inside the aircraft cabins, elevated cabin altitude, contamination from engine oil and hydraulic fluid, and disease transmission.

It is speculated that during the Severe Acute Respiratory Syndrome (SARS) outbreak in 2003, 22 passengers may have been infected by SARS in a flight from Hong Kong to Beijing (Olsen et al. 2003) due to possible release of the SARS viruses from infected passenger(s). Also, after the use of the nerve agent to attack the Tokyo subway in 1995 and the anthrax cases in Florida and Washington, DC in 2001, there have been concerns expressed of possible terrorist attacks by releasing chemical / biological agents in commercial airplanes.

It should be noted that the national need is not just limited to the protection from those persons with malicious intents, but rather it is concerned with the dispersion of bacteria and viruses from infected persons. With the outbreak of SARS and the severe economic impact it had on Asian airlines, disease transmission has risen to a top concern for the industry.

In order to respond to the necessary national needs, an integrated research program, related to aircraft cabin environment health, was launched at Kansas State University. The objectives of this program are:

- Assessing the understanding of contaminant transport within the aircraft cabins.
- Helping in the removal or the destruction of contaminants.
- Helping in the detection of contaminants inside the cabin.
- Attempting to prevent the aircraft cabin from being used as a means of contaminant deployment.

The research program was mainly divided into 4 main phases where each phase had its own objective as follows:

First and Second Phase : Investigation of the air flow characteristics.

Third Phase : Investigation of the gaseous species transport.  
Forth Phase : Investigation of the particle dispersion.

The recent work was related to the measurements and characterization of the tracer gas distribution.

The work conducted by Beneke (2010) concluded that there was particle transportation in the longitudinal direction of the mockup aircraft cabin. Also the work concluded that there was a clockwise swirl circulation inside the mockup cabin from the east wall to the west wall.

The main objective of the project reported in this thesis was to investigate the best placement location of a particulate detecting sensor in the lateral (side-to-side) and longitudinal (front-to-back) direction of the 11-row Boeing 767 mockup cabin available at the Airliner Cabin Environment Research (ACER) laboratory. To achieve this objective, talcum powder was released in multiple points at different locations inside the cabin. An Aerodynamic Particle Sizer (APS) unit was used to collect and categorize transported particles according to their diameter. For the lateral investigation, talcum powder was released in Row 2 and the particles were collected at six different locations in the lateral direction of the same row. For the longitudinal direction, the powder was released in a similar fashion in Row 2 and Row 6, each at a time, and the same procedure of collecting the particles was followed, but at different rows than the injection row.

## CHAPTER 2 - Literature Review

### 2.1 Overview

Every year, the number of people traveling by commercial aircrafts is increasing considerably. According to the National Academy Press publication entitled “The Airliner Cabin Environment and the Health of Passengers and Crew, 2002,” the number of air passengers worldwide has nearly quadrupled, from 383 million in 1970 to 1.5 billion in 1998. With more people traveling by airplane each year, air quality inside aircraft cabins has become of greater interest.

In addition to the increased density of population onboard aircrafts for traveling, there are other factors that raised the importance of the study of air quality inside aircraft cabins. One of these factors is the increase in the average trip length. (Lebbin, 2006).

Since, during a flight, people encounter a combination of environmental factors that includes low humidity, reduced air pressure, and potential exposure to air contaminants, such as ozone (O<sub>3</sub>), carbon monoxide (CO), various organic chemicals, and biological agents, flight crew and passengers have always been concerned about the quality of air available in the aircraft.

As per the Wendell H. Ford Aviation Investment and Reform Act for the 21<sup>st</sup> Century (PL106-181), section 725, the National Research Council (NRC) conducted studies to better understand air quality. These studies can help in identifying contaminants in the aircraft air and in developing recommendations for finding convenient means that can help in the reduction of such contaminants. The National Research Council (NRC), the principal operating agency of the National Academy of Sciences (NAS) and the National Academy of Engineering conducted the study and issued its report. The 2002 report, "*The Airliner Cabin Environment and the Health of Passengers and Crew*", included nine recommendations to the Federal Aviation Administration FAA and one to Congress that called for new regulations, further investigations in specified areas of concern, and increased efforts in public information, surveillance, and research.

The committee was charged to address the following topics:

1. Contaminants of concern, including pathogens and substances used to maintain and operate the aircraft, such as seasonal fuels and deicing fluids.
2. Cabin air supply systems and ways in which contaminants might enter the systems.
3. The toxic effects of the contaminants of concern, their byproducts, and degradation products, and other factors, such as temperature and relative humidity that might influence health effects.
4. Measurements of the contaminants of concern in the air of passengers cabins during domestic and foreign air transportation and comparison with measurements in public buildings, including airports.
5. Potential approaches to improve cabin air quality, such as an alternative air supply for the aircraft passengers and crew to replace the air supplied through the engines.

## **2.2 Aircraft Cabin Air Quality Factors**

The airplane cabin is a unique environment compared to most other forms of transportation. The environment is low in humidity, pressurized up to a cabin altitude of 8000 feet above the sea level and subjected to continuous noise, vibration, and accelerations in multiple directions (Lebbin, 2006). Unlike other forms of transportation, aircraft traveling allows for rapid movement of cabin occupants across many time zones in a single flight, with flight lengths from less than one hour to over 14 hours (O'donnell et al., 1991).

### ***2.2.1 Temperature***

According to the FAA Regulations, the aircraft shall be designed to provide a maximum temperature difference of no more than 3°C ( 5 °F ) between the different cabin zones. The acceptable range of temperature in the aircraft cabin is between 67-73 °F (19.5-23 °C). (O'Donnell et al., 1991)

### ***2.2.2 Relative Humidity***

The level of humidity in the living environment affects human beings in many ways. The common problems like dampness, condensation and dryness in our surroundings are just the results of humidity present in air. As both very high and very low humidity levels can

cause discomfort and various problems related to our health, it is very important that the right level of humidity be maintained.

Because of the temperature gradient, absolute humidity decreases rapidly with altitude. The NRC 2002 report indicated that the cabin relative humidity measured during the studied flights averaged approximately to 14%. A review of studies, conducted since the NAS report, shows that the average humidity levels in the aircraft cabins ranged from 14% to 19% RH at average temperatures of 23-24 °C (73-75 °F) (Nagda and Hodgson, 2001). "The humidity that is found in the cabin primarily arises from human respiration and food preparation" (Meyer, 1983). Levels will vary dramatically as a function of the number of persons onboard, the activity associated within the aircraft and the cabin air exchange rate. (Hocking, 2005).

"When the relative humidity drops below the comfort level, passengers are likely to experience that the air is dry. Dry air can cause health related problems like dry skin, nose and eye pain" (Meyer, 1983). In comprehensive review on the effects of humidity on comfort for building occupants, Berglund stated that such symptoms are likely to occur in low humidity levels when the dew point is less than 32 F (0 °C). The most common eye problems reported were conjunctival redness and dried eyes (Nagda and Hodgson, 2001). Furthermore, airline industries prefer a relative humidity below 25% to prevent condensation which can lead to corrosion, bacterial and fungal growth (Space et al., 2000).

### ***2.2.3 Pressure***

The U.S. Federal Aviation Regulations (FAR) state that the maximum operating altitude in commercial, pressurized aircraft shall be limited to 2450 m (8000 ft) (FAR 25.841). This limit was accepted by the U.S Civil Aeronautics Board in 1957 (Lebbin, 2006). This is seen as the best compromise between the occupant health and comfort on one hand, and the aircraft structure weight, which would increase with a higher pressure difference between the cabin and the outside, on the other hand.

The NRC's 2002 report suggested that pressurization of the cabin to equalize altitudes of up to 8000 ft, as well as changes in the normal rates of pressure during climb and descent, might pose a risk or create discomfort for some segments of the passengers, such as those with pulmonary or cardiovascular disease and infants. At this altitude, 8000 ft, the cabin

pressure is about 75.2 kPa (Lebbin, 2006). The 2003 HVAC Applications Handbook (ASHRAE, 2003) specifies the cabin-to-outside pressure difference to be within 8.6 psi (59.3 kPa).

The amount of oxygen absorbed from the surroundings, by the aircraft cabin body, is the major concern of the cabin pressurization. The amount of oxygen, that is present inside the cabin, affects the health of the passengers and the crew as well (Lebbin, 2006). Normal cabin altitude is well tolerated by healthy individuals.

#### ***2.2.4 Ventilation***

According to the FAA Regulations, section 25.831, it is required that "the ventilation system inside the aircraft cabin must be designed to provide a sufficient amount of uncontaminated air to enable the crew members to perform their duties without undue discomfort or fatigue and to provide reasonable passenger comfort." The FAA Regulations also requires 10 cfm (283.2 lit/min) of fresh air to be supplied per passenger in the cabin (O'Donnell et al., 1991). It should be noted that until the late 1980s about 20.5 cfm (570 lit/min) of fresh air was delivered to the cabin per passenger. Thus, in the modern aircraft, as per the FAA requirement, the fresh air delivery has been halved, but the total air circulation requirement remains the same. Consequently, the balance is supplied from re-circulated air.

In its 2002 report, "*The Airliner Cabin Environment and the Health of Passengers and Crew*", NRC repeated its 1986 recommendation that a regulation must be established to require air carriers to remove all passengers from an aircraft within 30 minutes after a ventilation failure or shutdown on the ground and also to require air carriers to use full ventilation on the ground whenever on-board or ground-based air conditioning is available.

#### ***2.2.5 Air Contaminants***

The aircraft cabin air contains a variety of contaminants coming from different sources. These sources might be the outside air, the passengers, the crew or even the aircraft itself. The major contaminants that are present in the cabin are mainly divided into physical, chemical, and biological air contaminants (Thibeault, 2002).

### *2.2.5.1 Physical and Chemical Air Contaminants*

Particulates or contaminants can contain almost any type of chemicals. According to the U.S. government air quality criteria definition, particulates are any dispersed matter, solid or liquid, in which the aggregates are larger than single gas molecules, but smaller than 0.5 mm in diameter (Meyer, 1983). Particles with a diameter ranging between 0.5 and 5 $\mu$ m are the most dangerous and shall be investigated carefully, because they are able of entering the respiratory tract and penetrate deeply into the lung (Meyer, 1983). Particles whose diameter is less than 0.5  $\mu$ m are normally exhaled. Particles with diameters larger than 5  $\mu$ m are trapped in the larynx or the bronchial tubes before they can reach the lung. (Meyer, 1983)

"The word particulate denotes both organic and inorganic materials. Small filaments and particulates up to 0.01  $\mu$ m in size are called smoke; particles from 0.1  $\mu$ m to the size of sand grains are called dust. The toxic effect of particulates depends on how deeply they can penetrate the respiratory system, what fraction is retained, and how well the body can cope with the toxic agents" (Meyer, 1983).

As mentioned earlier, the passengers or the cabin-crew might be one of the sources of the contaminants in the aircraft cabins. "The principle source of air contaminants by the human body is the expired air, the skin scales, the perspiration, the flatus, and the urine. The human body continually releases water vapor, carbon dioxide, and traces of over 100 other pollutants that can reach noticeable levels in small confined areas" (Meyer, 1983).

"The human body releases 1 liter or more of 37 °C air, saturated with moisture, with each exhalation. This exhaled air contains not only CO<sub>2</sub>, but also ammonia, CO, and acetone depending on the health and the diet of the human" (Meyer, 1983).

"Sweat also contains some 14 amino acids, primarily arginine, histidine and threonine. All of the above, plus many other particles, form the total human wastes which can reach up to 160 mg of micro-organisms, of which a fraction may be released to the air." (Meyer, 1983).

The most important source of indoor air particulates is tobacco smoke. As with all forms of smoke, it consists of a mixture of solids, liquids and dissolved gases. An average cigarette emits about 30 mg of respirable particulates. A pipe also emits about 30 mg and a cigar emits about 68 mg (Repace and Lowery, 1982). "The gas smoke contains 73% mole of Nitrogen, 10% CO<sub>2</sub>, 4.2% CO, 1% H<sub>2</sub>, 0.5% methane, and 0.3% acetone and traces of other

gases among which methanol makes up 700 ppm, methyl ethyl ketone 500 ppm, ammonia 300 ppm, NO<sub>2</sub> 250 ppm, methyl nitrite 200 ppm, and acrotoin 150 ppm" (Meyer, 1983).

In 2003, tobacco has been banned on all U.S. based air lines and on 91% of flights to and from U.S. (ASH). As a result, particle contaminants resulting from tobacco has been removed or reduced to very low limits.

#### ***2.2.5.2 Biological Air Contaminants***

Biological contaminants include bacteria, viruses, microbes, and spores. During the last century, people were extremely conscious of the role of indoor air as a carrier of microbes, because of the constant threat of pulmonary tuberculosis. Today, it is widely, but incorrectly assumed that infections are transmitted only by personal contact.

Some cases of Q fever (*Rickettsia burnetti* or *Coxiella burnetti* which is a unique genus classified between a virus and a bacteria) transmitted by airborne microbes have been documented, one of them in Oakland, CA (Lebbin, 2006). It should be noted that Jennison (1942) mentioned that each human sneeze releases up to 40,000 droplets, with sizes of 5-100 µm, that travel at a speed up to 40 m/s. Under these conditions, the droplets travel about 1 m before they partly evaporate, forming particles of a size between 1 and 10 µm that remain airborne and viable for some time. (Meyer, 1983).

For the aircraft cabin, the biological agents of interest have been influenza, severe acute respiratory syndrome (SARS), tuberculosis, and small pox. The low humidity levels typically found in aircraft cabins during flight can be important, as they don't allow bacteria to survive (Lebbin, 2006).

## CHAPTER 3 - Experimental Setup

This section describes the facilities and the instrumentation used during this project. It also outlines the manner in which the instruments were setup. These facilities and instrumentation are described in more details in the ``Draft Final Technical Report, Contaminant Transport in Airliner Cabins Project, Kansas State University, 2009.``

### 3.1 Cabin

An aircraft cabin mockup was built in the Airliner Cabin Environment Research (ACER) Laboratory at Kansas State University to simulate the Boeing 767 aircraft cabin environment. A schematic diagram of the mockup cabin is shown in Figure 3-1. This mockup cabin is 9.41 meters long and 4.72 meters wide and is one of the larger research mockup cabins in its class.

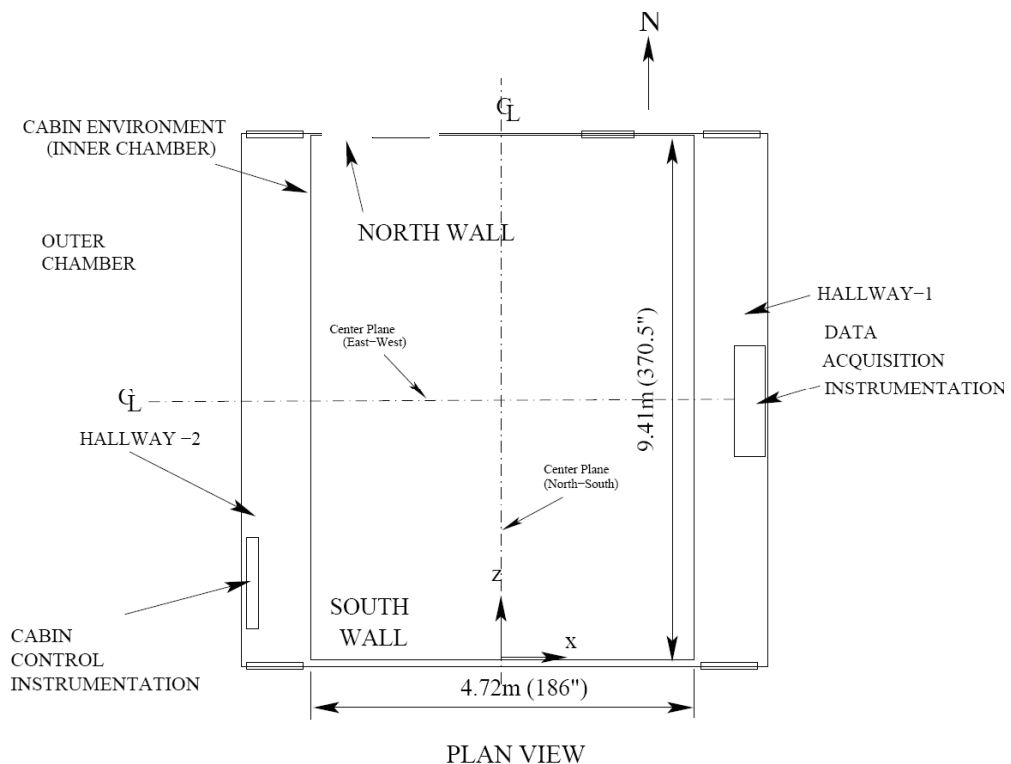
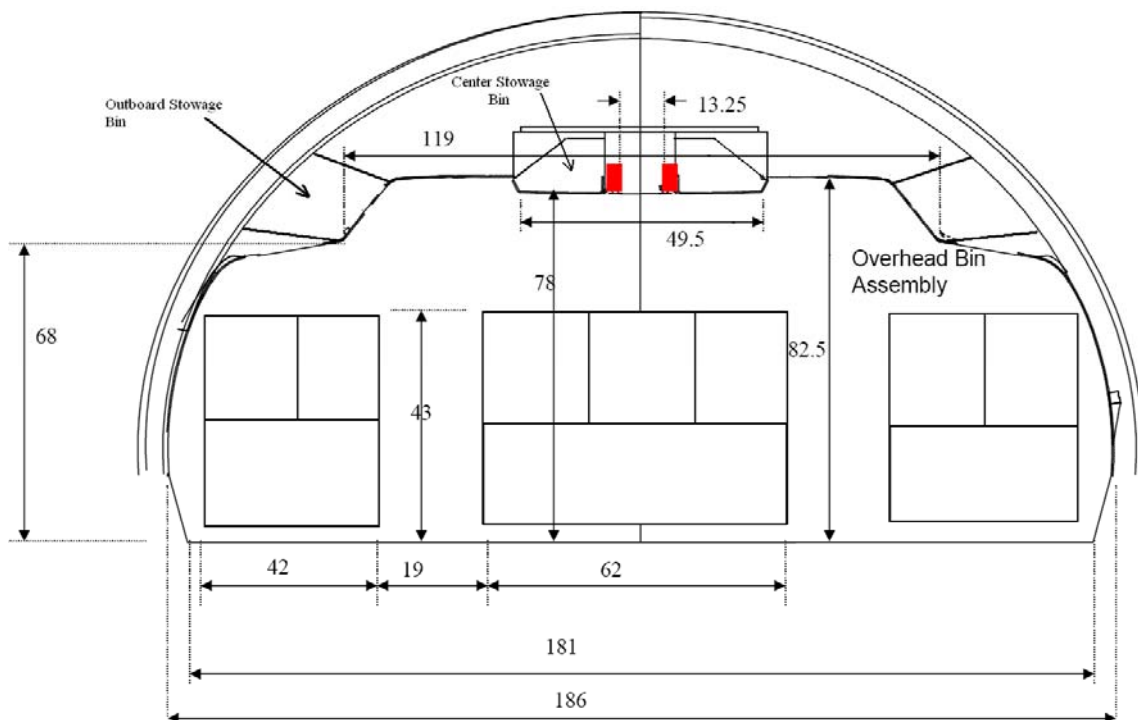


Figure 3-1 Cabin Chamber Overall Dimensions

The mockup cabin consists of 11 rows distributed along its longitudinal length with 7 seats in each row. For each row, two seats are located at the West wall and two at the East wall, while 3 seats are located at the center of the row. There are two outboard and two centered simulated stowage bins installed along the length of the cabin. The air diffusers are located between the two centered stowage bins. (Figure 3-2)

The remaining space between the upper parts of the inside and the outside of the mockup aircraft cabin is occupied by the air conditioning and the lightening systems' components. Two access doors to the cabin are provided in the north end which is considered as the rear of the cabin. Two hallways in the eastern and the western sides of the cabin are used to store the data acquisition system and the cabin control system.



**Figure 3-2 Cabin Cross-Sectional View**

### 3.1.1 Cabin Geometry

The mockup cabin dimensions are shown in Figures 3-1 and 3-2. The geometrical specifications of the cabin's interior profile can be determined by using the equations tabulated in Table 3-1. The segment number in each row is shown in Figure 3-3. Since the aircraft cabin is symmetrical, the cabin profile would be symmetrical as well. So only the west portion (approximately one half) of the cabin has been graphed and is shown in Figure 3-3.

**Table 3-1 Cabin Interior Profile Mathematical Equations**

Segment #	Start Point (width, height)	End Point (width, height)	Corresponded Mathematical Equation (y=Height, x=Width)
1	(20.661,0)	(39.485,154.419)	$(x - 251.472)^2 + (y - 50.221)^2 = (236.211)^2$
2	(39.485,154.419)	(52.46,162,975)	$y = (8 \times 10^{-8})x^3 - 0.0393x^2 + 4.268x + 46.672$
3	(52.46,162,975)	(98.536,172.2864)	$y = 0.2022x + 152.3672$
4	(98.536,172.2864)	(102.48,174.8672)	$(x - 97.284)^2 + (y - 174.872)^2 = 40.1956$
5	(102.48,174.8672)	(124.356,206.2)	$y = 1.4319x + 28.1311$
6	(124.356,206.2)	(128.35,208.3858)	$(x - 128.557)^2 + (y - 203.27)^2 = 26.2144$
7	(128.35,208.3858)	(206.46,211.54)	$y = 0.04043x + 203.1934$

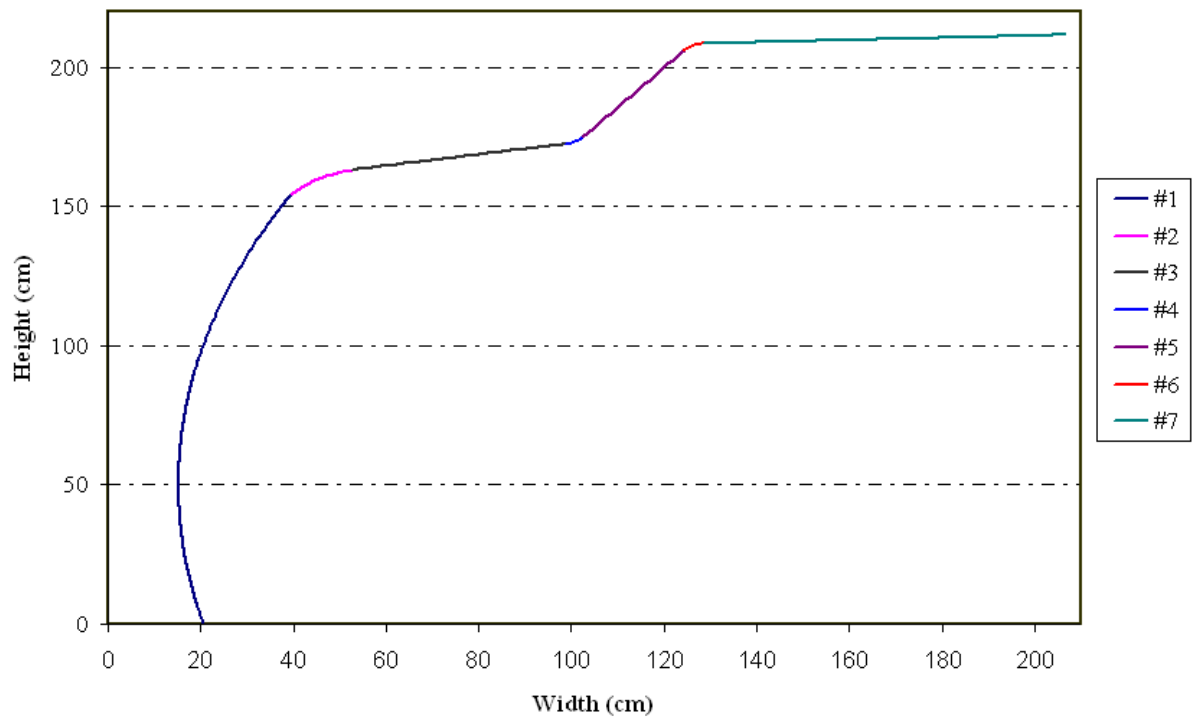


**Figure 3-3 Cabin Profile of the West Portion**

Note that the front of the aircraft has been located toward the south.

### ***3.1.2 Seat Locations***

The configuration of the first row of seats is shown in Figure 3-4. The exact location of the seats is determined by measuring the distances between the seats' mounting location and the south wall as well as between mounting location and cabin's floor center line. A sample of the mounting location of the seats is shown in Figure 3-5.

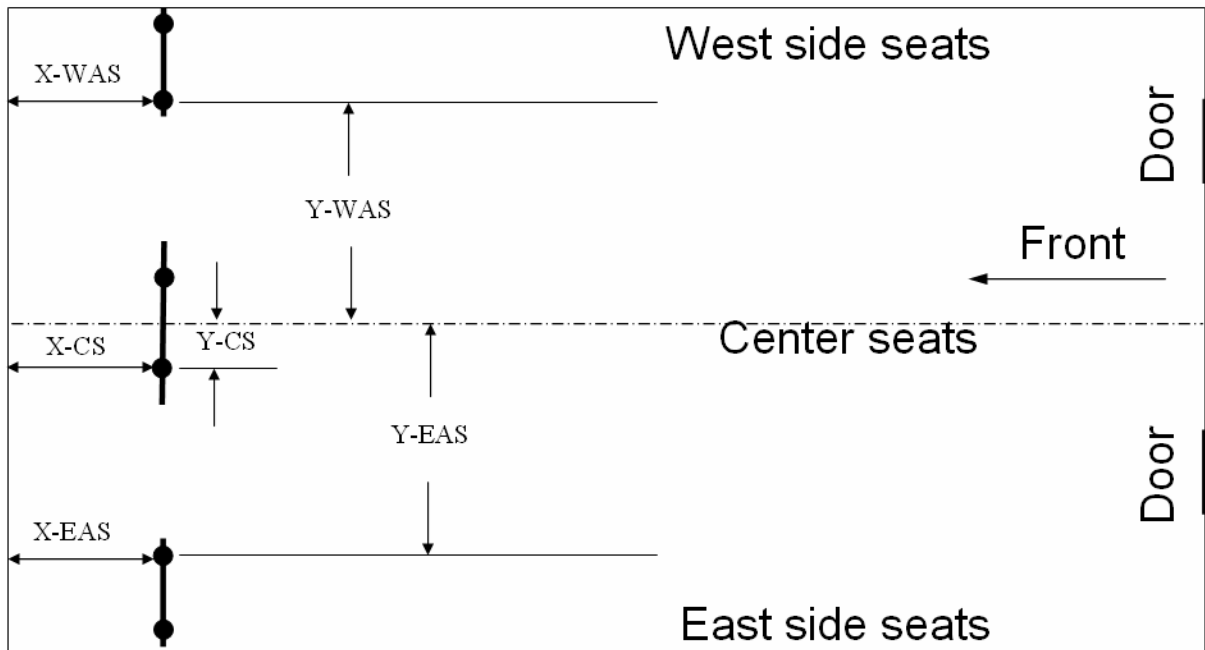


**Figure 3-4 First Row Location inside the Cabin**

Reference  
Mounting Point



**Figure 3-5 Reference Mounting Point**

### 3.1.3 Seat Geometry

Figures 3-6, 3-7, and 3-8 illustrate the geometrical dimensions of the seats used inside the simulation cabin.

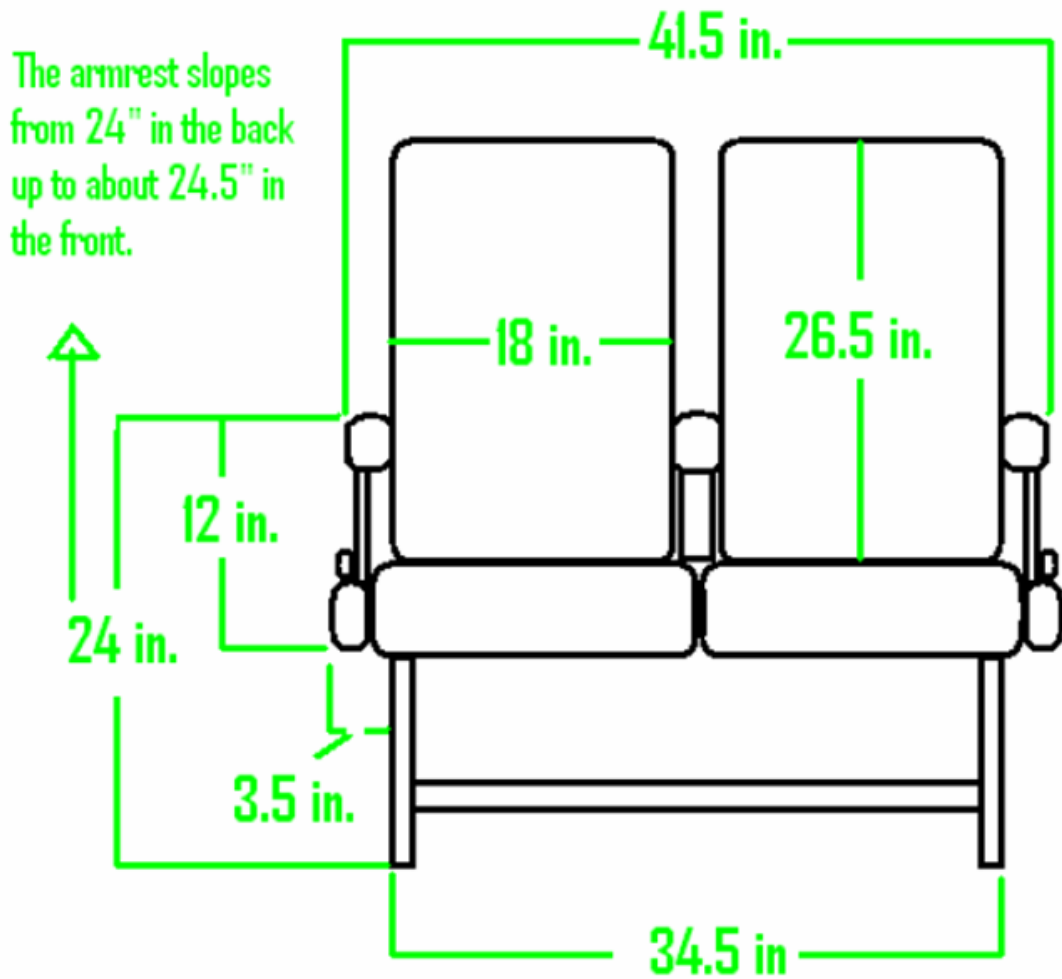


Figure 3-6 Front View Dimensions of the Side Seats



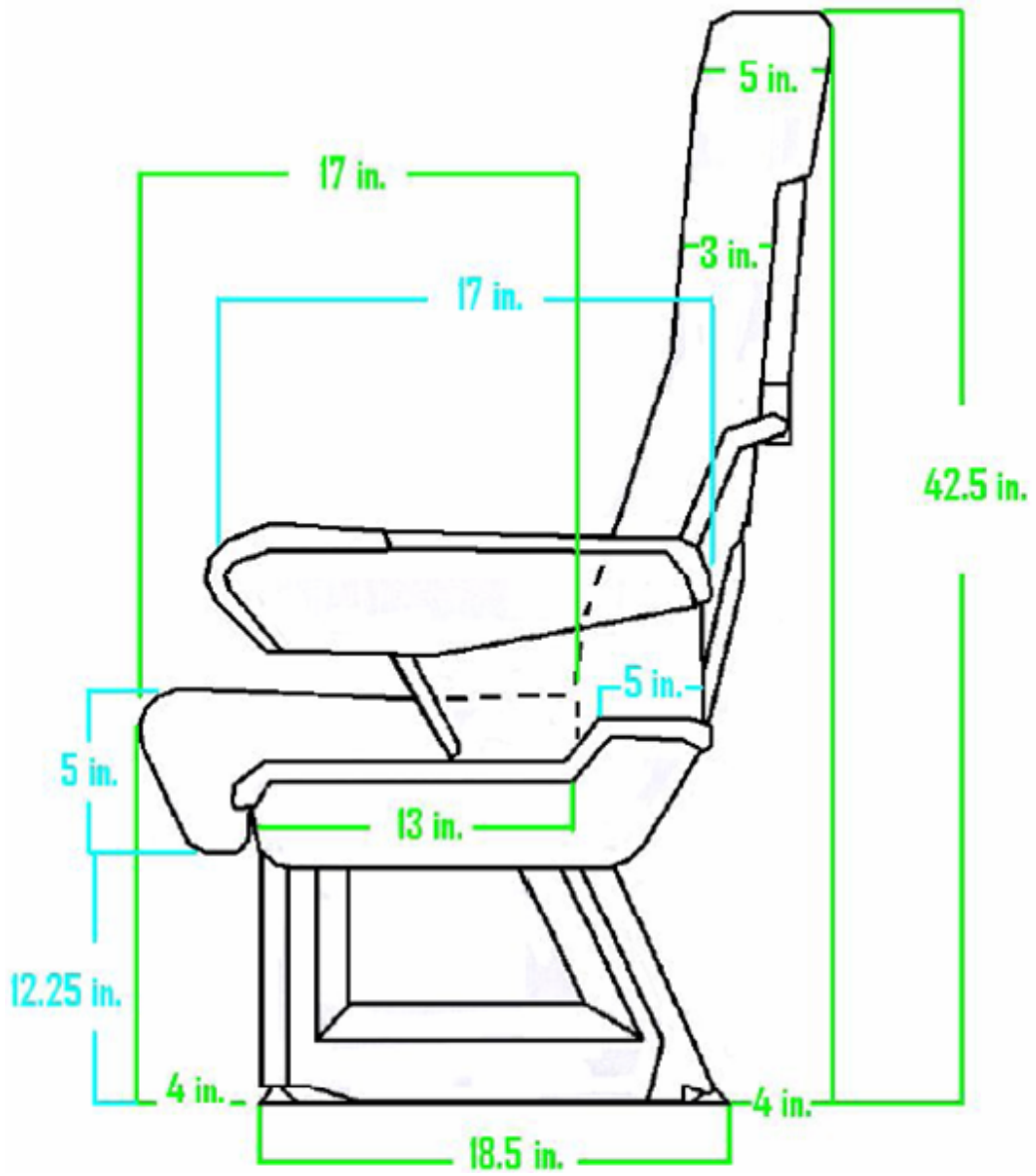


Figure 3-8 Side View Dimensions of the Seats

## **3.2 Air Supply System**

The chamber was supplied with 100% outside air, conditioned to 15.5 C (60 °F) at the upstream of the cabin main supply duct with a flow rate of 39.64 m<sup>3</sup>/min (1400 cfm). The diffusers and the ductwork that were used to supply the air into the cabin were from an actual Boeing 767. A commercial chiller unit was used to cool the outside incoming air into the required temperature when the air temperature was higher than what was required. At the same time a duct heater was used to control the temperature within  $\pm 0.5^{\circ}\text{F}$ . The chamber was maintained at a positive pressure at all times during experiments.

### ***3.2.1 Heating and Cooling Supply System***

The heating and cooling system, used to control the temperature of the air, is shown in Figures 3-9 and 3-10. This system has been designed (Draft Final Technical Report, Contaminant Transport in Airliner Cabins Project, 2009) to filter the incoming outside air and provide the supply air flow with the desired temperature.

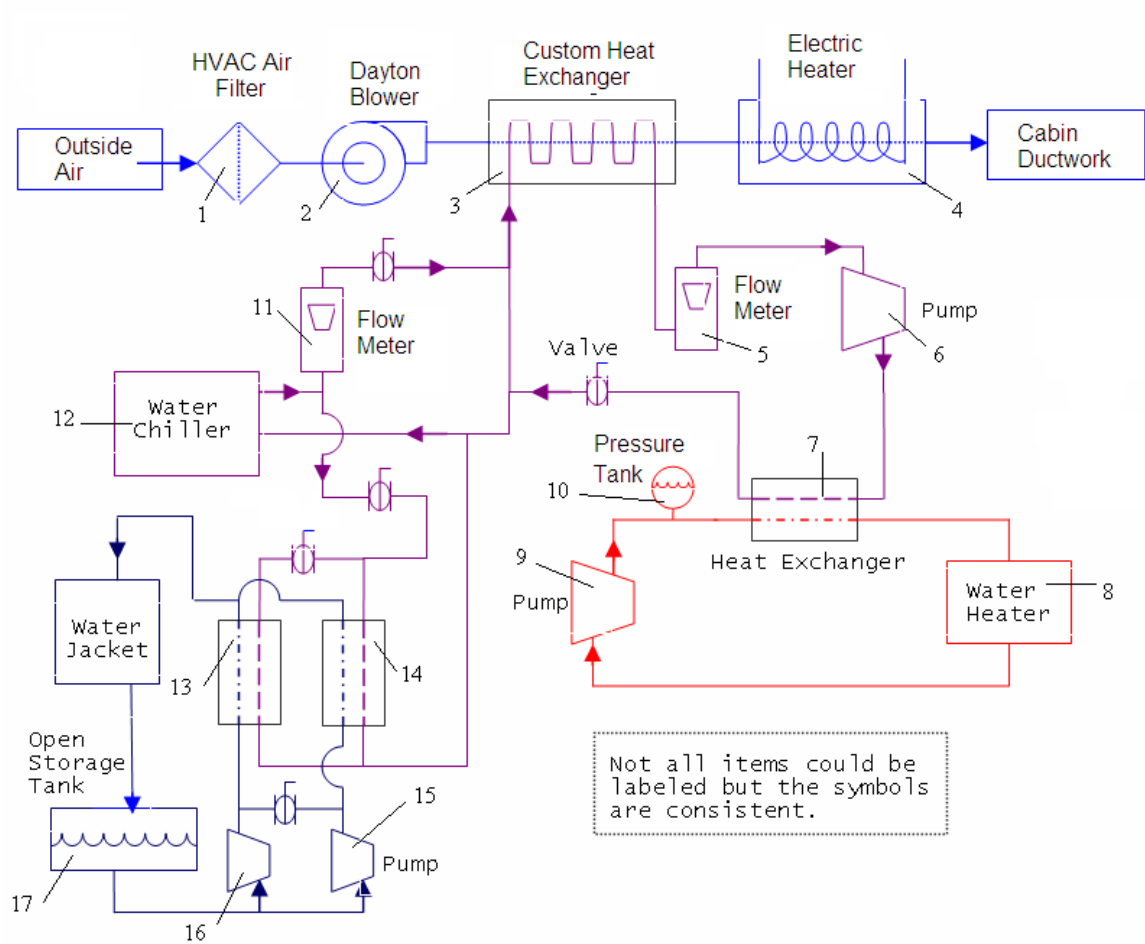


**Figure 3-9 Heating and Cooling System Details**



**Figure 3-10 A View of the Air Supply Heating & Cooling System Installation**

The technical specifications of the different components of the system, as numbered in Figure 3-9, are described as follows:

1. Filters- Ace 2025134, 20"×25" (2 filters in parallel)  
Yaskaw VFD Controllers-200V, 3 Phase, 2.2 Kw, Model #: C1MR-V7AM22P2
2. Dayton Blower-12 ¼ "
  - Airflow @ 0.250/1.500/3.000 Inch Static Pressure
  - 3012/2648/2020 CFM
  - Max Inlet Air Temperature 250° F
  - Blower Speed 2455 RPM
3. Custom Heat Exchanger- 24"×24"
4. Electric Heater
5. Omega Flow Meter – Model # : FL7204
  - 125 psig at 21°C (70°F)
  - 54°C (130°F) at 0 psig
  - Accuracy: 6% (Full Scale)
  - Repeatability: 2%
6. Marathon Electric Pump- Model #: COM 56C34D212OF Pfh
7. Alfa Laval Heat Exchanger- Model #: CB27-18H T06
8. Water Heater :  
Model # GT-199PV-N-1  
Serial # GTNG 0606 P 000253  
120 V 60 Hz  
Maximum Input : 199,900 Btu/hr                      Minimum Input : 19,000 Btu/hr
9. FHP Pump Model #: C4T34DC35A
10. Dayton Pressure Tank Model #: 4MY57
  - Capacity: 6.5 gal
  - 30 psi
11. King Flow Meter-7200series, Model #: 7205023133W
  - 1 to 200 GPM
  - ±3% to ±6% full scale accuracy
  - 1% to 2% repeatability

- 130°F (54°C) max
- 150 psig max

12. Accu Water Chiller- Model #: LQ2R1503

13. Alfa Laval Heat Exchanger – Model #: CB27-24L T06

14. Same as 13

15. Same as 6

16. Same as 6

17. Open Storage Tank

The heating and cooling air supply system consists of four main parts that have been distinguished in Figure 3-9 with different colors. These four parts are described as follows:

**a. Airflow Part:** This part is distinguished with blue color in Figure 3-9 and is shown separately in Figure 3-11 below. The outside air is drawn into the duct using a Dayton blower and then passes through the filter unit (1-2 in Figure 3-11). Exiting the filter, the air passes through the heat exchanger 3-4 (Figure 3-11) where the major temperature changes takes place.

In addition to the heat exchanger (3-4), an electric heater is used to help maintain the desired temperature for the supplied air (4-5 in Figure 3-11).

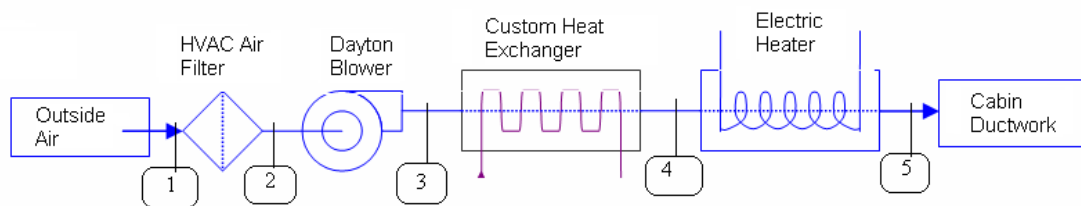


**Figure 3-11 Air flow parts and the components in the supply air heating and cooling system**

**b. Primary Water Loop:** This part, which provides the primary temperature control is shown in Figure 3-9 with purple color and has been shown separately in Figure 3-12.

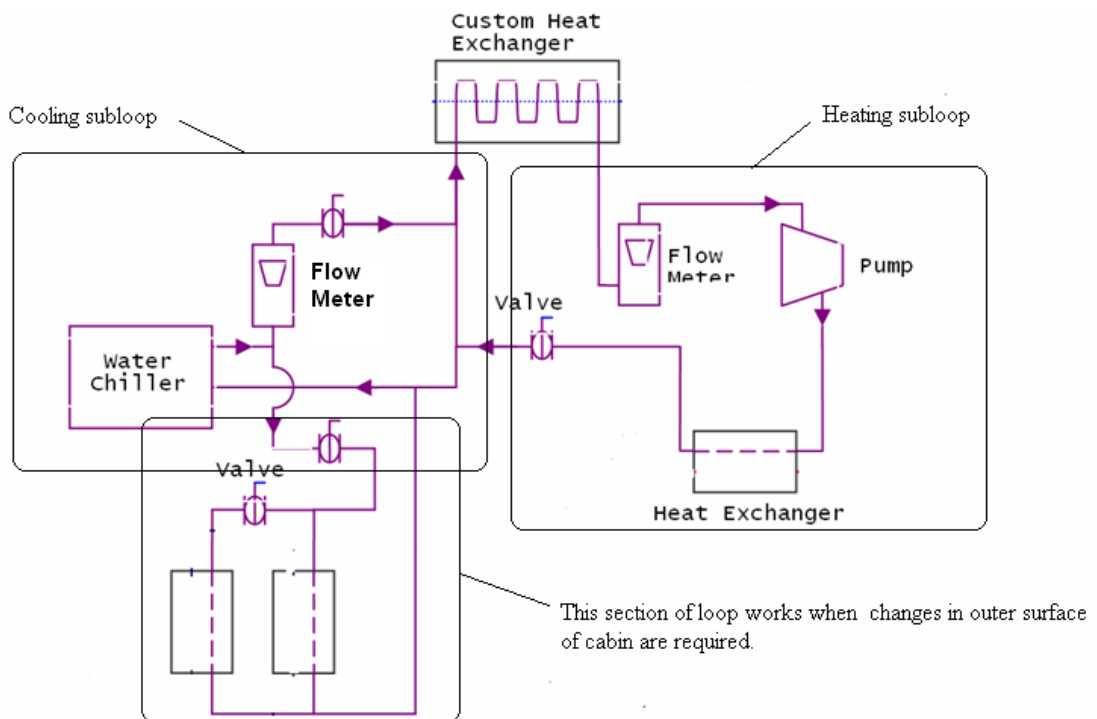


**Figure 3-12 Primary Water Loop**

Figure 3-13 shows a part of the installation of this loop.



**Figure 3-13 Primary Water Loop Installation**

As shown in the above figure, the Primary Water Loop contains three sections: The first section is the heating sub-loop (the primary water receives heat from the Heating Water Part through the heat exchanger of this sub-loop). The second section is the cooling sub-loop (the primary water's temperature decreases using a water chiller in this sub-loop) and the third section is a sub-loop used for the purpose of changing the temperature of the cabin's outer surface.

There are three scenarios that describe the working pattern of the Primary Water Loop. The control criterion of these scenarios is the outside air temperature:

1. *Outside air temperature is higher than 65°F (18 °C):*  
Under this condition, only the cooling sub-loop of the Primary Water Loop works to bring down the primary water's temperature below 55 °F.
2. *Outside air temperature is between 45°F (7.2 °C) and 65°F (18 °C):*  
Under this condition, both the heating and the cooling sub-loops work. Indeed, the heating sub-loop brings up the primary water temperature to a level that can be brought down to the designated temperature by using the chiller. Similarly, the cooling sub-loop brings down the primary water temperature to a level that according to the heating water capacity can be brought up to the designated range.
3. *Outside air temperature is lower than 45°F (7.2 °C):*  
Under this condition, only the heating sub-loop of the Primary Water Loop works.

It should be mentioned that all of the loop's valves are controlled by a Data Acquisition System (DAS) which controls the opening and the closing of the valves to maintain the required temperature inside the cabin.

**c. Heating Water Part:** As shown in Figure 3-9 (red colored) and in Figure 3-14, this part has the responsibility of providing heat for the heating sub-loop of the Primary Water Loop.

**d. Loop for changing cabin outer surface temperature:** The loop has been shown in Figure 3-15 and in general it is used when changes in the outer surface temperature of the cabin is required. The water jacket of this loop covers the sidewall surface of the cabin.

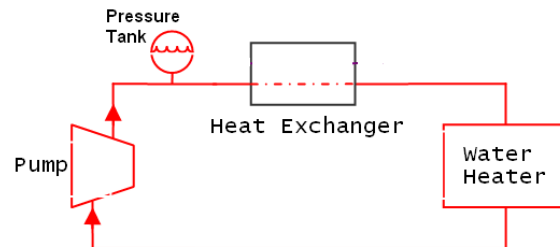


**Figure 3-14 Heating Water Loop**

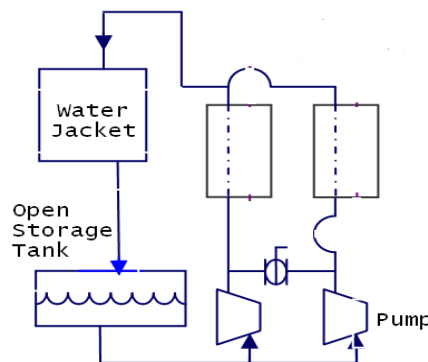


**Figure 3-15 Cabin Outer Surface Temperature Control Loop**

### ***3.2.2 Supply Air Instrumentation and Control***

The control system operation is based on two key parameters:

1. Desirable flow rate
2. Supply air temperature

As shown in Figure 3-1, the cabin control and instrumentation board is located in the west hallway. Data from all the sensors is sent to this board and then from this board is transferred to the computer to perform the required analysis. Based on the received data from the sensors, new orders are sent to the controllers. Figure 3-16 shows the different parts of the control system in which the arrows indicate the flow of data signals.

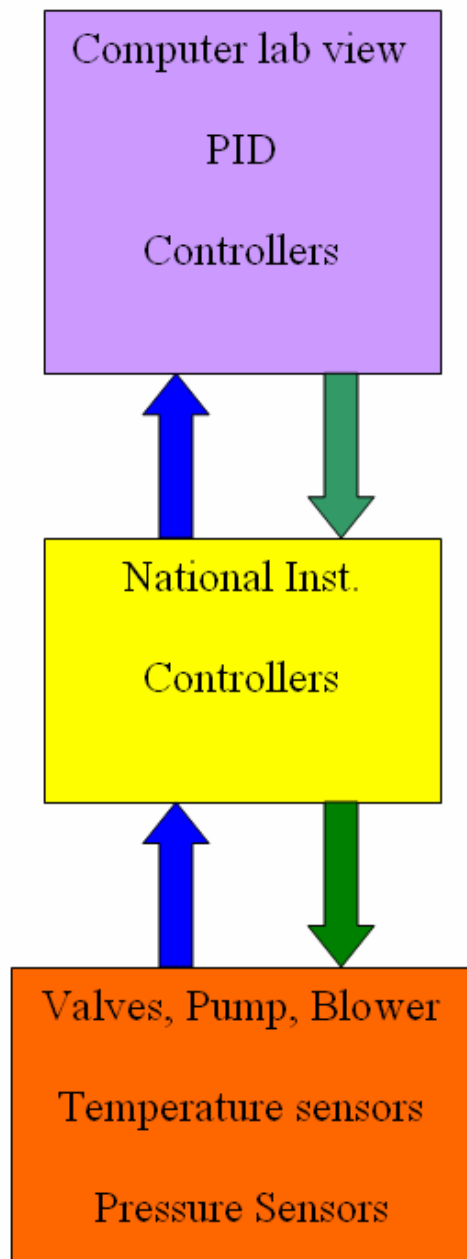


**Figure 3-16 Control System**

### 3.2.3 Air Distribution System

#### 3.2.3.1 Main Supply Duct Geometry

Figure 3-17 provides a schematic of the overall layout of the air supply ducting for the cabin mockup. The numbers on the duct refer to specific segments of the air supply duct. The red rectangular bar represents the cabin supply diffusers. The air supply duct is attached to the diffusers by 17 pairs of clear and smooth-wall plastic hoses (Figure 3.18-A). The numbers below the diffusers in Figure 3-17 refer to the supply hose pairs.

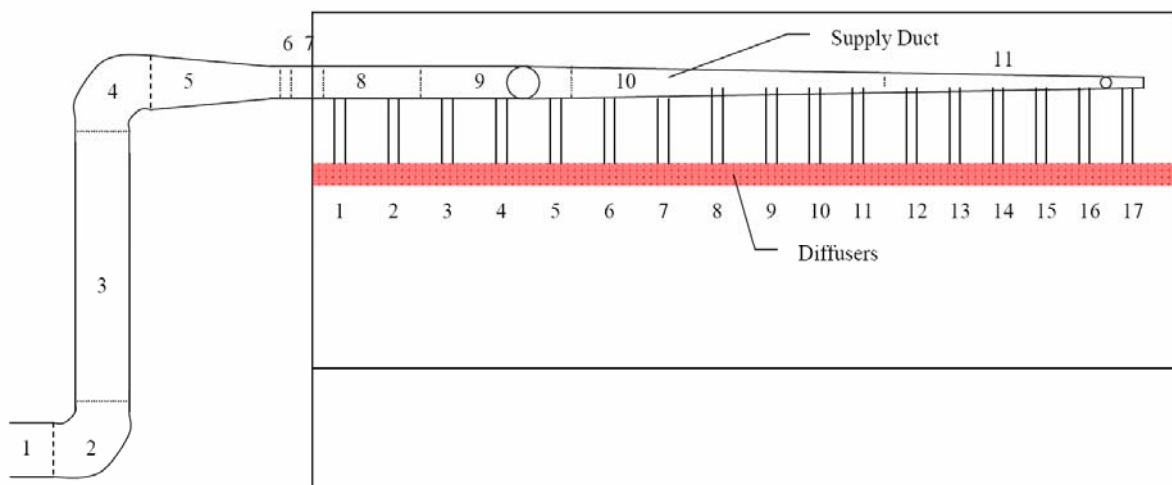


**Figure 3-17 Air Supply Ducting Layout**

The hose connectors extend approximately 1.5 inches from the supply duct (Figure 3.18-B). Inside the duct, the connector is flush with the supply duct wall. The edge between the supply duct and the connector is sharp (Figure 3.18-C). Each hose connector is fitted with a round and thin orifice as shown in (Figure 3.18-D). These orifices presumably are to aid the balance of the flow along the length of the cabin.



A) Plastic Lines from Supply Duct to Diffusers



B) A Typical Section of Supply Duct



C) Interior of Supply Duct Showing Hose Connector Interface



D) Close Up View of Supply Hose Connectors and Flow Restrictors



E) Hose Connection to Supply Duct



F) Hose Connection to Diffuser



G) Supply Duct Joint

**Figure 3-18 Air Supply Duct Details**

### **3.2.3.2 Diffuser Geometry**

This section describes the dimensions of the diffusers as they are installed in the cabin mockup. Figure 3-19 shows the location of the diffusers in the cabin as compared to other parts in the lateral direction. The diffusers are built of 11 ft sections as shown in Figure 3-26.A. The diffuser section mounts to the back side of the centered overhead bin assembly as shown in Figure 3-20. This figure shows the internal cross-section of the diffuser assembly. Air enters through hoses connected to the top of the diffuser assembly where it enters a plenum that extends the full length of the diffuser section. The diffuser is sealed to the back of the overhead bin assembly at the top. Air passes from the plenum through a narrow gap near the top of the assembly. This gap is established by small spacer buttons that are mounted on the edge of the lip (see Figure 3-26.C). The purpose of this narrow gap is to provide uniform flow over the full length of the diffuser section. This gap is approximately 0.125 inches wide.

After passing through this gap, the air passes into the diffuser that is formed between the diffuser assembly and the back of the overhead bin assembly. End caps plug both ends of the diffuser assembly as shown in Figure 3-26.D.

When mounted in the cabin, the diffusers form a single continuous unit from the front to the back end of the cabin as viewed from inside the cabin, as shown in Figure 3-21. However, there is no fluid path connection between the 11 ft diffuser sections since flow is blocked from flowing between sections by the end caps (Figure 3-26.D). Figure 3-22 shows the locations of the joints between the diffuser sections in the cabin mockup. The two back-to-back end caps take up approximately two inches of space. Thus, there are approximately two inches at each joint between the sections where there is no airflow.

Figure 3-23 shows the location of each connector to the air supply along the length of the diffuser sections. The locations are the same for each diffuser section and are the same from left-to-right. Figures 3-24 and 3-25 provide additional details for the diffuser dimensions.

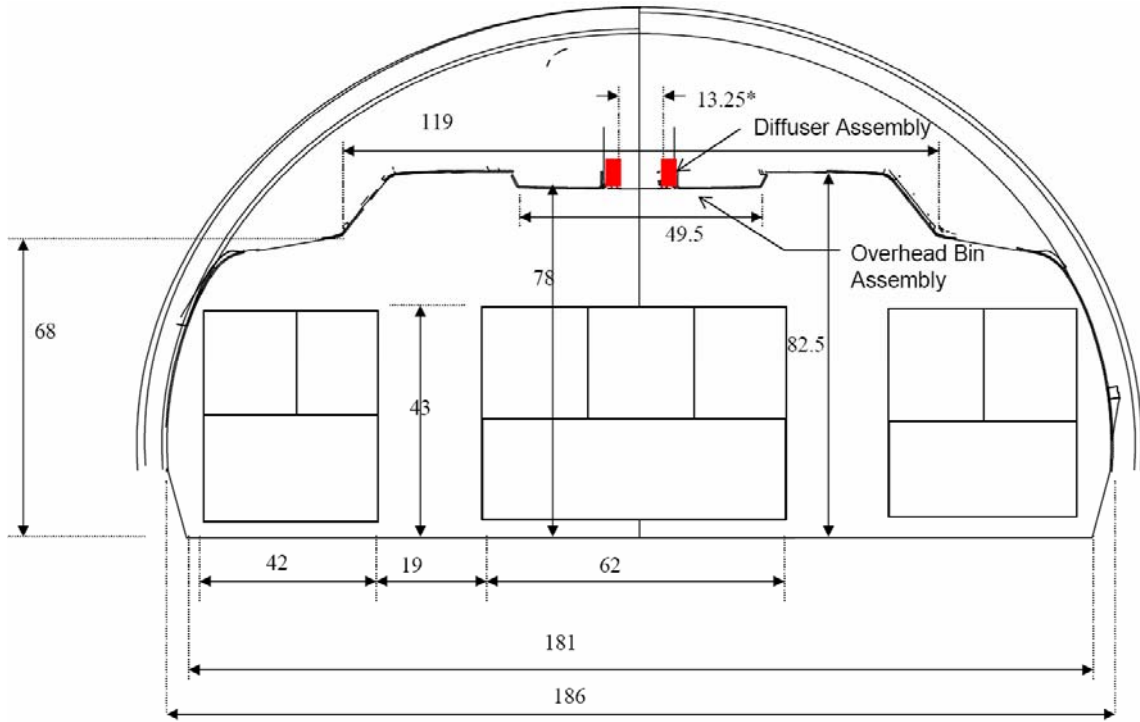


**Figure 3-19 Diffuser Location in the Cabin**

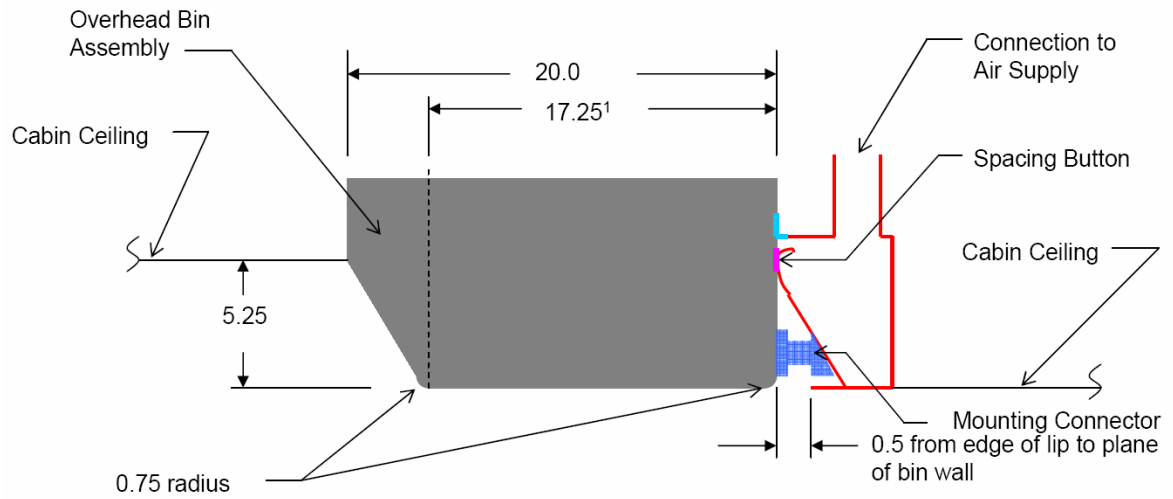


**Figure 3-20 Diffuser Assembly Mounting**



**Figure 3-21 Installation of the Diffuser Assemblies in the Cabin**

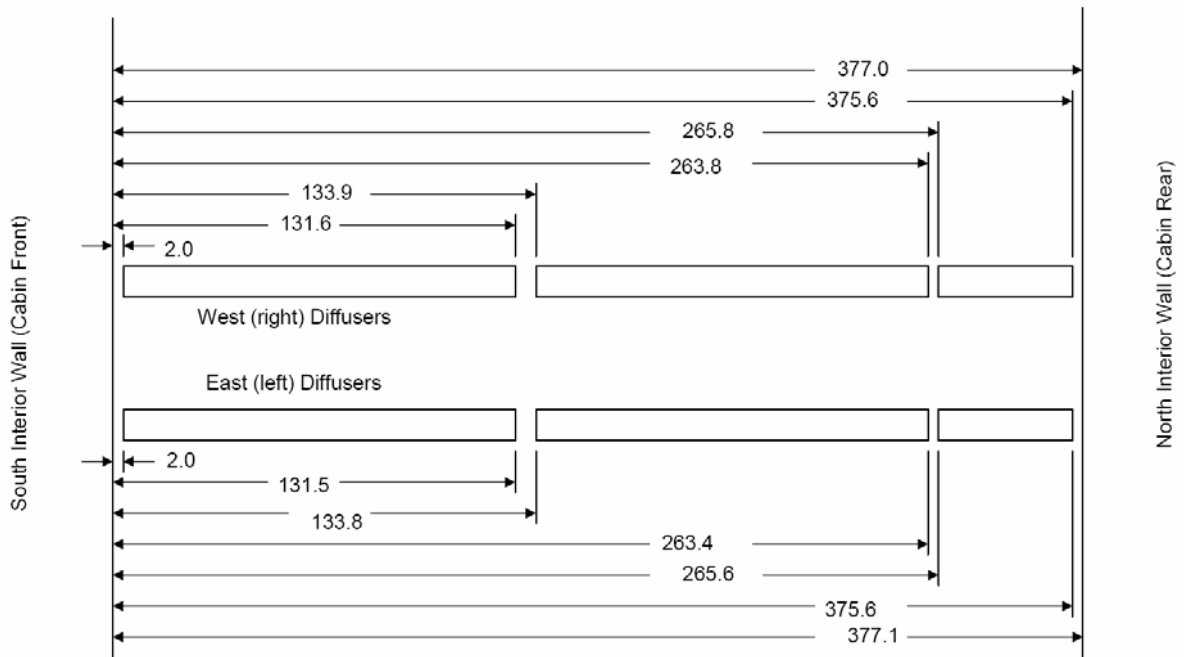


**Figure 3-22 Diffuser Joint Locations**

All dimensions are in inches. Dimensions are to the inside edge (face) of the diffuser plenum end caps.

Drawing is not to scale.

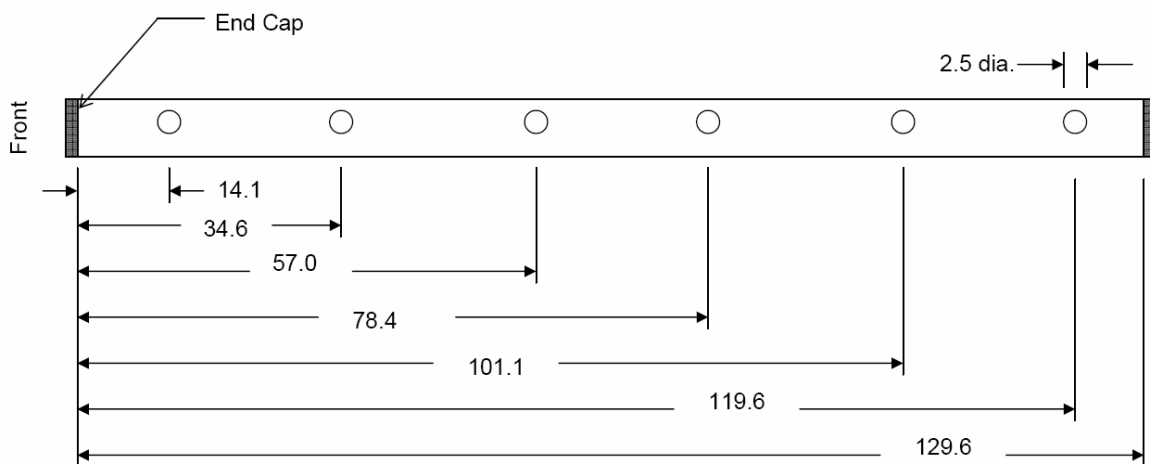


**Figure 3-23 Dimensions of the Air Supply Connections to the Diffuser Plenum**

All dimensions are in inches. Dimensions are to the inside edge (face) of the diffuser plenum end caps.

Drawing is not to scale.

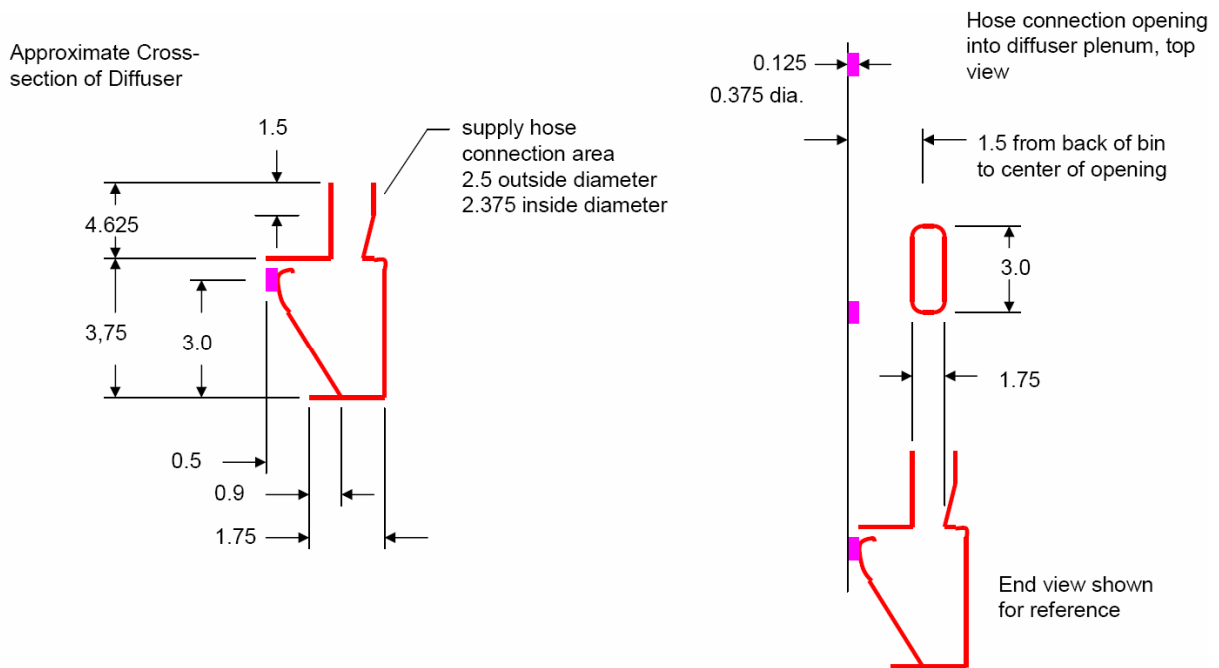


**Figure 3-24 Dimensions of the Diffusers**

All dimensions are in inches. Diffuser mounts to the back of the overhead bin assembly as shown in Figure 3-20 and the buttons shown in pink maintain the spacing from the back of the bin. The supply hose connection is circular and straight for the top 1.5 inches. The side away from the buttons tapers inward and there is a smooth transition to the oval shape where the hose connector is attached to the diffuser plenum. Internal to the diffuser plenum, the edges are flush and sharp along the 3 inch dimension and are flush and rounded with approximately a 0.375 inch radius along the ends of the port (1.75 inch dimension). Drawings are not to scale.

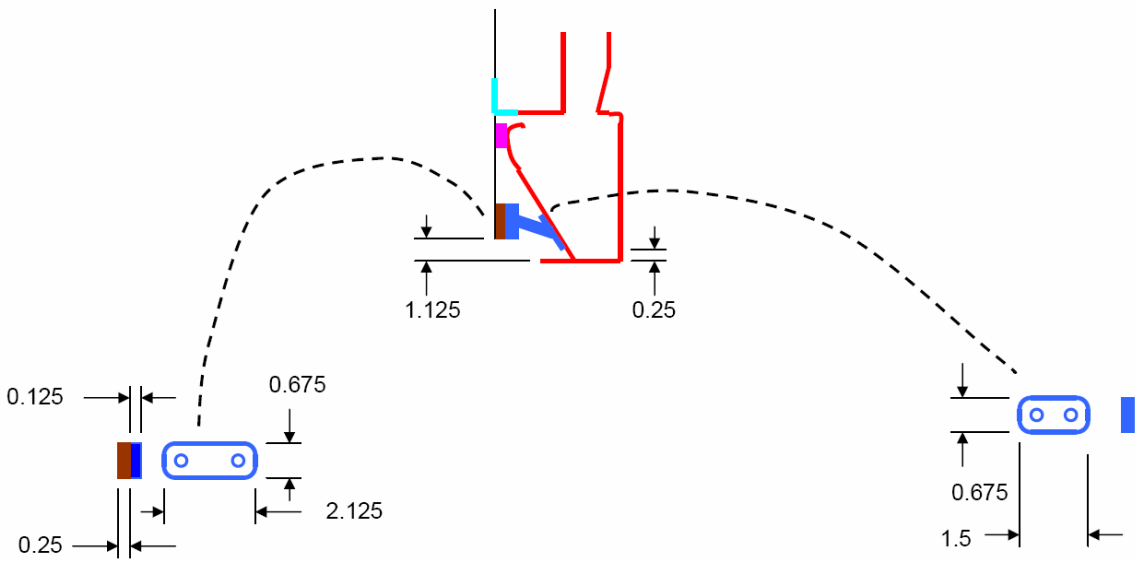


**Figure 3-25 Dimensions of the Connections**

All dimensions are in inches. The diffuser assemblies are attached to the back of the bin through a series of connectors near the bottom (Figure 3.26-C) and with a continuous metal angle at the top. In order to provide correct spacing, a quarter-inch plywood spacer, shown in brown, was placed between the back of the bin and the connector. The connector is attached to the bin with two round-head screws and to the plenum wall with two roundhead screws. Drawings are not to scale.



A) Complete Assembly Section



B) Cut Section Showing Internal Geometry



C) Detail of Connector and Spacing Buttons



D) Detail of End Cap

**Figure 3-26 Diffuser Assembly**

### **3.3 Powder Measurement**

During the tests, talcum powder was used to generate aerosolized fine particulates.

#### ***3.3.1 Powder Injection System***

Powder samples were placed in small plastic cups as shown in Figure 3-27. The weight of the powder was measured using an electronic balance by taking several samples. The weight of each sample is shown in Table 3-2. The average weight of the samples was found to be 41.3 mg with a standard deviation of 1.8 mg.



**Figure 3-27 Powder Cups**

**Table 3-2 Powder Samples Weight**

Powder Weight(mg)
38.8
41.6
39.8
43.7
42.7

### ***3.3.2 Powder Measurement Device***

The primary instrument used to measure the particle size and concentration in the cabin was a TSI Aerodynamic Particle Sizer (APS) system (TSI Model #3321, serial#70626096 named as Mercedes & serial#70742031 named as Porsche).

The theory of operation of the APS is that the particles are accelerated through the instrument to separate the particles into different size ranges. The size of the particles depends on the device. After acceleration, the particles pass through two broadly focused laser beams, scattering the light as they do so. While the size of the particle, identified by the diameter, is related to the time that it takes to cross both beams, the concentration is defined by the number of particles crossing the beams during a specified time interval.

The particle range spanned by the APS is from 0.5 to 20  $\mu\text{m}$  in both aerodynamic size and light scattering signal. One issue of the disadvantages of the use of the APS is that coincidence loss can occur, when two particles cross the beams at the same time and are counted as a single particle, for concentration higher than 1000 particle/ $\text{cm}^3$  (Cox and Miro, 1997).

For more technical details about the method of operation of the APS, refer to the "Instruction Manual" that accompanied the device. The Aerosol Instrument Manager (AIM) software, that accompanied the device, was used to collect the data.(Appendix C)

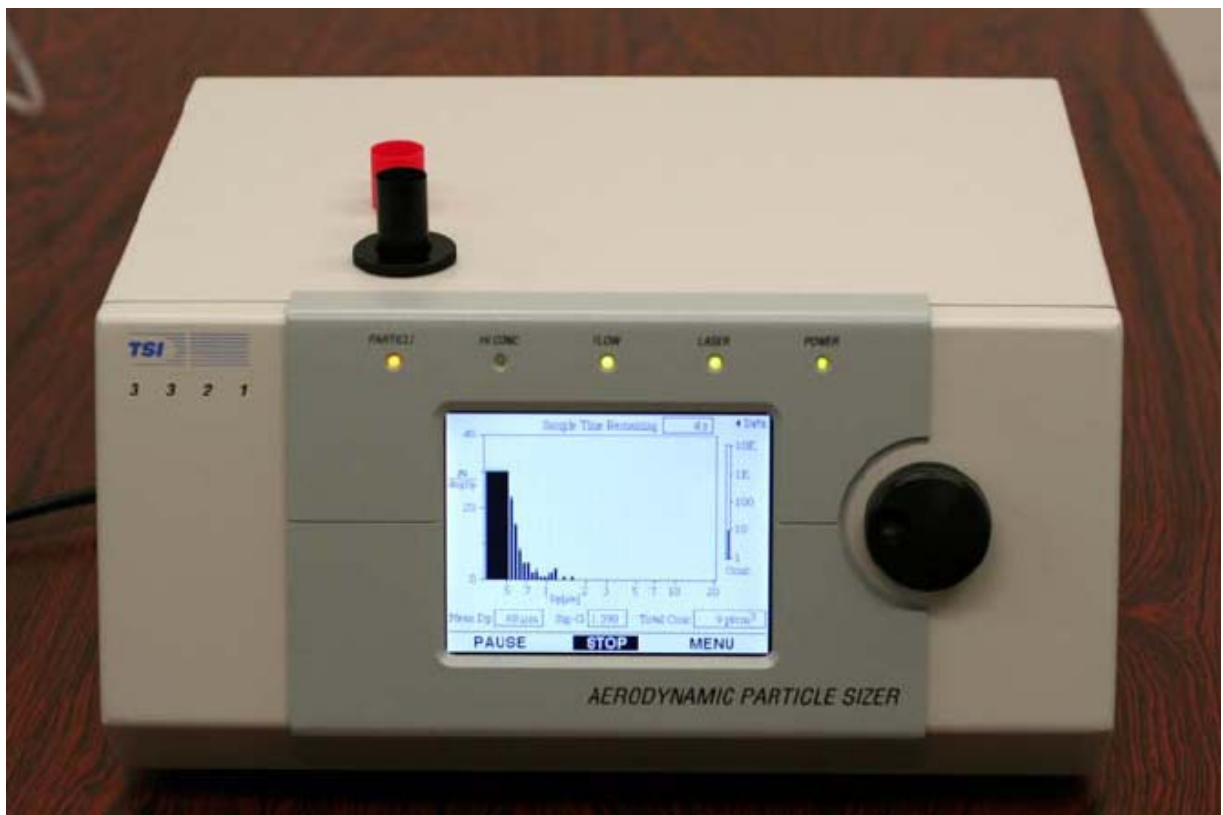


**Figure 3-28 Aerodynamic Particle Sizer (APS)**

### 3.4 Experimental Methodology

The main tasks to be accomplished were:

- i. Determining the sensor's optimal placement location (strongest signal and fastest detection time) in row 2 by comparing different results at various selected locations in the lateral direction (side-to-side).
- ii. Determining the differences in the detection time and in the total exposure at different locations in the longitudinal direction (front-to-back) in a way to figure out the optimum separating distance between two consecutive detection sensors in the longitudinal direction.

#### *OPTIMAL SENSOR LOCATION IN THE LATERAL DIRECTION:*

Powder was released separately in each seat of Row 2 (A through G) at a height of 30 inches above the cabin mockup floor. This height is a good representation of the sneezing of an infected person or the spread of any particle from a pressurized tank by a terrorist as he/she will be carrying the tank in between his legs.

For every injection from each seat, the particles were collected in 6 different locations in the lateral direction of Row 2 as shown in Figure 3-29. The exact co-ordinates of the 6 locations inside the cabin are shown in Table 3-3. The Aerodynamic Particle Sizer (APS) unit was used to collect the particles at these locations.

**Table 3-3 Particulate Detection Locations' Co-ordinates in the Lateral Direction of Row 2**

Location	Dist. From South Wall	On the Cabin Center	Height	Dist. from West Wall	Dist. from East Wall
I	65"	Yes	72"		
II	33"	Yes	9"		
III	33"	No	48"	7"	
IV	33"	No	48"		7"
V	33"	No	9"	10"	
VI	33"	No	9"		10"

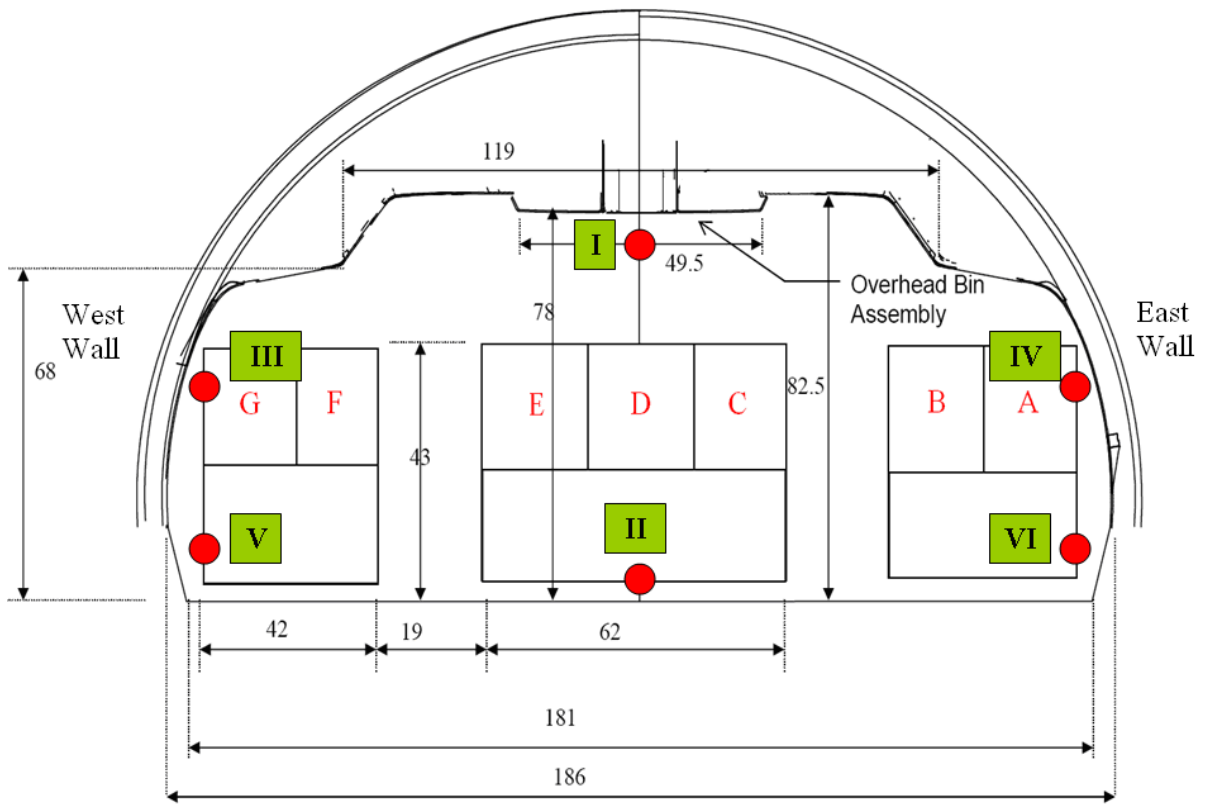


**Figure 3-29 Different Detection Locations in the Lateral Direction**

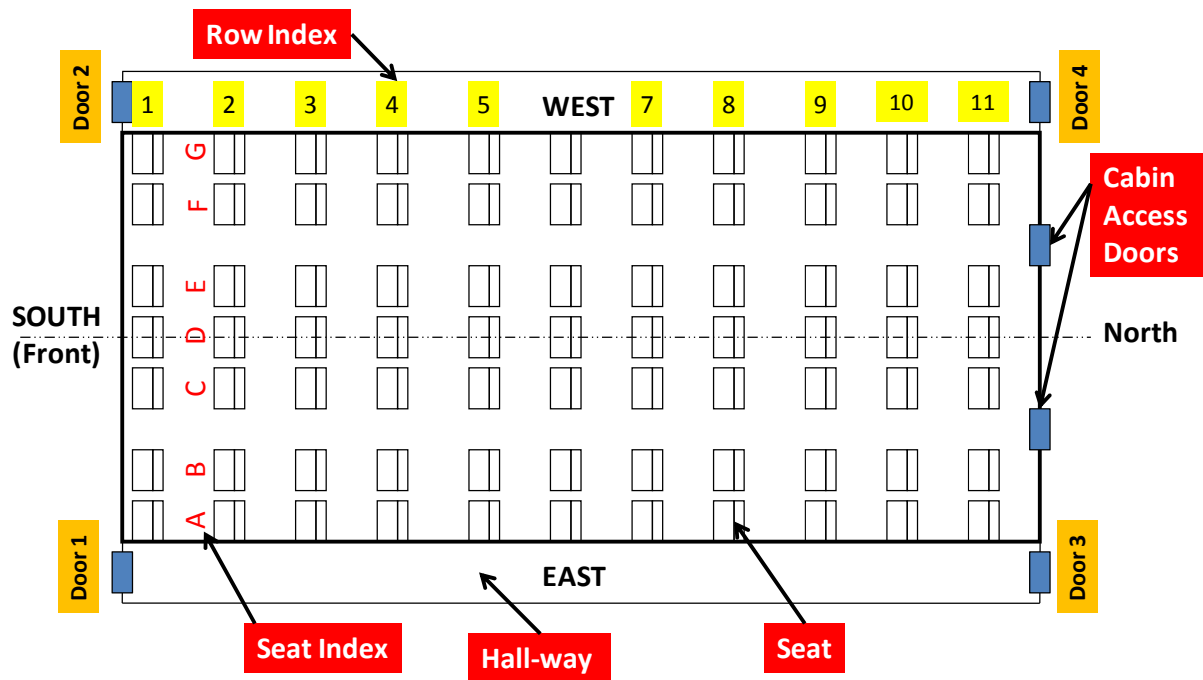


**Figure 3-30 Schematic Diagram of the Mockup Cabin**

The reasons for selecting the sensor locations, as shown in Figure 3-29, are the following:

- Sensors I and II : since it was shown in previous studies that there exist two large airflow circulations in the lateral direction (Figure 3-31), any particle released at any seat should have the tendency to pass through these two locations.
- Sensors III and IV: at 48 inches above the cabin floor which is approximately equivalent to the height of the head of a seated passenger in an aircraft cabin. If an infected person sneezes or spreads out any virus from a pressurized tank and he/she is sitting in one of the side seats near the windows, the plume of sneezing or injection will tend to move up and may pass by these proposed locations.
- Sensors V and VI: located near the exhaust ports. Any suspended particles ultimately will pass by these locations. The advantage of this location is that the concentrations should be representative of mixed cabin air. The disadvantage is that the

concentration will be diluted by mixing. Additionally, the response may not be very fast.

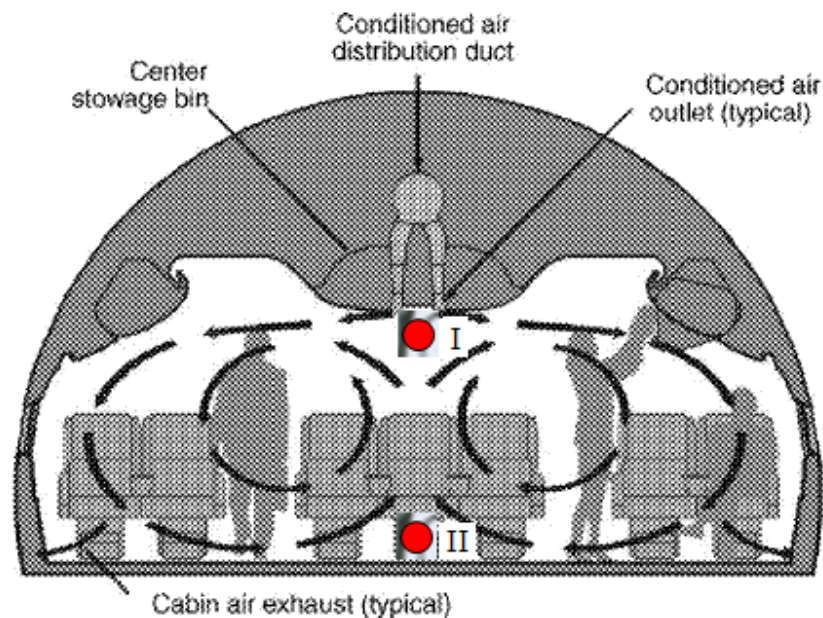


**Figure 3-31 Air Flow Distribution in the Lateral Direction**

For every injection in each seat, the tests were repeated 3-times for statistical consistency. The duration of each test was 15 minutes. Ten minutes waiting period was used before each test to allow the particulates from the previous test to exhaust out from the cabin and thus forming zero particle count by the APS unit.

Two criteria were used in determining the best location of the sensor. The first one was the maximum total exposure (maximum number of particles collected), while the second criterion was the fastest detection time which is the time period required by the APS to start detecting and counting the particles, in a given location, after their release. The maximum total exposure can be used as a criterion for selecting the sensor location if we just need to check whether there is a contaminant in the cabin or not. This type of sensors can be named as "Detection Sensors". The second criterion, which is the fastest detection time, can be used in the case when an action against the detected contaminant is to be taken. This action can be an automatic response by the environmental control system (ECS) such as increasing the

flow rate, going to a 100% outside air, going to 100% recirculation air, dispersing a decontaminant, using oxygen masks, etc.... This type of sensors can be named as "Action Sensors".

The location with maximum exposure will be considered as the best location for placing a "detection sensor", while the location with the minimum detection times will be considered as the best location for placing an "action sensor". A combination of the two criteria will be used in determining the best placement location in this study.

#### *LONGITUDINAL INVESTIGATION :*

After determining the best location for the sensor in the lateral direction, the differences in the "total exposure" and in the "detection time" between different locations in the longitudinal direction were examined. The same testing procedures, as in the lateral study discussed above, were repeated where the powder was released separately in each seat of "Row 2" and then the APS was used to collect the particles in rows 1, 2, 3, 4, and 5.

Furthermore, the injection system was moved into Row 6 which is in the middle of the cabin. Powder was released in each seat (A through G) and particles were collected in Row 6 (the row where powder was released), Row 5, and Row 7, consecutively.

## CHAPTER 4 - Results

This section shows the results of the data collected at different locations in the lateral and longitudinal directions for particle diameters ranging from 0.5 $\mu\text{m}$  to 5  $\mu\text{m}$ . This range demonstrates most of the bacteria and viruses diameter sizes. Note that although many viruses have diameters smaller than 0.5  $\mu\text{m}$ , particles with diameters smaller than 0.5  $\mu\text{m}$  were excluded due to the APS unit inconsistency when counting particles with diameters below 0.5  $\mu\text{m}$  as will be discussed in the APS verification section. Also it was noted in “section 2.2.5.1” that particles with diameters smaller than 0.5  $\mu\text{m}$  are normally exhaled from the human body and that particles with diameters larger than 5  $\mu\text{m}$  are trapped in the larynx or the bronchial tubes before they can reach the lung. For these reasons, the study will focus on particles whose diameters range between 0.5 and 5  $\mu\text{m}$ .

Before showing the results, a normalization technique will be discussed upon which the normalization of the collected particle counts was based.

### 4.1 Normalization Procedures

All of the collected data were normalized by using the concentration measurement near the source point. As a result, the normalized value will be the ratio of the total number of particle counts at a given location to the total number of particles collected at the release point. Thus, the normalized count can be determined using Equation 4.1:

$$\text{Normalized Count} = \frac{\text{Total Number of Counts}}{C_{\text{source}}} \quad (4.1)$$

where the "Total Number of Counts" at a given location is the total number of all particles collected at that location during the whole period of the test which is 15 minutes, and  $C_{\text{source}}$  is the total number of particles collected at the source.

#### ***4.1.1 Experimental Determination of the Total Number of Particles at the Source***

The orifice of the APS unit was placed very close to the powder release points in Row 2 as shown in Figure 4-1. Different amounts of powder were released. These amounts were taken as a multiple of the original amount which was used during the lateral and the longitudinal investigations. Taking the ratio of these multiples with respect to the original amount, these multiples can be categorized as:

- ½ amount
- 1 ( Original )
- Double amount

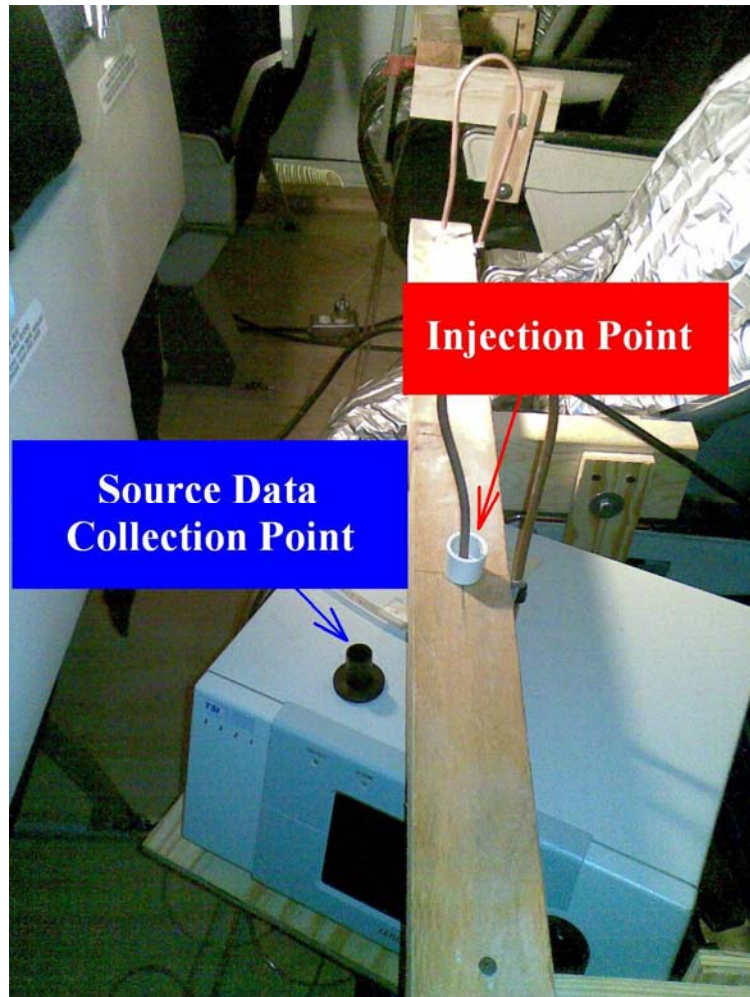


**Figure 4-1 APS Alignment during Particle Determination at the Source**

Three locations were considered for investigating the source strength. These locations are:

- Seat 2A
- Seat 2D
- Seat 2F

For "Seat 2A", the powder ratios were released in seat 2A and the particles were collected, using the APS, very close to the release point as shown in Figure 4-1. The same procedures were repeated for "Seat 2D" and "Seat 2F".

For each case three tests were run for each amount for consistency. The obtained results are shown in Figure 4-2.

Combining the data collected for each amount released in the three locations in one figure and taking the average of each set yields the red line shown in Figure 4-2. The equation of this line is

$$y = 19873.2x - 5460.8$$

where y is the Particle Count and x is the ratio of the released amount of powder to the original amount released during the tests.

For our normalization purposes, we shall substitute  $x = 1$  which yields a total number of particles of 14413 that represents  $C_{\text{source-exp}}$ .

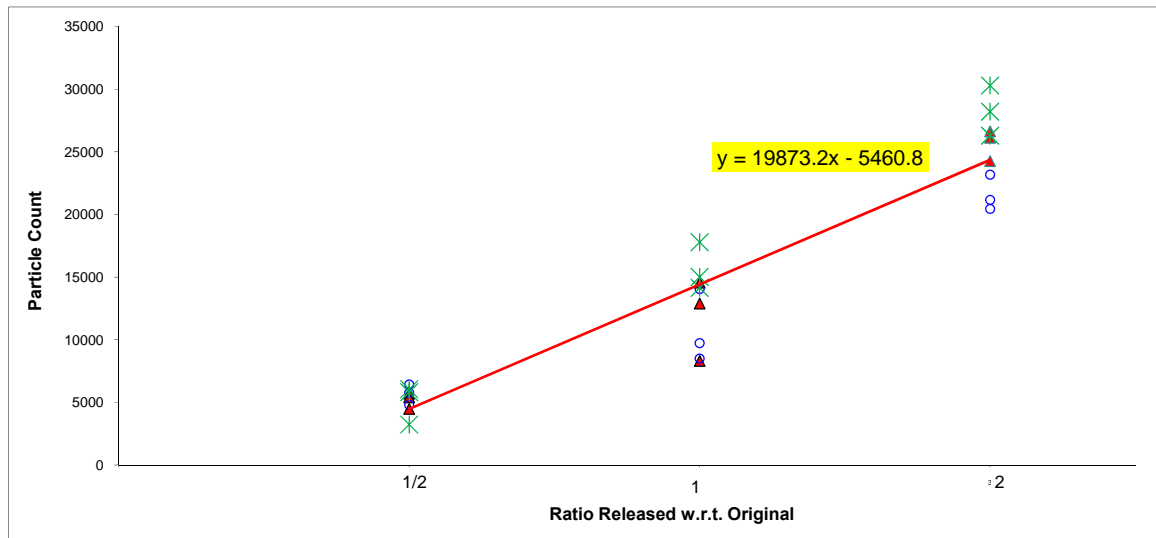


**Figure 4-2 Powder Particles Collected at the Release Point with Different Release Quantities**

## 4.2 Detection Times and Normalized Particle Counts in the Lateral Direction of Row 2:

This section addresses the results of the data collected in the 6 locations in the lateral direction. The data were classified into two main categories. The first one is the detection time, while the second one is the normalized particle counts.

Analyzing the particle counts collected by the APS, the time at which the base count of zero jumps to some higher values was considered as the detection time. Figure 4-3 through Figure 4-14 show the detection times and the normalized counts in the lateral direction of row 2.

**Location I:**

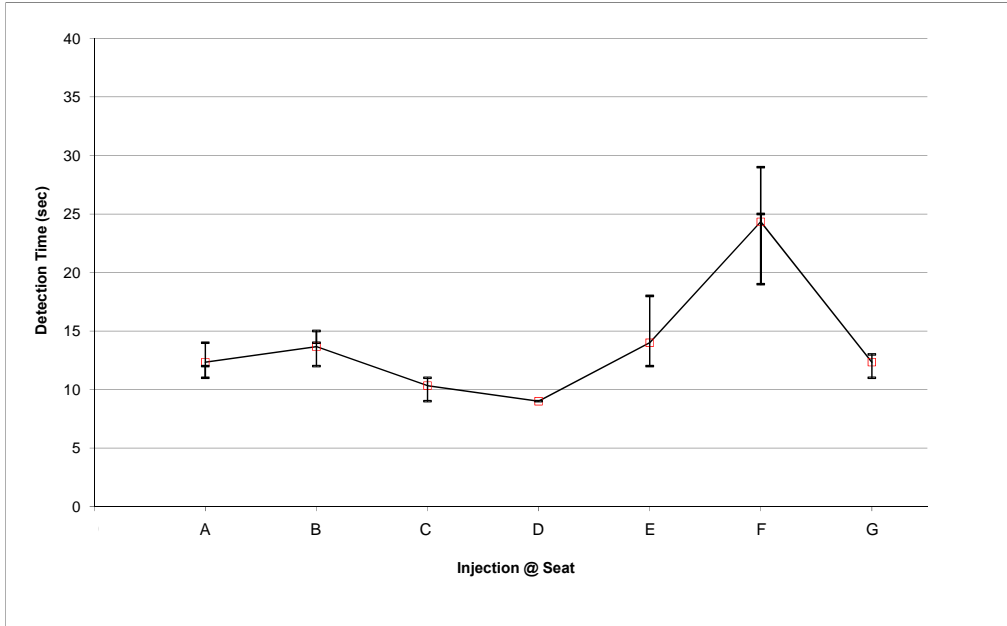


**Figure 4-3 Detection Times at Location I - Row 2 (Injection in Row 2)**

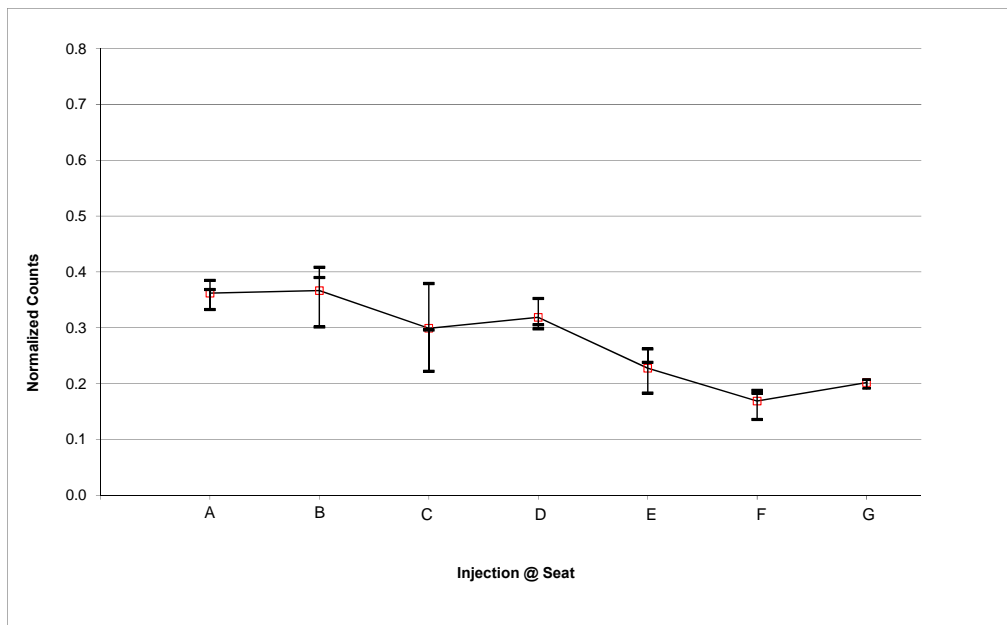


**Figure 4-4 Normalized Counts - Location I - Row 2 (Injection in Row 2)**

**Location II:**

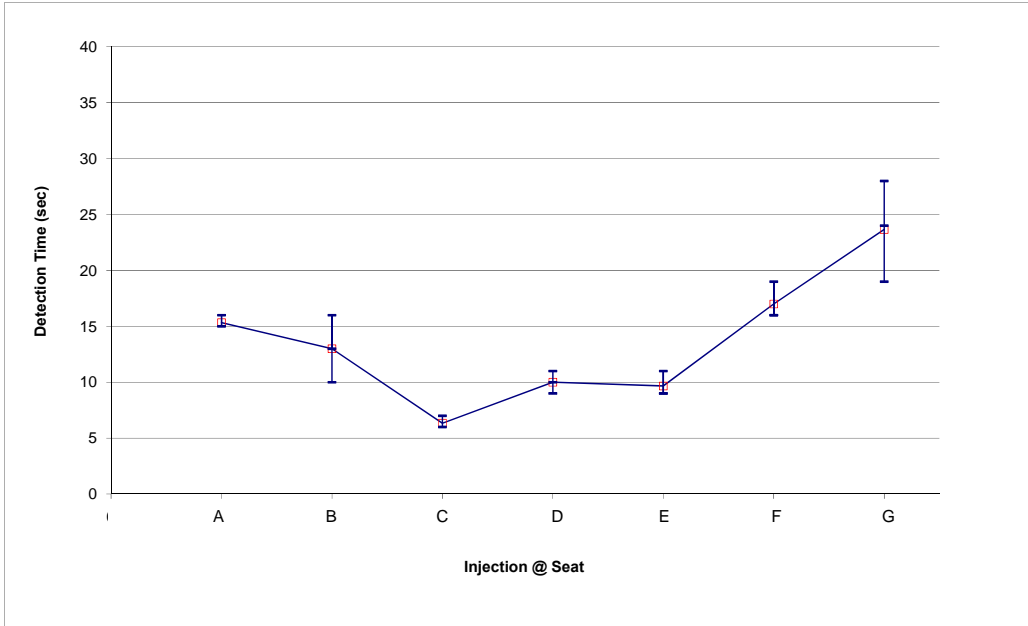


**Figure 4-5 Detection Times at Location II - Row 2 (Injection in Row 2)**

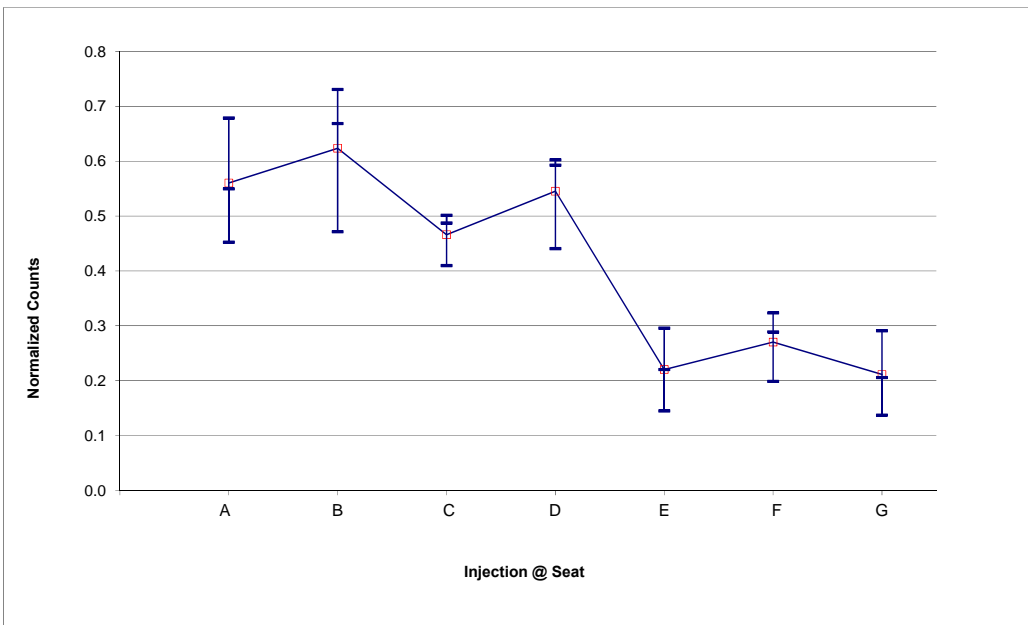


**Figure 4-6 Normalized Counts at Location II - Row 2 (Injection in Row 2)**

**Location III:**

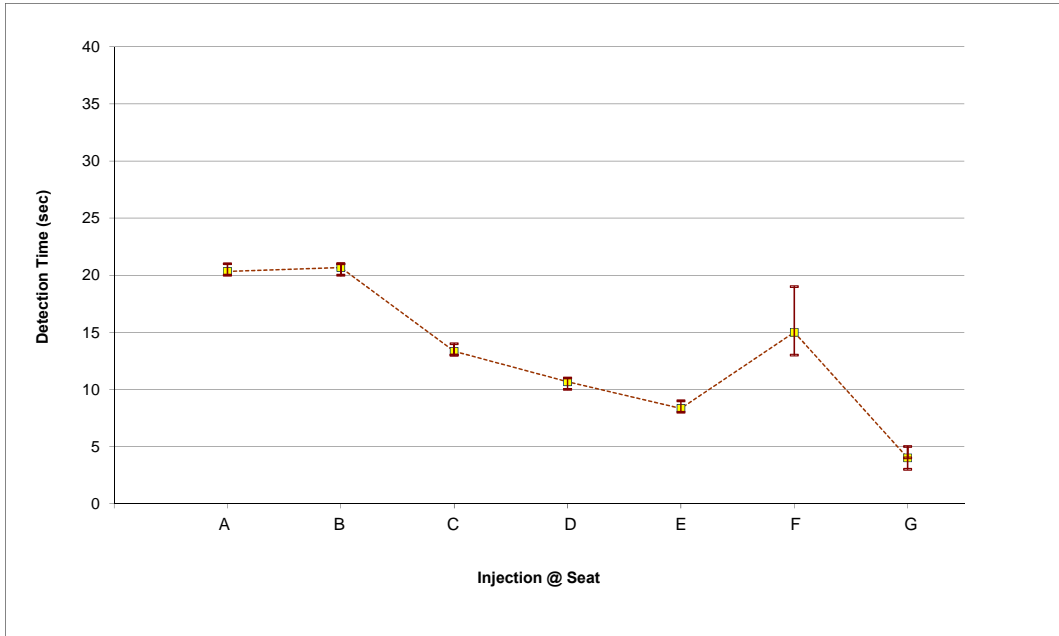


**Figure 4-7 Detection Times at Location III - Row 2 (Injection in Row 2)**

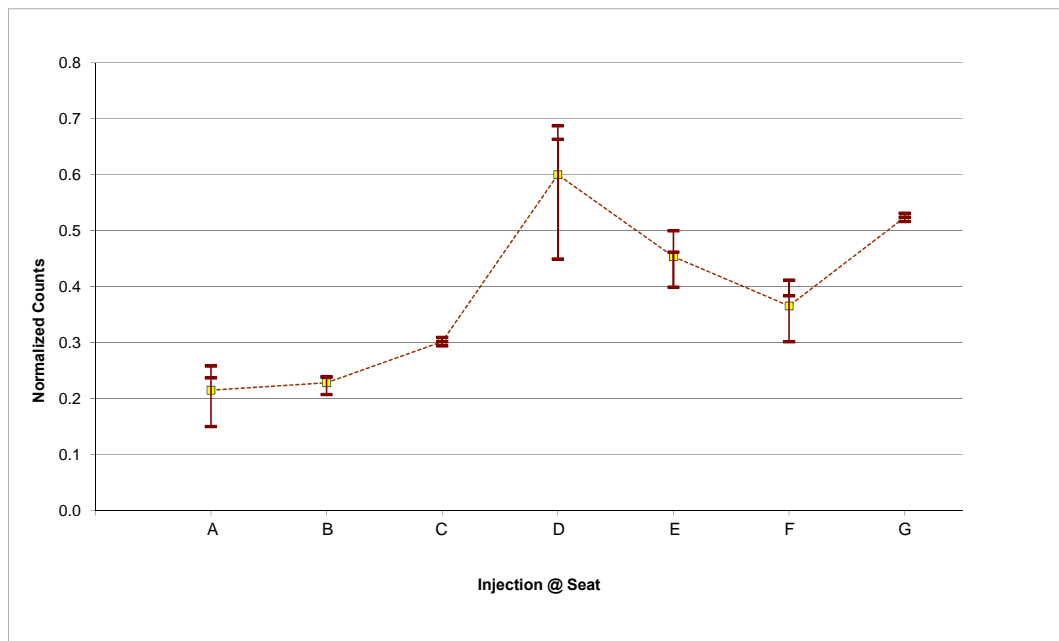


**Figure 4-8 Normalized Counts at Location III - Row 2 (Injection in Row 2)**

**Location IV:**

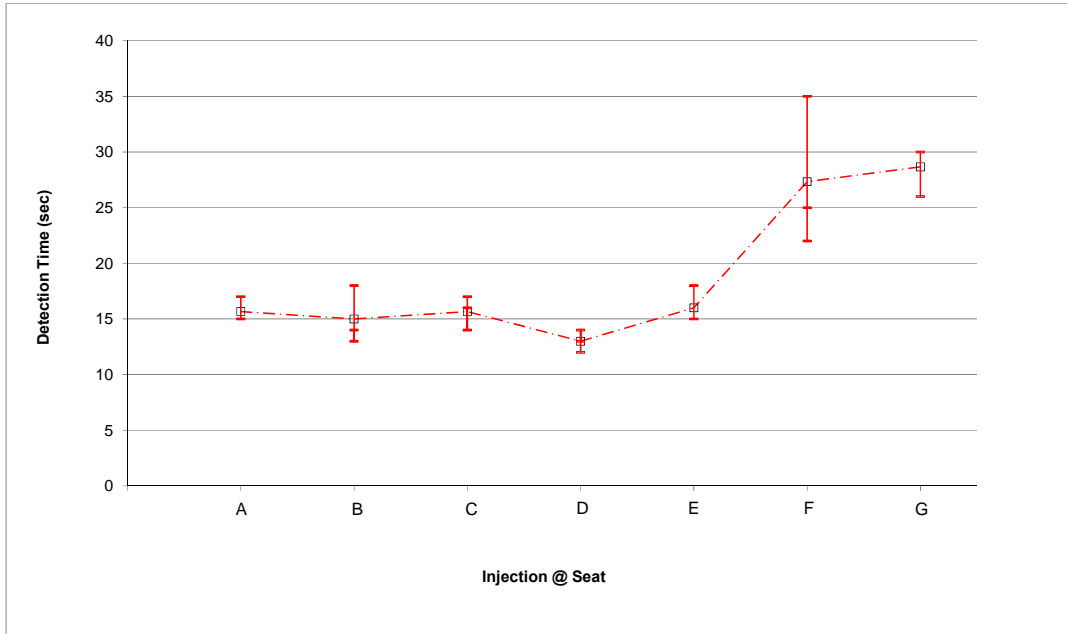


**Figure 4-9 Detection Times at Location IV - Row 2 (Injection in Row 2)**

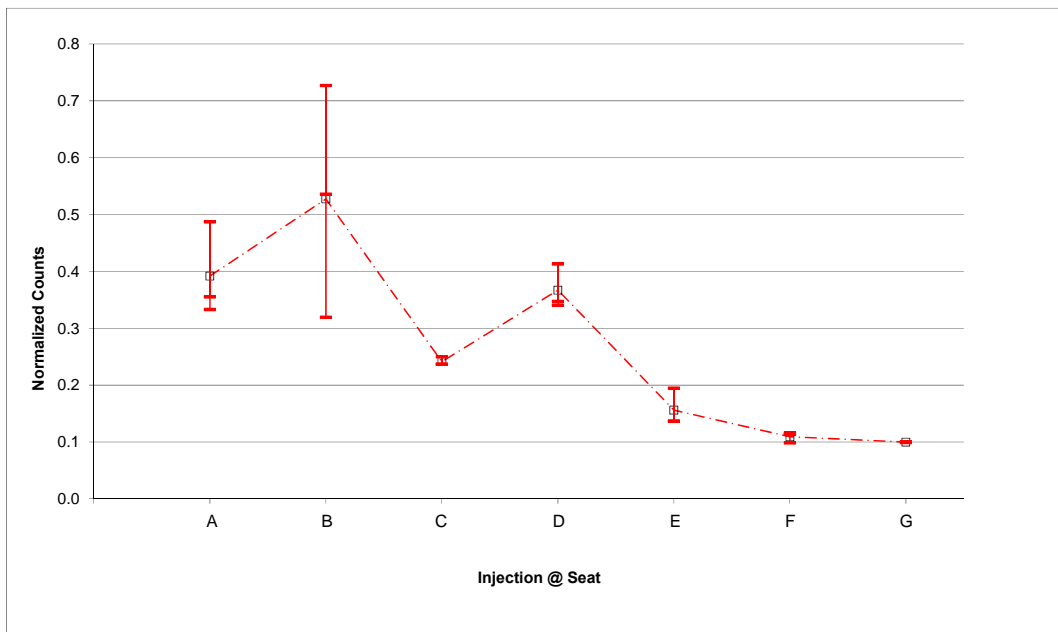


**Figure 4-10 Normalized Counts at Location IV - Row 2 (Injection in Row 2)**

**Location V:**

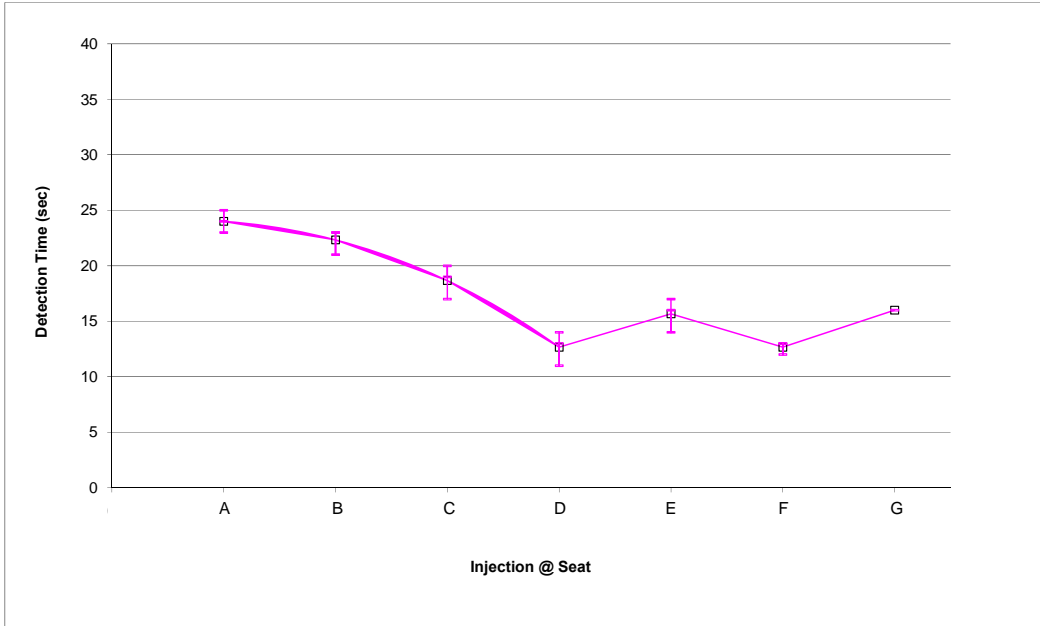


**Figure 4-11 Detection Times at Location V - Row 2 (Injection in Row 2)**

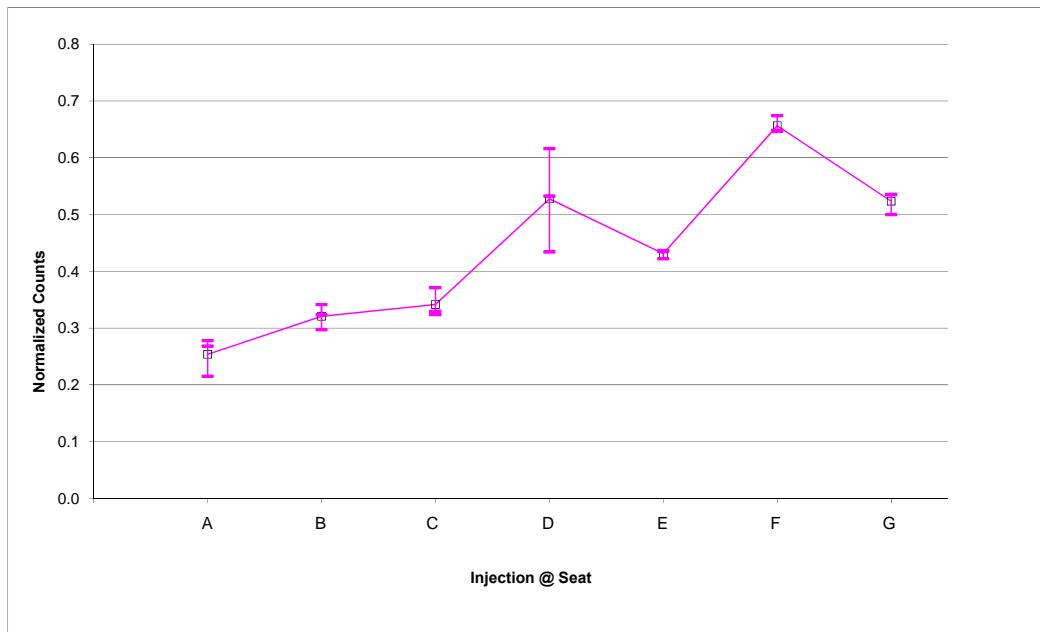


**Figure 4-12 Normalized Counts at Location V - Row 2 (Injection in Row 2)**

**Location VI:**

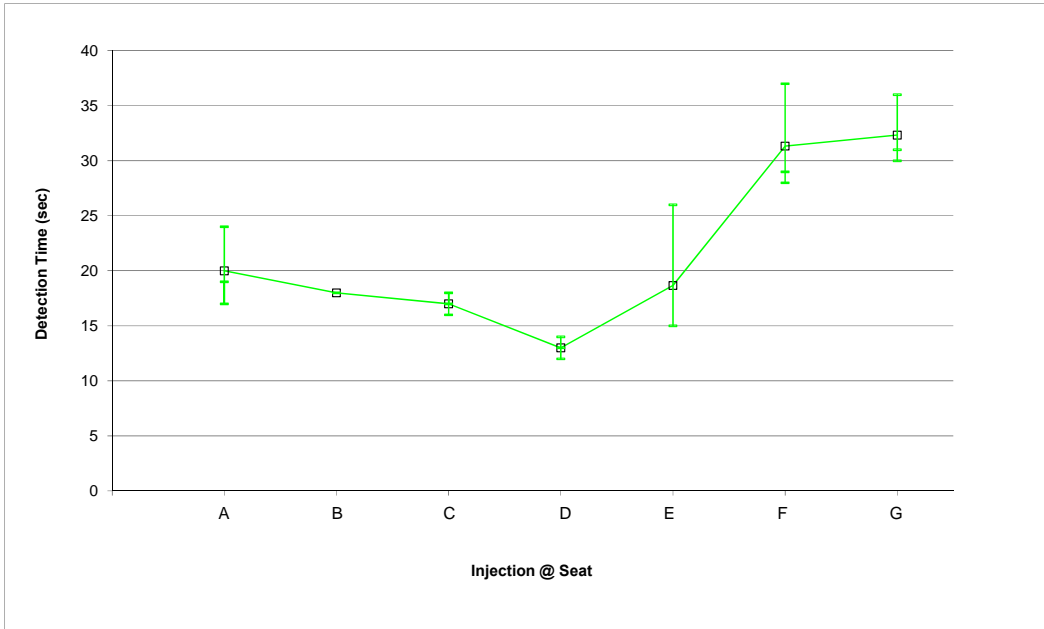


**Figure 4-13 Detection Times at Location VI - Row 2 (Injection in Row 2)**

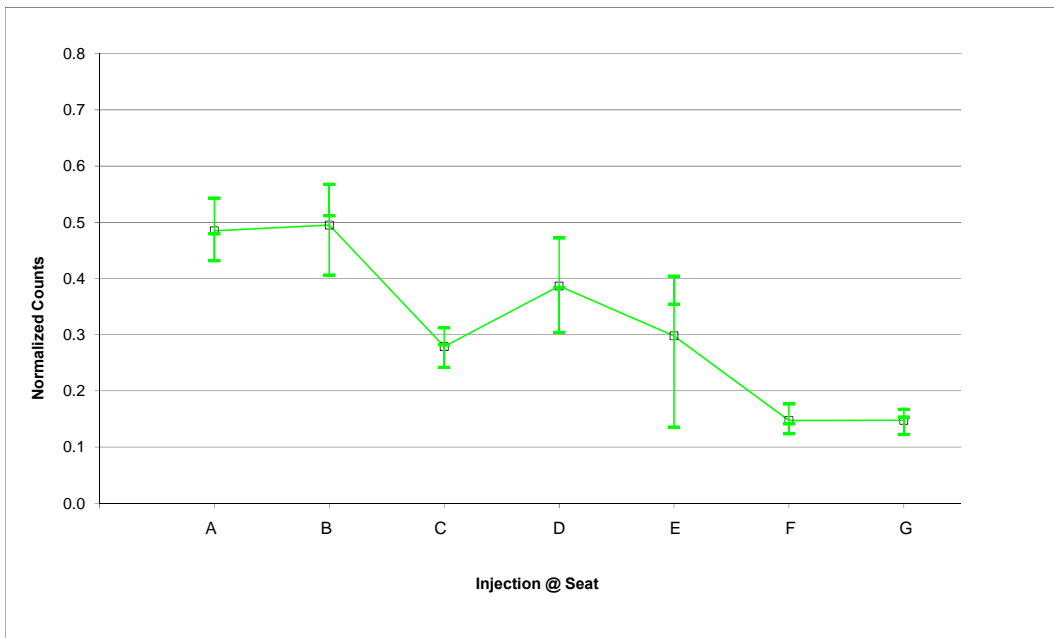


**Figure 4-14 Normalized Counts at Location VI - Row 2 (Injection in Row 2)**

### **4.3 Detection Times and Normalized Particle Counts in the Longitudinal Direction:**

As will be shown in Chapter 5, the best location out of the six locations considered for placing a sensor in the lateral direction is in Location II if only one sensor is to be used in a row.

Two locations were considered for powder release during the longitudinal investigation. The first one was in Row 2, while the second one was in Row 6.

#### ***4.3.1 Longitudinal Investigation – Injection in Row 2***

After choosing Location II as the best location in the lateral direction, powder was released separately in each seat of Row 2 and the particles were collected in Row 1, Row 2, Row 3, Row 4, and Row 5 in the same locations as Location II, but in different rows as shown in Figure 4-15. All locations were on the center line as shown in Figure 4-15 and their heights were the same as that of Location II. The location of the APS in each of row 1, 2, 3, 4, and 5 from the South Wall of the mockup cabin is 4 inches, 33 inches, 63 inches, 100 inches, and 133 inches, respectively.

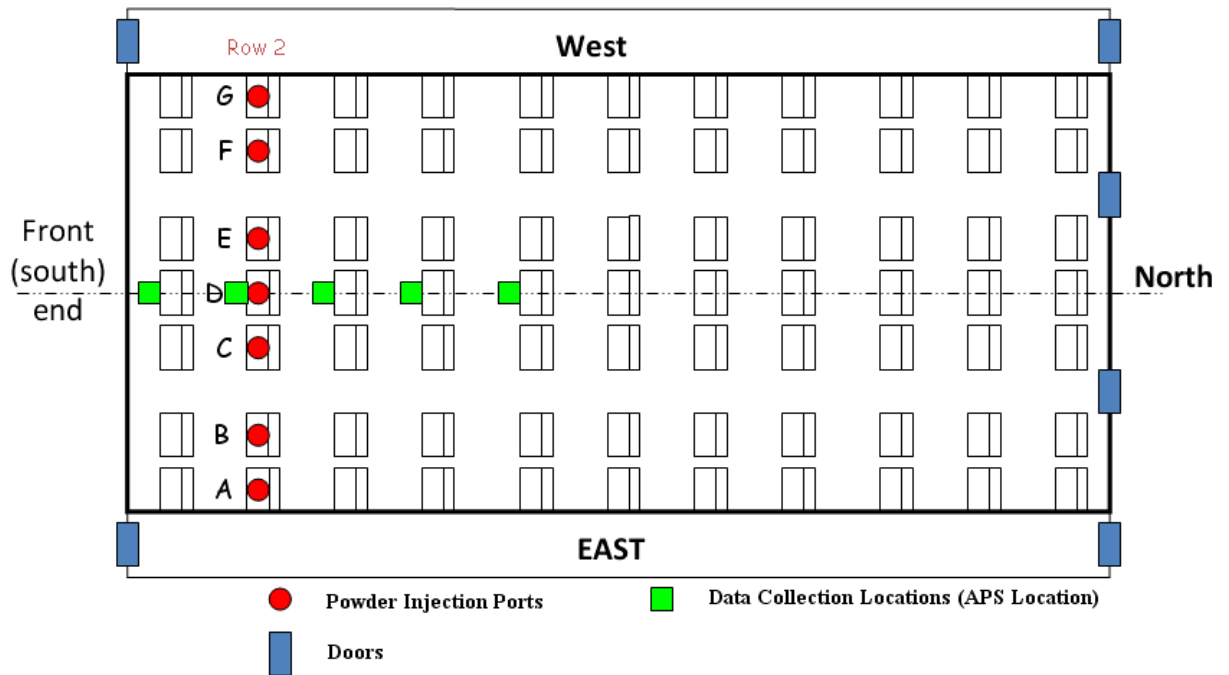


**Figure 4-15 Longitudinal Data Collection Locations when Injecting in Row 2**

The results of the detection times obtained at the 5 rows are shown in Figure 4-16, while the obtained normalized particle counts are shown in Figure 4-17.

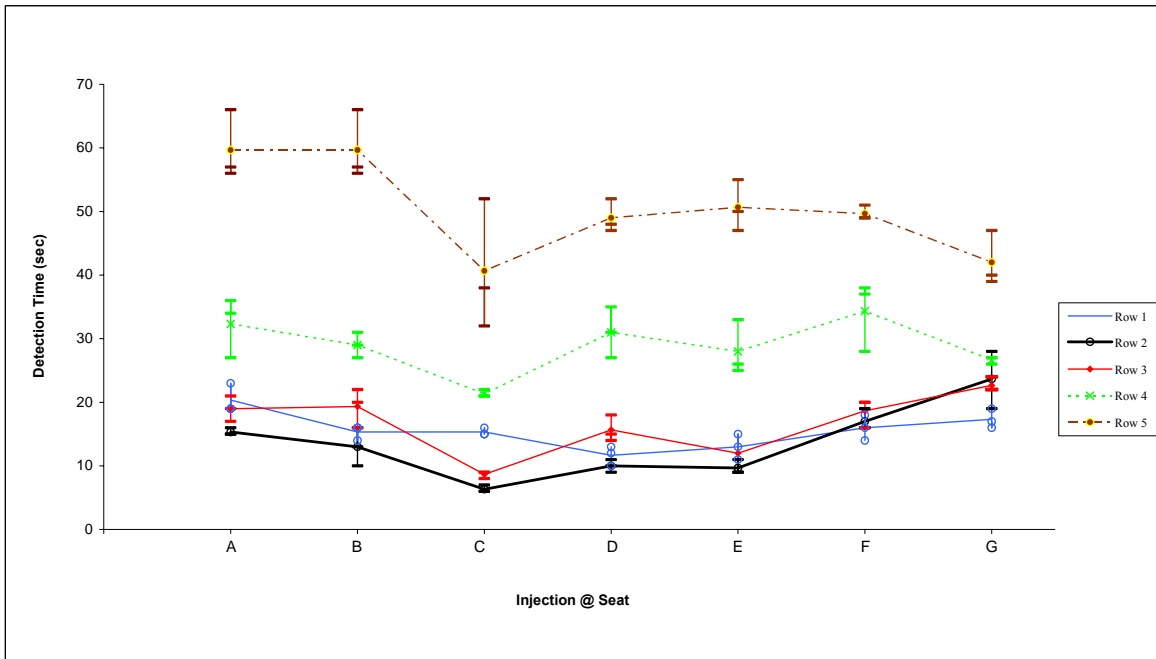


**Figure 4-16 Detection Times at Location II in Different Longitudinal Locations ( Injection in Row 2 )**

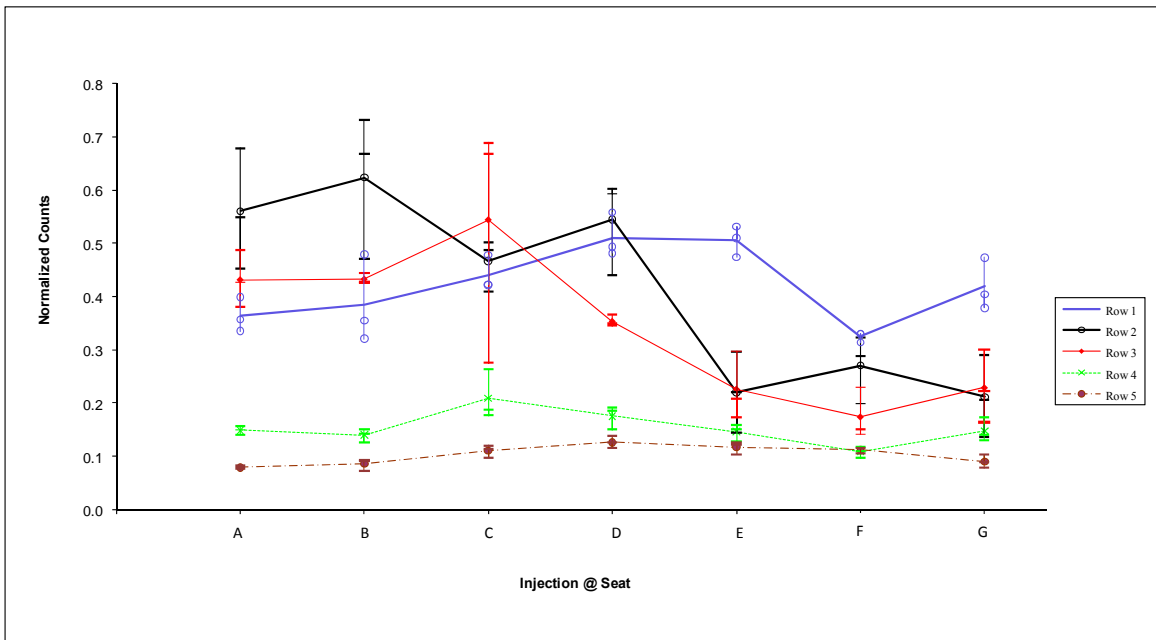


**Figure 4-17 Normalized Particle Counts at Location II in Different Longitudinal Locations (Injection in Row 2)**

### 4.3.2 Longitudinal Investigation – Injection in Row 6

The source was moved to the middle of the cabin (Row 6) to check whether the results will be similar to those obtained in the front section of the cabin when the release was in Row 2. Data were collected in rows 5, 6, and 7. In Chapter 5, it will be shown that a sensor at Location II can detect particulates when released in the same row of the sensor placement, in the back row or in the front row. Beyond that distance, there will be a risk at some points. For that, the particles here were collected in rows 5, 6, and 7 only as shown in Figure 4-18.

The results of the detection times and the normalized particle counts are shown in Figure 4-19 and Figure 4-20, respectively.

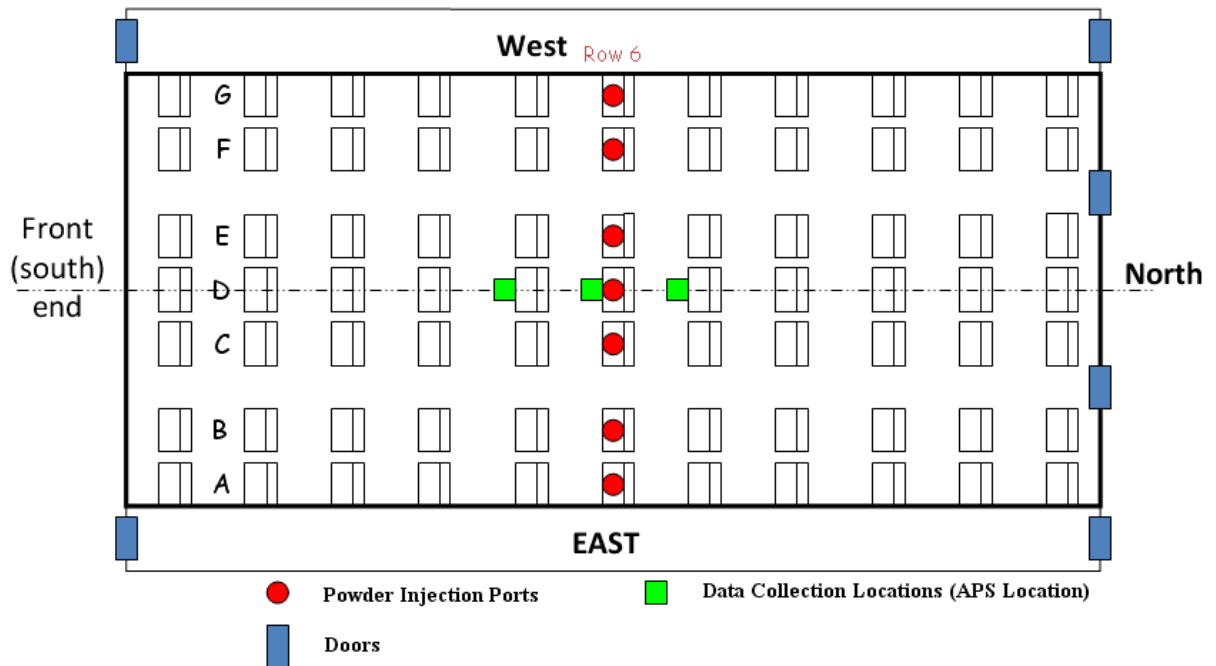
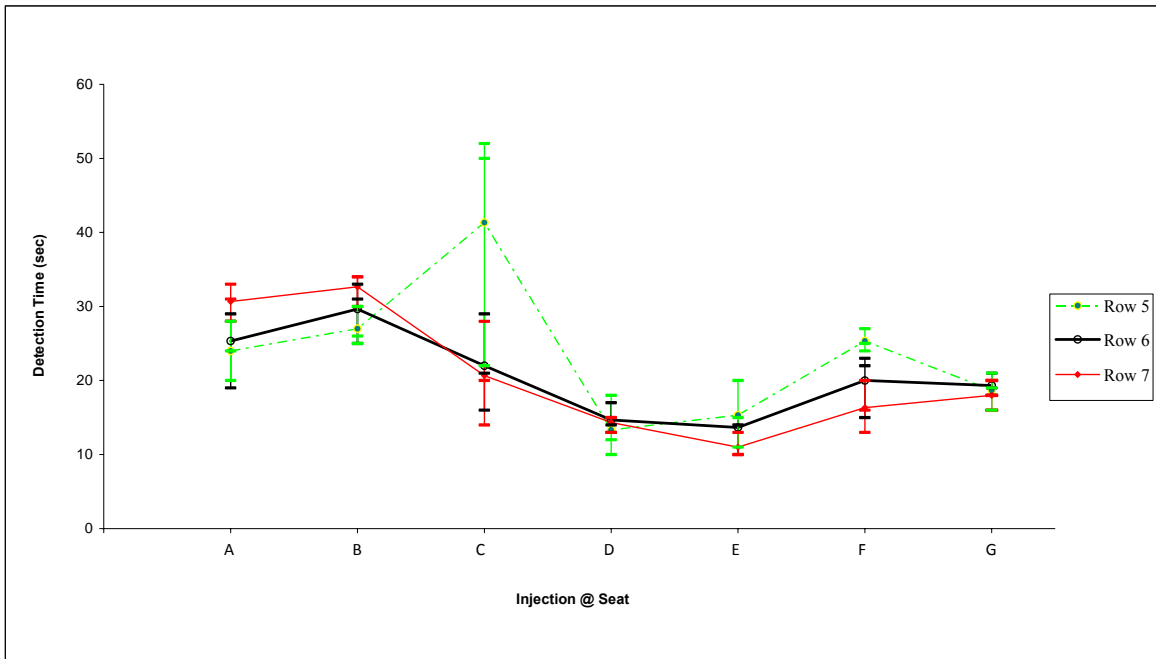
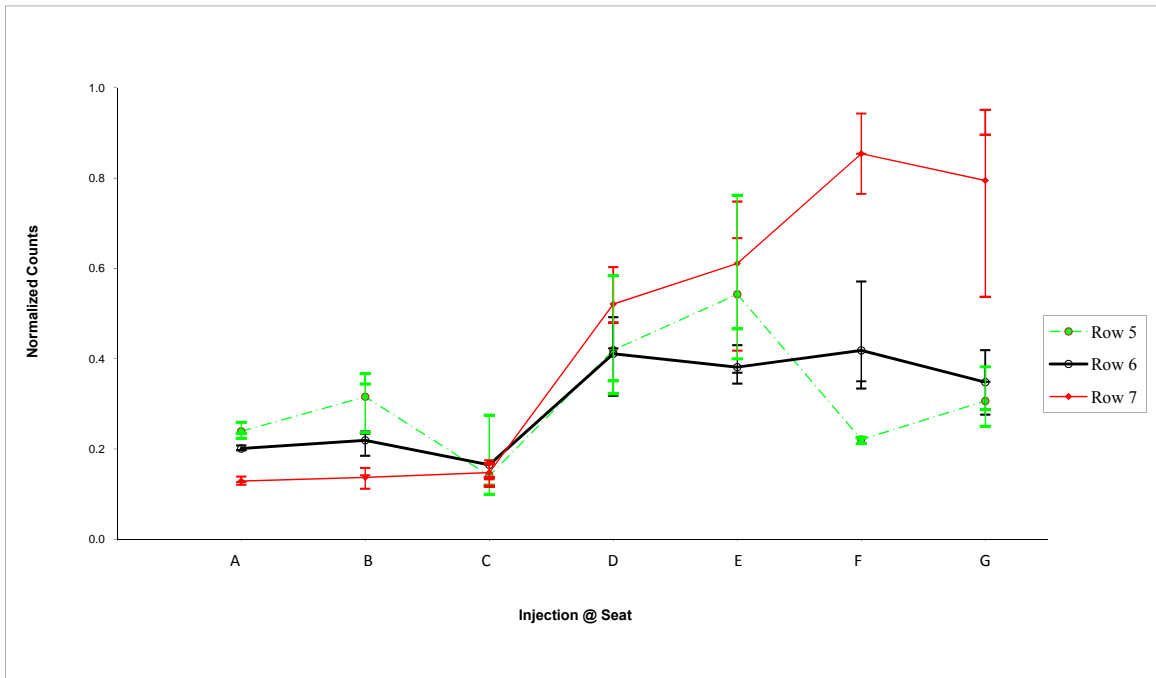


Figure 4-18 Longitudinal Data Collection Locations (Injecting in Row 6)



**Figure 4-19 Detection Times at Loc. II in Different Longitudinal Locations (Injection in Row 6)**



**Figure 4-20 Normalized Counts at Loc. II in Different Longitudinal Locations (Injection in Row 6)**

## **CHAPTER 5 - Data Analysis**

### **5.1 Analysis of the Data Collected in the Lateral Direction of Row 2**

The detection time results and the normalized particle counts collected in the lateral direction of Row 2 are shown Figure 4-3 along through Figure 4-14. To achieve an efficient comparison between all the considered locations in the lateral direction, all the results related to the detection time were combined in one chart and so were the results related to the normalized particle counts. Since we have three tests for every injection point in each location, the chart would be very messy if all points were plotted. For that, the average of the three tests was plotted.

The average detection times for all locations in the lateral direction of Row 2 are shown in Figure 5-1, while the average normalized particles counts for all locations in the lateral direction of Row 2 are shown in Figure 5-2.

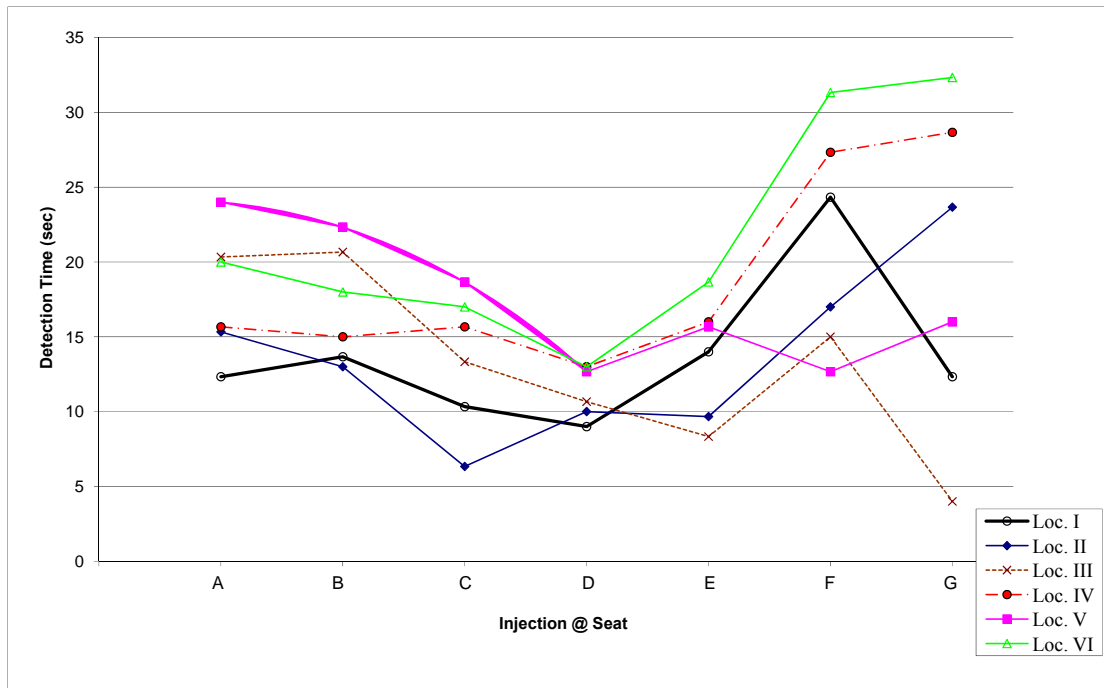


**Figure 5-1 Detection Times of the Data Collected in the Lateral Direction of Row 2 (Injection in Row 2)**

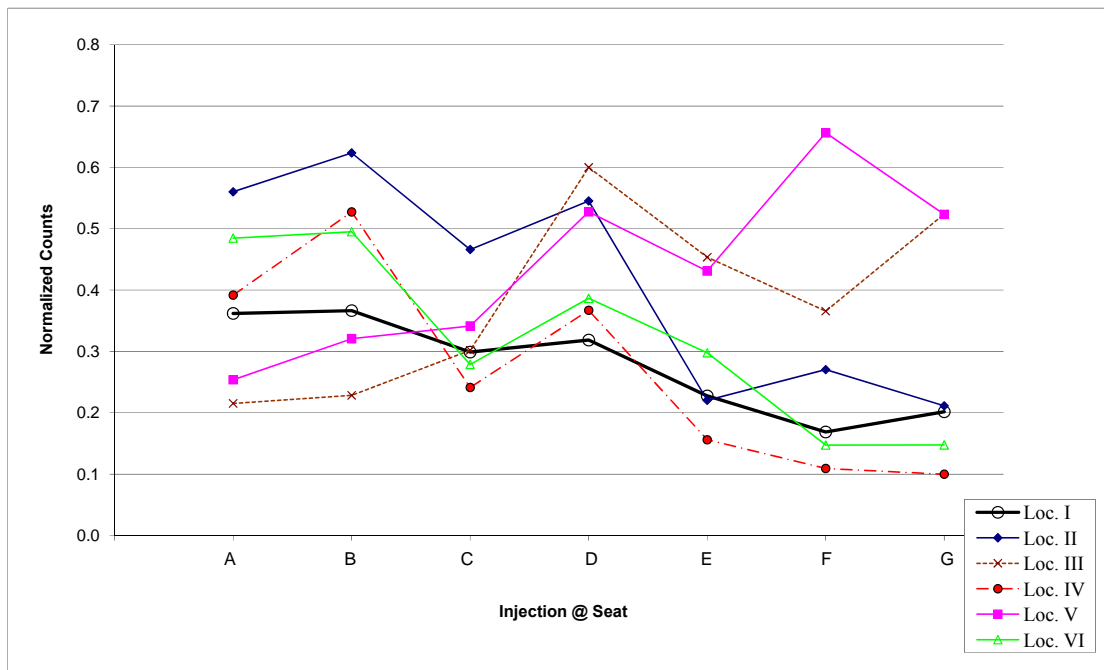


**Figure 5-2 Normalized Counts of the Data Collected in the Lateral Direction of Row 2 (Injection in Row 2)**

The results from Figure 5-1 show that Location IV and Location VI have almost the longest detection times, thus, these two locations are eliminated from further consideration as compared to other locations. Location I and Location II curves are the lowest two curves representing the lowest detection times when releasing in seats A, B, C, and D. It should be noted that at some points the results obtained in Location I are higher than those obtained in Location II and at other points are lower, but as mentioned before the results shown in Figure 5-1 and Figure 5-2 represent the averages of the three tests and thus any of the conducted tests might be lower or higher than the average. This can give a conclusion that at these points ( A to D ) Location I and Location II are at the same level of consideration. For the case of injection in seats E and F, Location II with Location III have the lowest detection times. For injection in seat G, Location III is classified as the lowest record followed by Location I, Location V and then Location II. Note that Location V can also be eliminated from the comparisons when compared with Location III, because the detection times of Location III are lower than those for Location V at all points except at F where both of them are very close to each other. Consequently, if one chooses locations based on the detection time only, Location I, Location II, and Location III are recommended.

Analyzing Figure 5-2, which summarizes the normalized total counts at each location in the lateral direction of Row 2, it is noticed that Location I has much lower counts than Location II, for all seats ( A through G ), and lower than Location III for injection in seats C, D, E, F, and G. As a result, Location I is eliminated from the comparison of the lateral locations. This elimination yields Location II and Location III as the best locations for placing a sensor inside the cabin in the lateral direction.

Therefore, if a combination of sensors is to be used, then Location II and Location III are recommended, while if only one location is to be selected, then Location II is to be recommended due to the following reasons:

- Location II has lower detection times when releasing particles in seats A through D (Figure 5-1) and higher particle counts when releasing in seats A through C.
- Location II and Location III have almost the same average detection times when releasing particles in seat E and seat F (Figure 5-1).
- Location II and Location III have almost the same average particle counts when releasing from seat D. (Figure 5-2)

There are some drawbacks for the selection of Location II over Location III, such as:

- Location III has a lower detection time only when releasing in seat G.
- Location III has a higher total particle counts when injecting in seats E, F, and G.

It should be noted that these drawbacks are due to the fact that Location III is just above the release point in seat G which can help in reducing the risks of these drawbacks. Suppose that an infected person sneezes while sitting in seat G, but instead of keeping his head straight, he turned it to the left. The situation here will be changed and the plume of sneezing may not go directly to Location III due to the high level of turbulence inside the cabin. The effect of the release direction will be investigated in "Appendix D".

It should be noted that if an "Action Sensor" is to be considered, then Location I, II, and III are recommended since the action sensor mainly depends on the detection time. On the other hand, if the interest is to employ a "Detection Sensor," then Location II and Location V are recommended to be used together since they have the highest counts compared to all other locations.

## **5.2 Analysis of the Data Collected in the Longitudinal Direction of the Cabin**

After the selection of Location II as the best location for placing a sensor in the lateral direction, the detection times and the particle counts acquired by this location at different rows in the longitudinal direction were investigated. The results were shown earlier in chapter 4 for the two cases. The first case was when the release of powder was in Row 2 and the second case was when the release was in Row 6.

### ***5.2.1 Injection in Row 2***

The primary goal of the longitudinal investigation was to figure out the maximum distance that should separate two consecutive sensors in the longitudinal direction. (Refer to Figure 4-15 for further details).

Starting with the results in Figure 4-16, which summarizes the detection times obtained at Location II in rows 1, 2, 3, 4, and 5, it is noticed that there is a strong overlapping in the results obtained for Row 1, Row 2, and Row 3. Row 5 curve is clearly out of the range for all seats (A through G) and Row 4 as well, except for the injection in seat G.

Therefore, when releasing particles in Row 2 we have almost the same results or at least acceptable results obtained in Row 1, 2, and 3. As a result, depending on the detection time only, a particulate release in a given location is well detected in the same row of release, in the front or the back rows as well.

Again, the normalized particle counts in Figure 4-17 show that the results of Row 4 and Row 5 are out of the range, except at point E, where they're close to the results of Row 2 and Row 3 results. Row 4 curve has another overlapping point at G. Rows 1, 2, and 3 overlap in the cases when releasing in seats A through D and beyond that Row 2 and Row 3 continue overlapping, while Row 1 records higher particle counts.

The same conclusion can be set for the normalized particle counts as in the case of the detection time which is that a sensor can be used to cover the same row it is placed in  $\pm 1$  row. (i.e. front and back rows)

### ***5.2.2 Injection in Row 6***

It was shown in "Section 5.2.1" that a sensor can be used to detect the particulates released in the same row of release  $\pm 1$  row. This result was based on the case of powder release in all seats of Row 2. To confirm the above result, the injection ports were moved into the middle section of the cabin (Row 6) and the particles were collected in Rows 5, 6, and 7 as shown in Figure 4-18. The results of the data collected were shown previously in Figure 4-19 and Figure 4-20.

All of the three rows overlap over each other, in the case of the detection time analysis, except for Row 5 at point C where it has two outliers. Again, in the case of the total particle counts, the three rows overlap for all seats from A to E. For the case of the release in F and G, Row 7 jumps to 0.8-0.9.

Ignoring the two outliers at point C in the detection time analysis, we can say that a sensor can be used to cover the row where it is placed and the front and the back rows as well.

### 5.2.3 Comparing the longitudinal results when injecting in Row 2 and in Row 6:

Combining the results of Rows 1, 2, and 3 when releasing the powder in Row 2 with the results of Row 5, 6, and 7 when releasing in Row 6 gives the two figures shown below (Figure 5-3 and Figure 5-4).

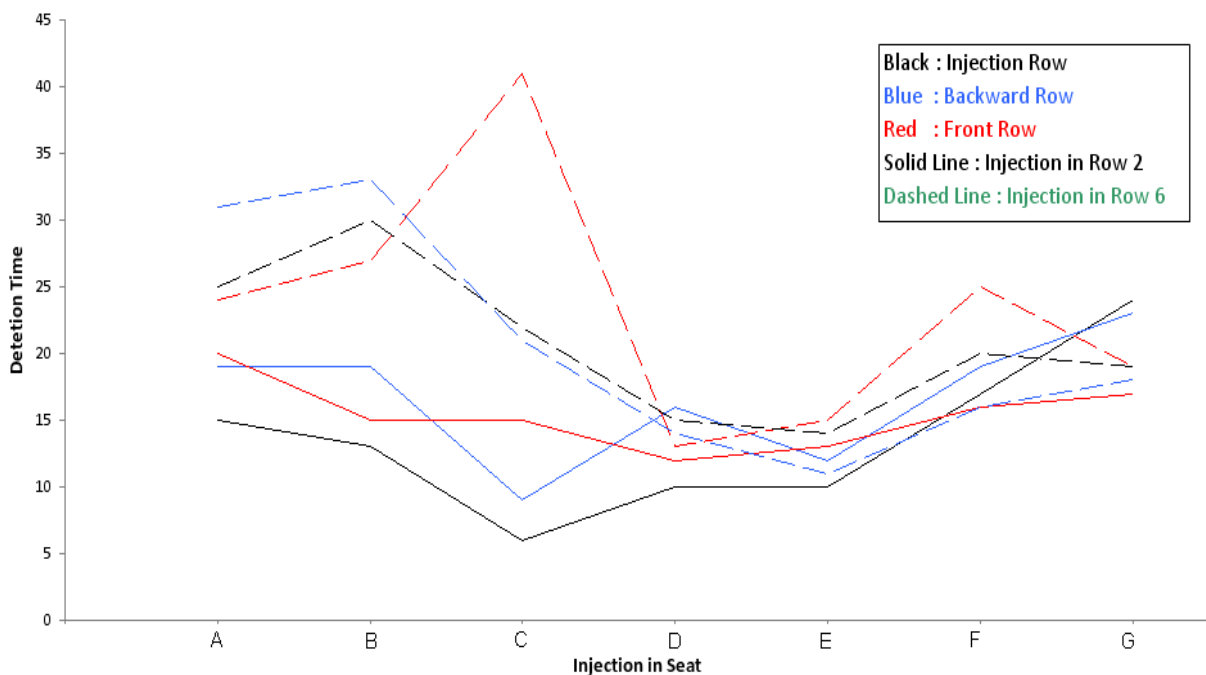


**Figure 5-3 Detection Times in Different Longitudinal Locations  
(Injecting in Row 2 & Row 6)**

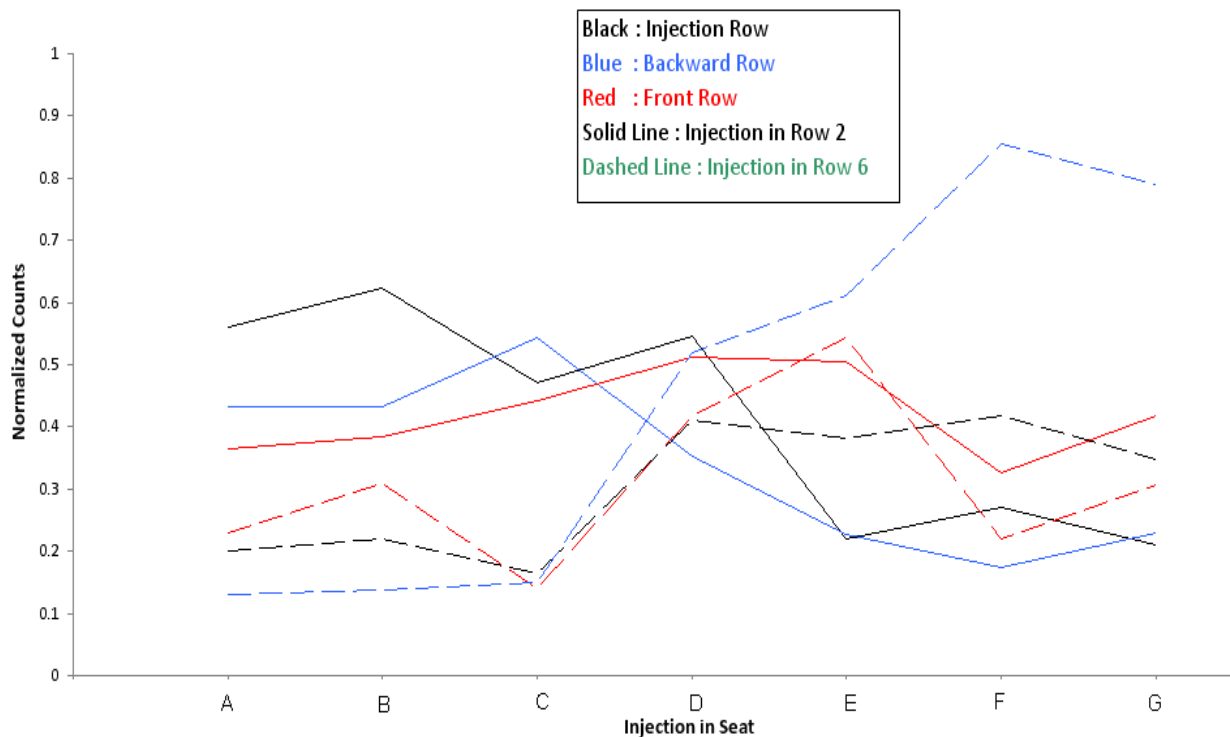


**Figure 5-4 Normalized Counts at Different Longitudinal Locations  
(Injection in Row 2 & Row 6)**

From the results of Figure 5-3, it can be concluded that when injecting in seats A, B, and C in the middle of the cabin it takes more time to reach Location II in Rows 5, 6, and 7 when compared to the results of the case when releasing in Row 2. From point D to G, all curves overlap.

The normalized particle counts chart (Figure 5-4) shows that more particles are detected in the front region of the cabin than in the middle region at Location II, when releasing powder in seats A, B, and C. The opposite is true when injection takes place in seats E, F, and G.

These results can be used to show that there are several swirls (eddies) inside the cabin in the longitudinal direction; A first guess would be that there is a clock-wise directed

swirl in the front section of the cabin as shown in Figure 5-5. This swirl breaks in the middle section of the cabin since more particles were detected in the middle section in Location II when injecting in seats E, F, and G. Additional evidence for this result is that more particles were detected in Row 7 than in Row 5 and 6 when the particle releases were in seats E, F, and G.

Another conclusion might be that there is a counterclockwise directed swirl in the middle of the cabin. The clockwise swirl in the front of the cabin was based on the fact that more particles moved to Location II in Row 1, 2, and 3 when releasing in seats A, B, C and D of Row 2 than when releasing in seats E, F and G of the same row. The counterclockwise directed swirl in the middle of the cabin was based on the fact that more particles moved to Location II in Row 5, 6, and 7 when releasing in seats D, E, F, and G of Row 6 than when releasing in seats A, B, and C.

The fact that more particles were collected at Location II in Row 7 than in Row 6 and in Row 5, when releasing particles in seats E, F, and G of Row 6, gives more evidence to support towards the first guess which is that the front clockwise directed swirl breaks in the region around Row 7.

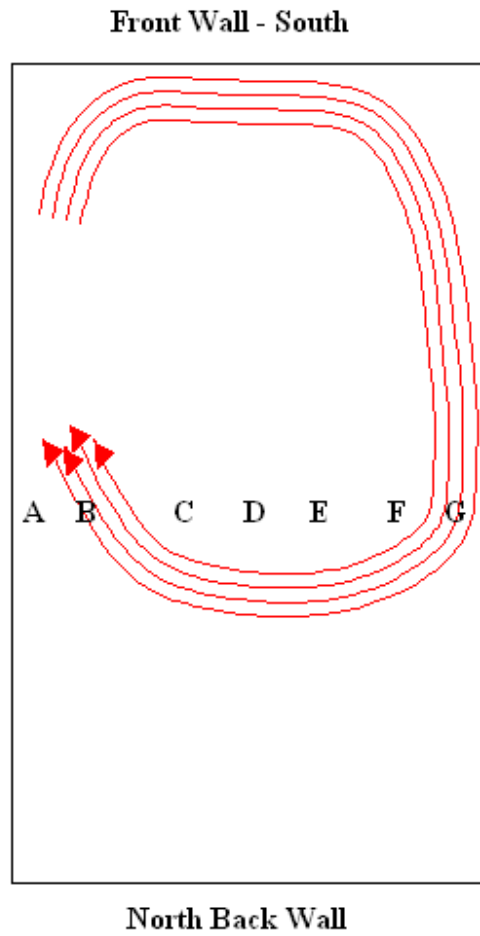


**Figure 5-5 Sketch of the Assumed Swirl in the Front part of the Cabin**

### **5.3 Uncertainty Analysis**

An uncertainty analysis for the detection time results and the normalized particle counts was performed for both the lateral and the longitudinal cases. The results were then combined with other uncertainties such as that of the APS unit itself and the uncertainty of the powder injection system.

### 5.3.1 Uncertainty Analysis of the Results Collected in the Lateral Locations (Row 2)

In each location of the six lateral locations in Row 2, we have seven release points (A → G). The release of powder in each seat was repeated 3 times giving the rise of a mean value and a standard deviation for every release point in each location. These values were used to calculate the standard error for each location. The standard error of the mean was determined using equation (5.1), which was defined as:

$$S.E = \pm t_{95\%} \times \frac{\sigma}{\sqrt{N}} \quad (5.1)$$

where - S.E is the standard error of the mean

-  $\sigma$  is the standard deviation

- N is the number of samples (number of tests repeated for every release point)

and -  $t_{95\%}$  is defined as the 95% confidence level factor. For a Gaussian distribution there is a 5% probability that the true value is away from the mean. The  $t_{95\%}$  depends on the degree of freedom of the samples which in turn depends on the sample size considered.

To compare the overall result of each location with the other locations, it is better to define an overall standard error for each location by using the pooling method (Gibbons and Coleman, 2001). The pooling method, for independent events, is to put all the results obtained from every release point in A through G at a given location in one group then to find the standard deviation, the standard error, and the relative uncertainty of that group. The standard deviation for each location is found by combining all the standard deviations of the results of A through G and it is calculated by using equation (5.2) which was defined as:

$$\sigma_{Loc.} = \sqrt{\sigma_A^2 + \sigma_B^2 + \sigma_C^2 + \sigma_D^2 + \sigma_E^2 + \sigma_F^2 + \sigma_G^2} \quad (5.2)$$

After defining the standard deviation for each location, the standard error is calculated by using equation (5.1), but  $\sigma$  is replaced with  $\sigma_{Loc.}$  and N represents the total number of all tests related to a given location. Thus, N is equal to 21 since we have 7 release

points with 3 tests in each point. The  $t_{95\%}$  for a sample size of 21 samples is 2.086 (Gibbons and Coleman, 2001).

Hoffman and Gardner (1983) mentioned that in the pooling method for the independent events the mean of the total group will be the algebraic summation of the individual means of each group contained in the pool, while the standard deviation is the same as was defined in equation (5.2).

The relative uncertainty, which is a measure of variability, is defined as the ratio of the standard error to the mean.

$$u = \frac{S.E}{MEAN} \quad (5.3)$$

where

- u is the relative uncertainty
- S.E. is the standard error

Equation (5.1) is used to compute the standard errors for each release point at each location in the lateral direction. The value of the  $t_{95\%}$  is 4.303 since the sample size is 3 and the degree of freedom of the samples is 2. The results of the relative uncertainties for the detection times and for the normalized counts, for the locations in the lateral direction of row 2, are shown in Table 5-1 and in Table 5-2, respectively.

**Table 5-1 Relative uncertainties of the detection times in the lateral direction of row 2  
(In seconds)**

	A	B	C	D	E	F	G
Loc. I	0.31	0.28	0.27	0.00	0.61	0.51	0.23
Loc. II	0.09	0.57	0.22	0.25	0.29	0.25	0.47
Loc. III	0.07	0.06	0.11	0.13	0.17	0.57	0.62
Loc. IV	0.18	0.44	0.24	0.19	0.27	0.62	0.20
Loc. V	0.10	0.13	0.20	0.29	0.24	0.11	0.00
Loc. VI	0.45	0.00	0.15	0.19	0.44	0.39	0.25

The relative uncertainty of the normalized counts is computed by combining the relative uncertainty of the test itself and the relative uncertainty of the data collected at the source.

$$\text{Normalized Count} = \frac{\text{Test Total Counts}}{\text{Total Counts at the Source}}$$

$$u_{\text{Normalized-Count}}^2 = u_{\text{test}}^2 + u_{\text{source}}^2$$

where  $u_{\text{test}}$  is the relative uncertainty of each test and  $u_{\text{source}}$  is the relative uncertainty of the source.

The relative uncertainty of the data collected near the source is calculated by considering the results obtained in 'section 4.1.1'. Since 9 samples were collected near the source, a value of  $\pm 2.306$  was used for the  $t_{95\%}$  and hence,  $u_{\text{source}}$  was found to be  $\pm 0.16$  ( $\pm 16\%$ ).

**Table 5-2 Relative uncertainties of the normalized particle count results collected in the lateral direction of row 2**

	A	B	C	D	E	F	G
Loc. I	0.24	0.43	0.68	0.28	0.47	0.46	0.23
Loc. II	0.50	0.44	0.26	0.41	0.34	0.32	0.31
Loc. III	0.39	0.26	0.17	0.40	0.32	0.42	0.16
Loc. IV	0.21	0.34	0.18	0.32	0.17	0.27	0.16
Loc. V	0.37	0.23	0.25	0.46	0.17	0.17	0.19
Loc. VI	0.33	0.44	0.35	0.56	0.60	0.48	0.41

Table 5-3 and Table 5-4 show the total standard errors and the total relative uncertainty for the detection times and the normalized counts results for all locations in the lateral direction of Row 2. Since the sample size in this case is 21,  $t_{95\%}$  is  $\pm 2.086$ . Similarly,  $u_{\text{source}}$  was considered when determining the relative uncertainty of the normalized counts.

**Table 5-3 Total Standard Errors and Total Relative Uncertainties of the Detection Time Results Collected in the Lateral Direction (seconds)**

	Total Standard Error	Relative Uncertainty
Loc. I	3.10	0.22
Loc. II	2.70	0.20
Loc. III	1.74	0.13
Loc. IV	3.71	0.19
Loc. V	1.40	0.08
Loc. VI	4.30	0.20

**Table 5-4 Total Standard Errors and Total Relative Uncertainties of the Normalized Counts Results Collected in the Lateral Direction**

	Total Standard Error	Relative Uncertainty
Loc. I	0.16	0.25
Loc. II	0.19	0.31
Loc. III	0.17	0.25
Loc. IV	0.18	0.41
Loc. V	0.16	0.19
Loc. VI	0.18	0.32

In section 5.1, Location II and Location III were compared with each other depending on the mean value only and Location II was more acceptable than Location III, and thus, was selected as a representative location for placing a sensor in the lateral direction. If Location II had more variability than Location III, then we would have needed to carry out more investigations to check the decision that was taken. Since the relative uncertainty is a direct measure of the level of variability, we can say that Location II and Location III had approximately the same level of variability, because Location II had a relative uncertainty of  $\pm 0.2$  for ‘Detection Time Analysis’ (Table5-3) and  $\pm 0.31$  for the normalized counts (Table5-4) where as they were  $\pm 0.13$  for the detection time and  $\pm 0.25$  for the normalized counts of Location III.

### ***5.3.2 Uncertainty Analysis of the Results Collected in the Longitudinal Locations***

#### ***5.3.2.1 Injection in Row 2***

The same principles that were used in the lateral analysis were used here in the calculations of the standard errors, the total standard deviation of each location, the total standard error, and the relative uncertainty.

Equation (5-1) was used again here to estimate the standard errors of the detection time results and the normalized counts, while equation (5-2) and equation (5-3) were used to calculate the relative uncertainties. The relative uncertainty of the source was taken in account for the normalized counts relative uncertainty analysis. The relative uncertainties results are shown in Table 5-5 for the detection times and in Table 5-6 for the normalized particle counts.

**Table 5-5 Total Standard Errors and Total Relative Uncertainties of the Detection Time Results Collected in the Longitudinal Locations (Injection in Row 2) (seconds)**

	Total Standard Error	Relative Uncertainty
Row 1	2	0.13
Row 2	2.7	0.19
Row 3	2.4	0.14
Row 4	4.4	0.15
Row 5	6.6	0.13

**Table 5-6 Total Standard Errors and Total Relative Uncertainties of the Normalized Counts Results Collected in the Longitudinal Locations (Injection in Row 2)**

	Total Standard Error	Relative Uncertainty
Row 1	0.16	0.21
Row 2	0.18	0.31
Row 3	0.19	0.38
Row 4	0.16	0.24
Row 5	0.15	0.20

From the detection time results (Table 5-5), the relative uncertainties are almost the same. The normalized particle counts uncertainties (Table 5-6) ranged between  $\pm 0.20$  and  $\pm 0.38$ .

### **5.3.2.2 Injection in Row 6**

Similarly as in “section 5.3.2.1”, the standard errors and the relative uncertainties were calculated for the case when releasing powder in Row 6. The results are shown in Table 5-7 and Table 5-8.

The two tables show that Row 5 has a higher level of variability than Row 6 and Row 7 when injection was in Row 6.

**Table 5-7 Total Standard Errors and Total Relative Uncertainties of the Detection Time Results Collected in the Longitudinal Locations (Injection in Row 6) (seconds)**

	Total Standard Error	Relative Uncertainty
Row 5	8.50	0.36
Row 6	4.90	0.24
Row 7	4.11	0.20

**Table 5-8 Total Standard Errors and Total Relative Uncertain of the Normalized Counts Results Collected in the Longitudinal Locations (Injection in Row 6)**

	Total Standard Error	Relative Uncertainty
Row 5	0.19	0.41
Row 6	0.18	0.35
Row 7	0.20	0.35

Comparing the relative uncertainties of rows 5, 6, and 7 with rows 1, 2, and 3 for both cases, the detections times and the normalized counts, it is clear that the middle section of the cabin has a higher level of variability than the front section. This result might be an indication that there is a higher level of disturbance in the middle of the cabin.

### ***5.3.3 Uncertainty of the Powder Samples Used in the Tests***

In addition to the uncertainties obtained in the data collection during the tests, there is another type of variability associated with the tests. This type of variability is the variability of the powder samples used. To better understand this level of variability, five samples were weighed (Table 3-2) and the average weight was found to be 41.3 mg with a standard deviation of 1.8 mg. (section 3.3.1).

The standard error of the average weight was calculated by using equation (5.1)

$$\begin{aligned}
 S.E_p &= \pm t_{95\%} \times \frac{\sigma}{\sqrt{N}} \\
 &= \pm 2.776 \times \frac{1.8}{\sqrt{5}} \\
 &= \pm 2.24 \text{ mg}
 \end{aligned}$$

Therefore, the relative uncertainty is

$$u_p = \frac{\text{S.E}_p}{\text{mean}} = \pm 0.054 = \pm 5.4\%$$

### ***5.3.4 Total Relative Uncertainty***

A total relative uncertainty calculation for the whole experiment would be more efficient as it will allow us to compare the uncertainty of the final results and decisions.

The total relative uncertainty combines the uncertainty of all random variables that occurred during the tests with the biased uncertainty. The bias uncertainty is represented by the APS unit uncertainty which was estimated by the manufacturer to have a value of  $\pm 10\%$ . The uncertainties of the other variables include the uncertainty of the powder samples and the uncertainty of the data collected.

Therefore, the total relative uncertainty can be represented by equation (5.4) as:

$$u_T = \sqrt{u_p^2 + u_c^2 + u_{APS}^2} \quad (5.4)$$

where

- $u_T$  is the total relative uncertainty of the experiments
- $u_p$  is the relative uncertainty of powder samples
- $u_c$  is the relative uncertainty of the data collected
- $u_{APS}$  is the APS uncertainty (bias uncertainty) which is  $\pm 10\%$

Thus, the total relative uncertainty of the data collected in the lateral locations is as shown in Table 5-9.

**Table 5-9 Total Relative Uncertainties of the Data Collected in the Lateral Locations**

**(Row 2)**

Location		Loc. I	Loc. II	Loc. III	Loc. IV	Loc. V	Loc. VI
Total Relative Uncertainty	Detection Time	0.25	0.23	0.17	0.22	0.14	0.23
	Normalized Counts	0.27	0.33	0.27	0.43	0.22	0.34

Table 5-10 shows the relative uncertainties when combining the uncertainties of the two criteria, the "Detection Time" and the "Normalized Counts", together using equation (5.5).

$$u_{combined}^2 = u_{Detection-time}^2 + u_{Normalized-Counts}^2 \quad (5.5)$$

**Table 5-10 Combined Total Uncertainties of the Data Collected in the Lateral Direction**

**(Row 2)**

Location	Loc. I	Loc. II	Loc. III	Loc. IV	Loc. V	Loc. VI
Total Relative Uncertainty	0.37	0.40	0.32	0.48	0.26	0.41

Therefore, from the above two tables ( 5-9 and 5-10 ), we conclude that the relative uncertainties of the locations in the lateral direction of row 2 range between ±26% to ±48%.

For the data collected in the longitudinal direction, both cases of injection in Row 2 and in Row 6, the total relative uncertainties were calculated and are shown in Table 5-11 and Table 5-12.

**Table 5-11 Combined Total Relative Uncertainties of the Data Collected in the Longitudinal Locations (Injection in Row 2)**

Row	1	2	3	4	5
Total Uncertainty	0.27	0.38	0.42	0.30	0.26

**Table 5-12 Combined Total Uncertainties of the Data Collected in Longitudinal Locations  
(Injection in Row 6)**

Row	5	6	7
Total Uncertainty	0.56	0.44	0.42

The combined total relative uncertainties in the front rows and in the middle rows of the cabin ranged between  $\pm 26\%$  to  $\pm 56\%$ .

The above uncertainty calculations yielded  $\pm 56\%$  relative uncertainty which was in the middle section of the cabin. This is mainly due to the small sample sizes considered and due to the high disturbance inside the cabin. Also a value of  $\pm 10\%$  for the APS affects the results. If we want to minimize the uncertainty level, enough tests should be conducted in order to reasonably represent each location with low variability levels. It should be mentioned that due to some of the assumptions in the “root mean squared” method, this method may not be the best method to use for the calculation of the relative uncertainty in this project.

## **CHAPTER 6 - Instruments and Cabin Verification**

This chapter describes the various tests and procedures that were followed and performed, to ensure accurate results and presents the results of these tests.

### **6.1 APS Verification**

In order for the tests measurements to be accurate and precise, the reliability of the measurements taken by the APS unit was investigated by conducting comparison tests. Two units, of the same manufacturer, were already available at the Airliner Cabin Environment Research (ACER) laboratory. In order to widen the range of accuracy, a third unit was borrowed from another department and it was included in the comparison tests. For familiarity reasons, the three units were named as: Porsche, Mercedes, and Bio. The first two were those units that were already available in the laboratory, while the Bio was the one that was borrowed.

The comparison tests were conducted in the 11-row mockup cabin at two different locations. Figure 6-1 shows these locations and Figure 6-2 shows the general arrangement of the units in each location. The distance between the nozzles (orifices) of the APS units was kept as minimum as possible by aligning the units 90 degrees with respect to each other. Three tests were conducted in each location and the APS units were rotated during each test (each unit location was replaced by the other unit) to make sure that the alignment of the APS units had no effects on the results obtained.

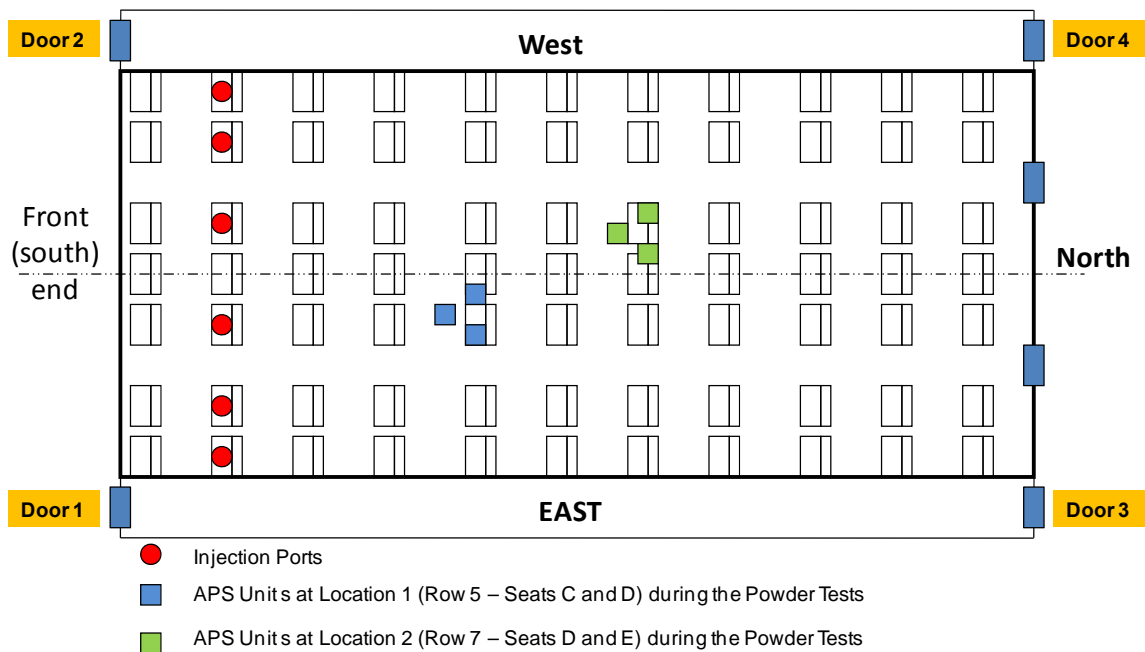


**Figure 6-1 Comparison Tests Setup inside the Cabin**

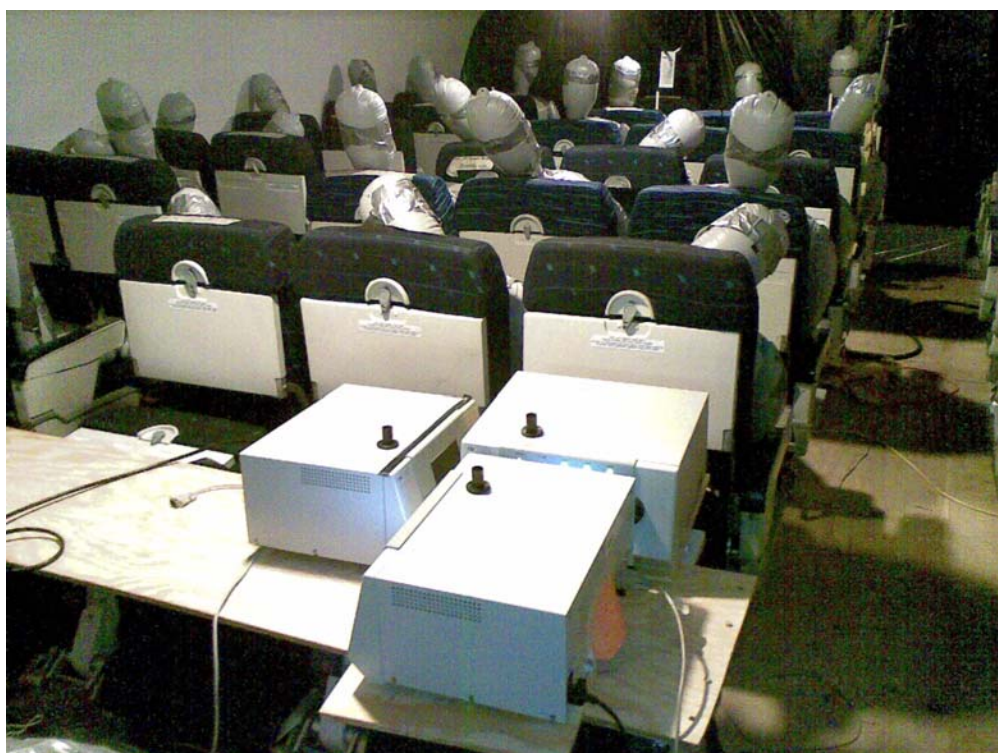


**Figure 6-2 APS Units Alignment in the Cabin Mockup**

During each test, smoke was injected continuously in Row 2 over the whole period of the test, which was 15 minutes, as shown in Figure 6-1. The smoke was released in all seats at the same time, except the middle seat which did not have a smoke release port. The supply air temperature, into the cabin main supply duct, was maintained at 15.5 °C (60°F) with 39.64 m<sup>3</sup>/min (1400 cfm) airflow rate.

The total number of particles collected by each unit in each location during each test is plotted in Figure 6-3. The results obtained in Location 2 are plotted in a separate figure as shown in Figure 6-4, because they are much lower than those obtained in Location 1 and they cannot be investigated using Figure 6-3.

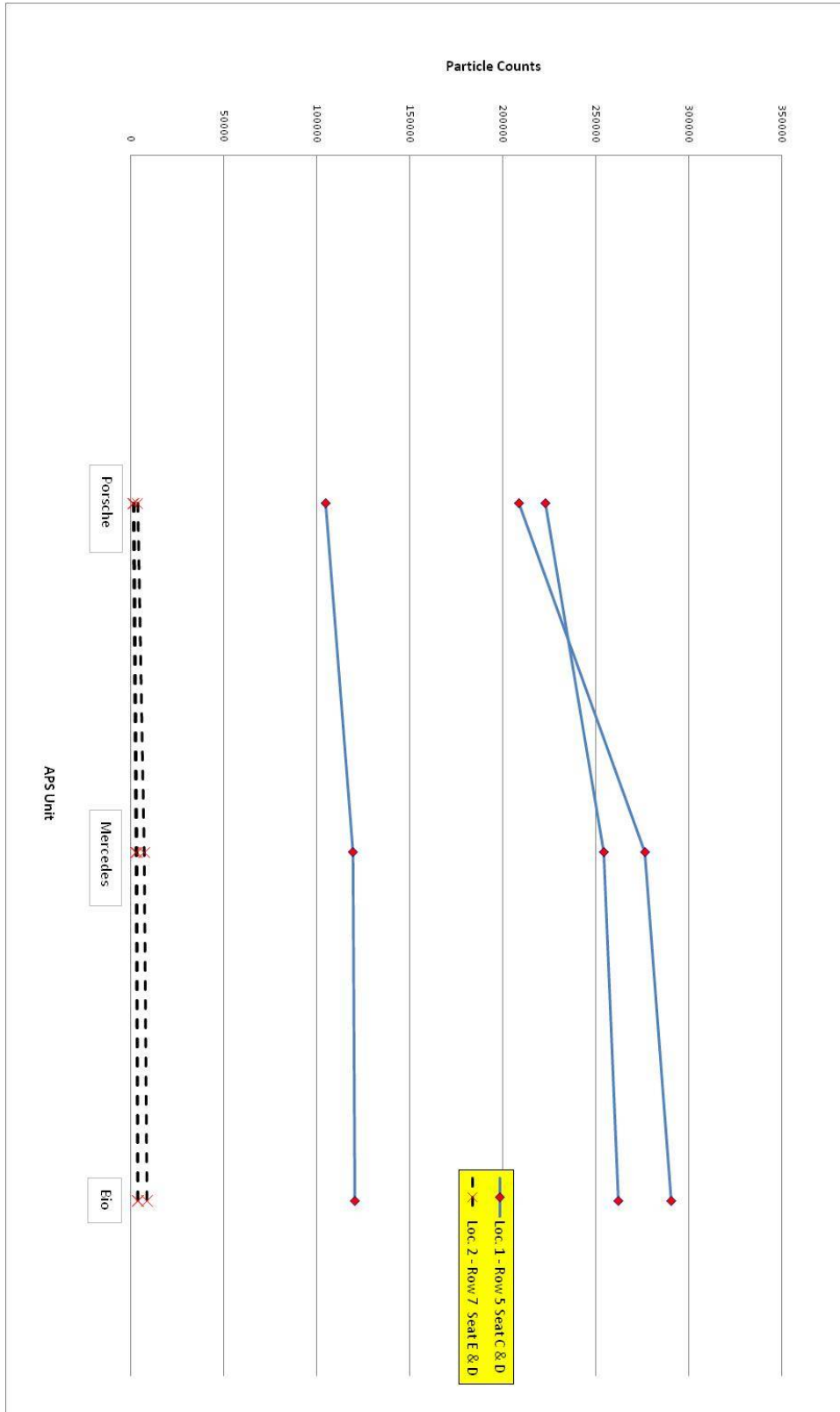


**Figure 6-3 APS Comparison Results - Location 1 and Location 2**

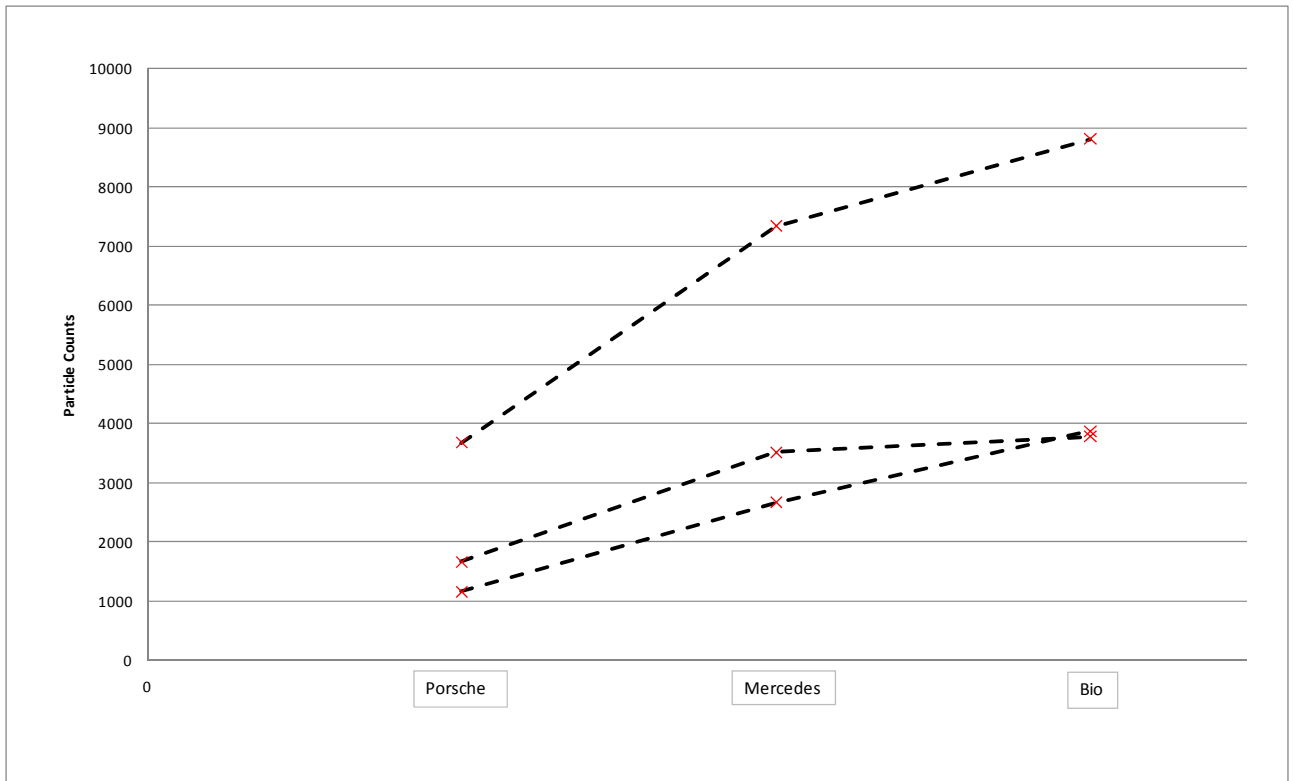


**Figure 6-4 APS Comparison Results - Location 2 only**

It is clear from Figure 6-3 and Figure 6-4 that the "Porsche" unit detects less number of particles than the "Mercedes" and "Bio", although the "Porsche" was newly calibrated.

Figures 6-5, 6-6, and 6-7 show the average transient particles exposure of the three tests by each unit at Location 1 for different particle sizes. The plots were averaged over 15 seconds.

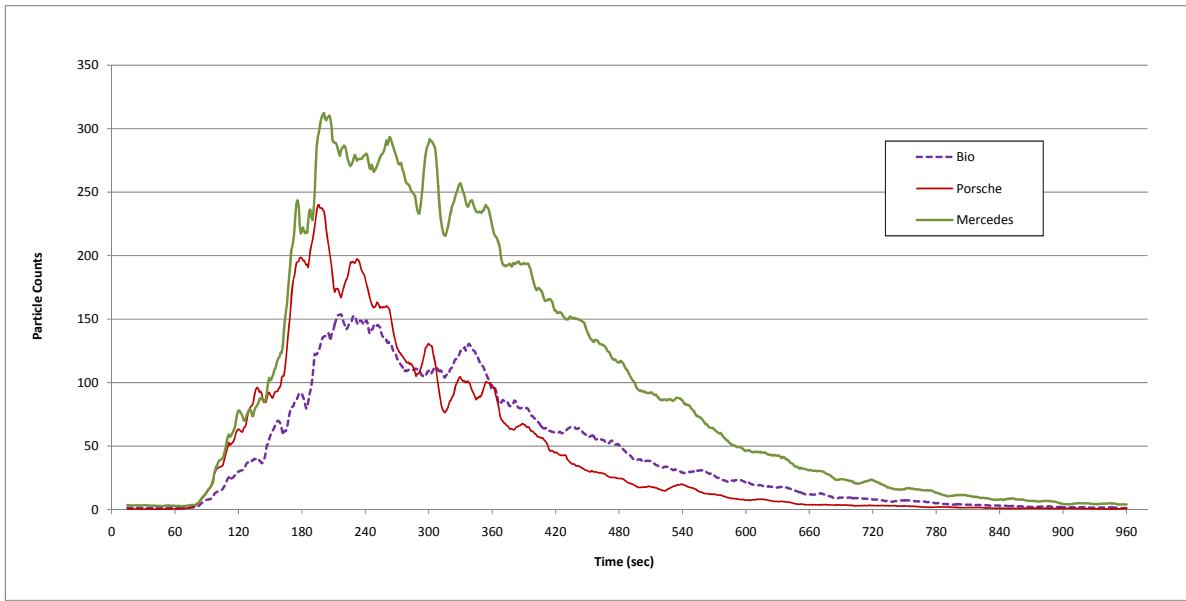


**Figure 6-5 APS Comparison Results -  $d < 0.5 \mu\text{m}$**

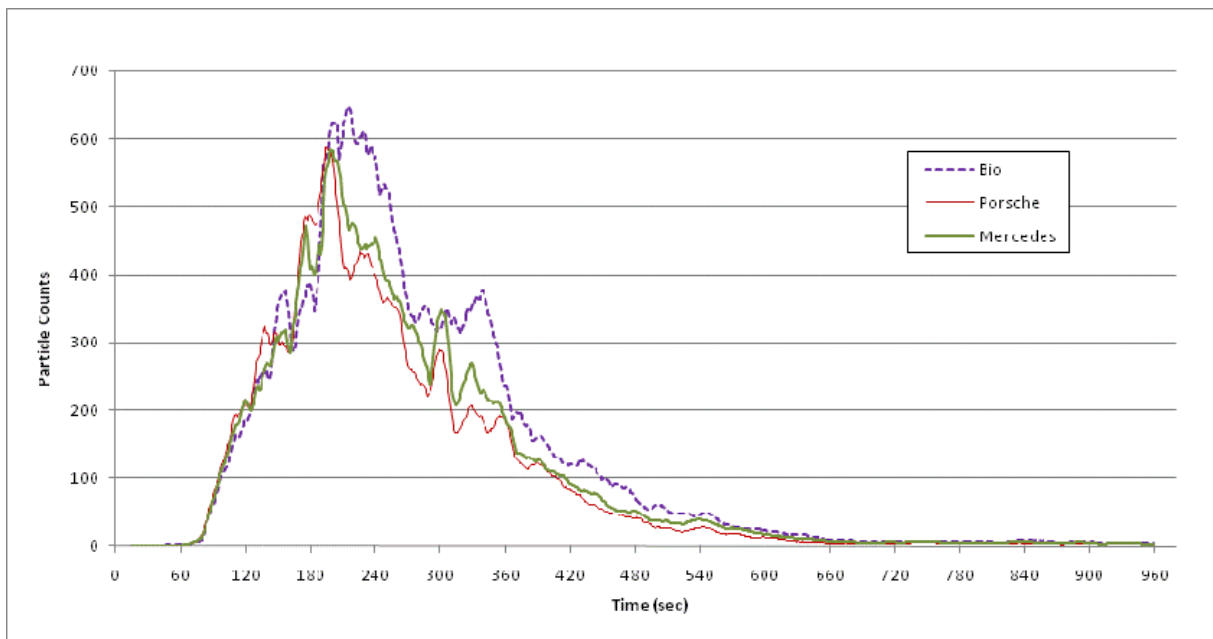


**Figure 6-6 APS Comparison Results -  $0.5 \mu\text{m} < d < 1 \mu\text{m}$**

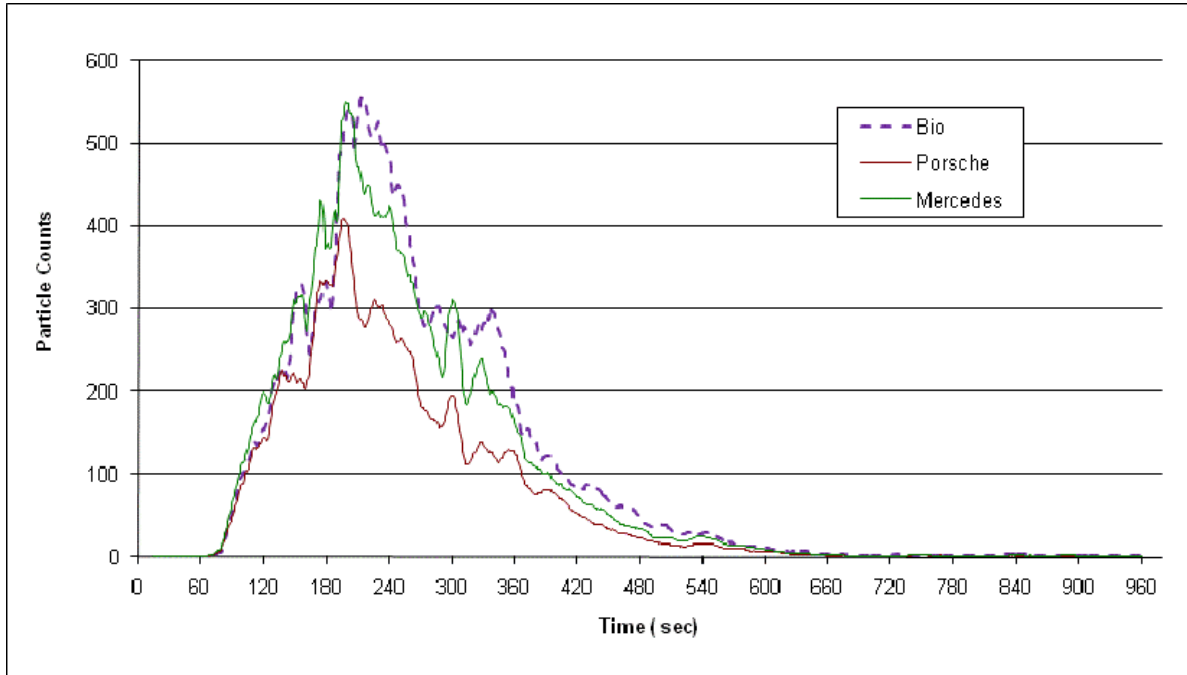


**Figure 6-7 APS Comparison Results -  $1\mu\text{m} < d < 5\mu\text{m}$**

Figure 6-5 ( $d < 0.5 \mu\text{m}$ ) shows that none of the 3 units matches. This is due to the efficiency of the APS units which, as per the manufacturer, decreases as the collected particles become smaller. The APS units have higher discrepancy and variability as the particles diameter becomes smaller and smaller and can reach up to  $\pm 67\%$  variability with particles as small as  $0.2 \mu\text{m}$ . In order to prevent such discrepancy, which can increase the uncertainty of the tests, particles with diameter less than  $0.5 \mu\text{m}$  were not considered in the analysis.

Figure 6-6 shows that the 3 units are approximately matching for the specified range of particle size. Again, Figure 6-7 confirms the results of Figures 6-3 and 6-4 which is that the "Porsche" unit collects lower number of particles than the other two units.

Recommendations:

- i. Use the "Mercedes" unit in the investigation tests since it highly matched with the "Bio" unit.
- ii. Check the "Porsche" unit as per TSI recommendations as follows:
  - a. Check the flow rates attained by the pumps of the APS units.
  - b. Check and clean the nozzles of the units as they are very sensitive and any particle accumulation inside them can alter the results collected.

The flow rate of the "Porsche" and "Mercedes" was checked at two different locations. These two locations as identified by the instruction manual of the device are named as "Sample" and "Sheath". Measuring the flow rate in (l/min) at these two different locations and taking the total yields the results shown in Table 6-1. It was found that the two units attain approximately the same flow rate and there was not that much difference between them. (1.25% difference)

**Table 6-1 Flow Rate ( l/min ) Comparison between the Two APS Units**

	Sample		Sheath		Total	
	Mercedes	Porsche	Mercedes	Porsche	Mercedes	Porsche
	0.898	0.901	3.73	3.685	4.628	4.586
	0.895	0.905	3.735	3.669	4.63	4.574
	0.9	0.907	3.717	3.665	4.617	4.572
	0.899	0.906	3.73	3.651	4.629	4.557
	0.897	0.912	3.737	3.651	4.634	4.563
	0.898	0.914	3.726	3.65	4.624	4.564
	0.935	0.904	3.687	3.666	4.622	4.57
	0.935	0.915	3.687	3.64	4.622	4.555
	0.938	0.908	3.683	3.655	4.621	4.563
	0.899	0.911	3.717	3.651	4.616	4.562
Average	0.909	0.908	3.715	3.658	4.624	4.567
% Difference	0.12		1.52		1.25	

After checking the flow rates, the inner and the outer nozzles of the two units were disassembled and cleaned. It was found that approximately one third of the inner nozzle area of the "Porsche" was blocked with some particles. The two APS units were tested again in

the cabin after cleaning them. Powder (not smoke) was released in all seats of Row 2 and the APS units were located in Row 4-Seats D and E. Four tests were conducted and the two units were aligned in a specific orientation during the first two tests. The APS units were replaced with each other, during the other two tests, to make sure that the location had no effects on the tests results.

The total particle counts collected during each test by each unit are shown in Table 6-2 and the averages of the four tests for each unit are plotted against time in Figure 6-8.

**Table 6-2 Total Particle Counts – APS Verification # 2**

	Porsche	Mercedes
Test 1	19046	19169
Test 2	22901	22134
Test 3	26211	26172
Test 4	18218	18196

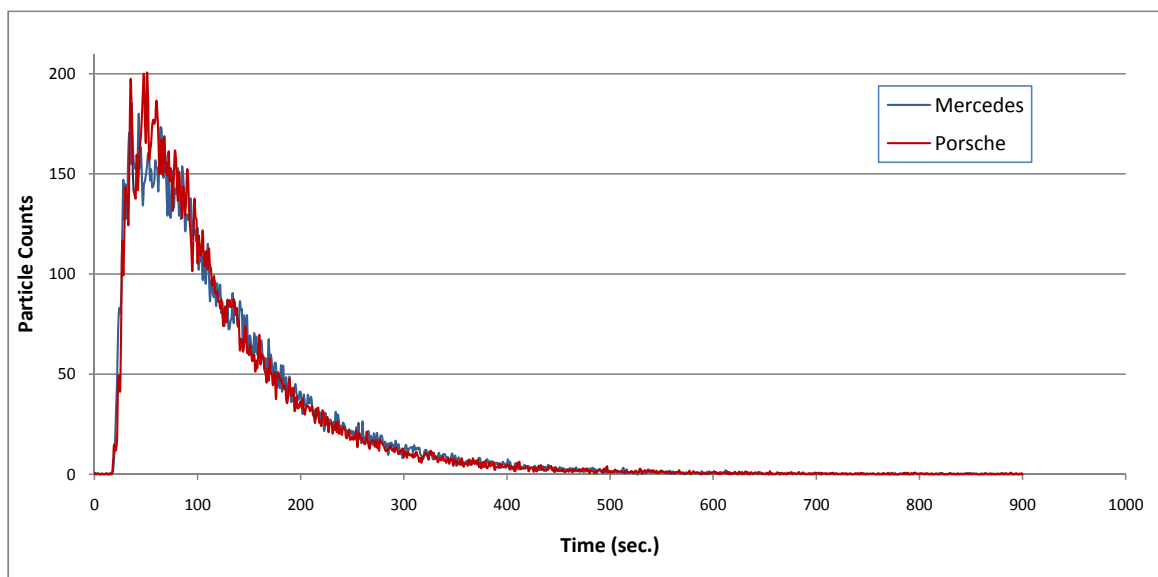


**Figure 6-8 Total Particle Counts Collected by the Two APS Units after Cleaning the Nozzles (0.5 – 5  $\mu$ m)**

It can be seen from Table 6-2 and Figure 6-8 that the two units are matching very well after cleaning the nozzles. It should be mentioned that the APS unit named as “Mercedes” (serial # 70626096) was the only unit used during this project. The above validation process showed that this unit was functioning properly as compared to the “Bio” and to the “Porsche”

(serial # 70742031) after cleaning. Therefore, no action is needed to be taken for the project's results that were obtained earlier.

## 6.2 Powder Injection System Verification

Before starting the tests, the accuracy of the powder injection system was tested and checked to make sure that the variability obtained was within acceptable ranges. The injection system was controlled by Labview software (Refer to Appendix B). A schematic of the system is shown in Figure 6-9.

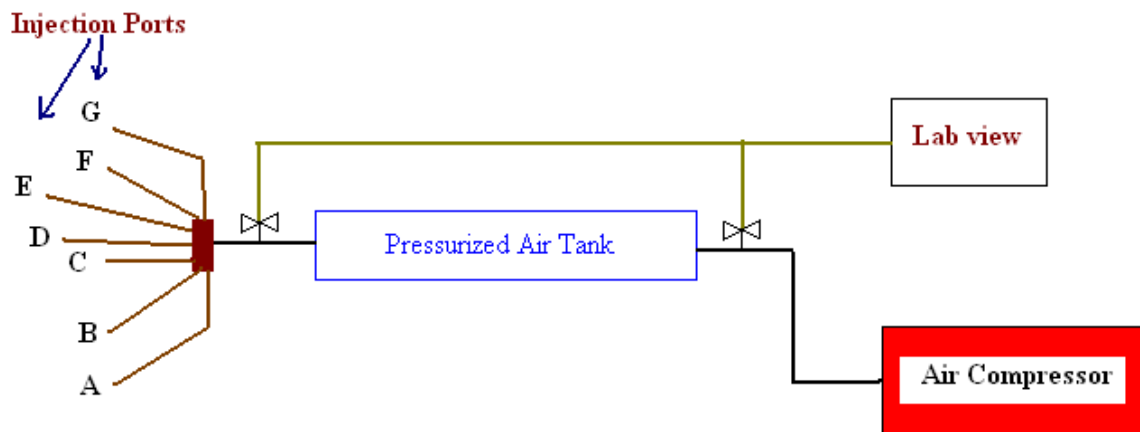


**Figure 6-9 Schematic Diagram of the Powder Injection System**

The compressor charges the air tank (1175 ml) with air to a specified pressure during a specified duration of time. All of these specified parameters are controlled by the computer using Labview (Appendix B). At the moment of injection, the output valve (the discharge valve), which is shown near the injection ports in Figure 6-9, is opened instantly for 150 ms and the air moves out through plastic tubes into copper tubes which in turn direct the air into the powder that is placed in small plastic cups. The copper tubes, the plastic tubes, and the cups, that were used to hold the powder, are shown in Figure 6-10. Once the air is injected through the ports into the cup, the powder spreads out forming a 10 inch high powder cloud as shown in Figure 6-11.



**Figure 6-10 Details of the Injection System**

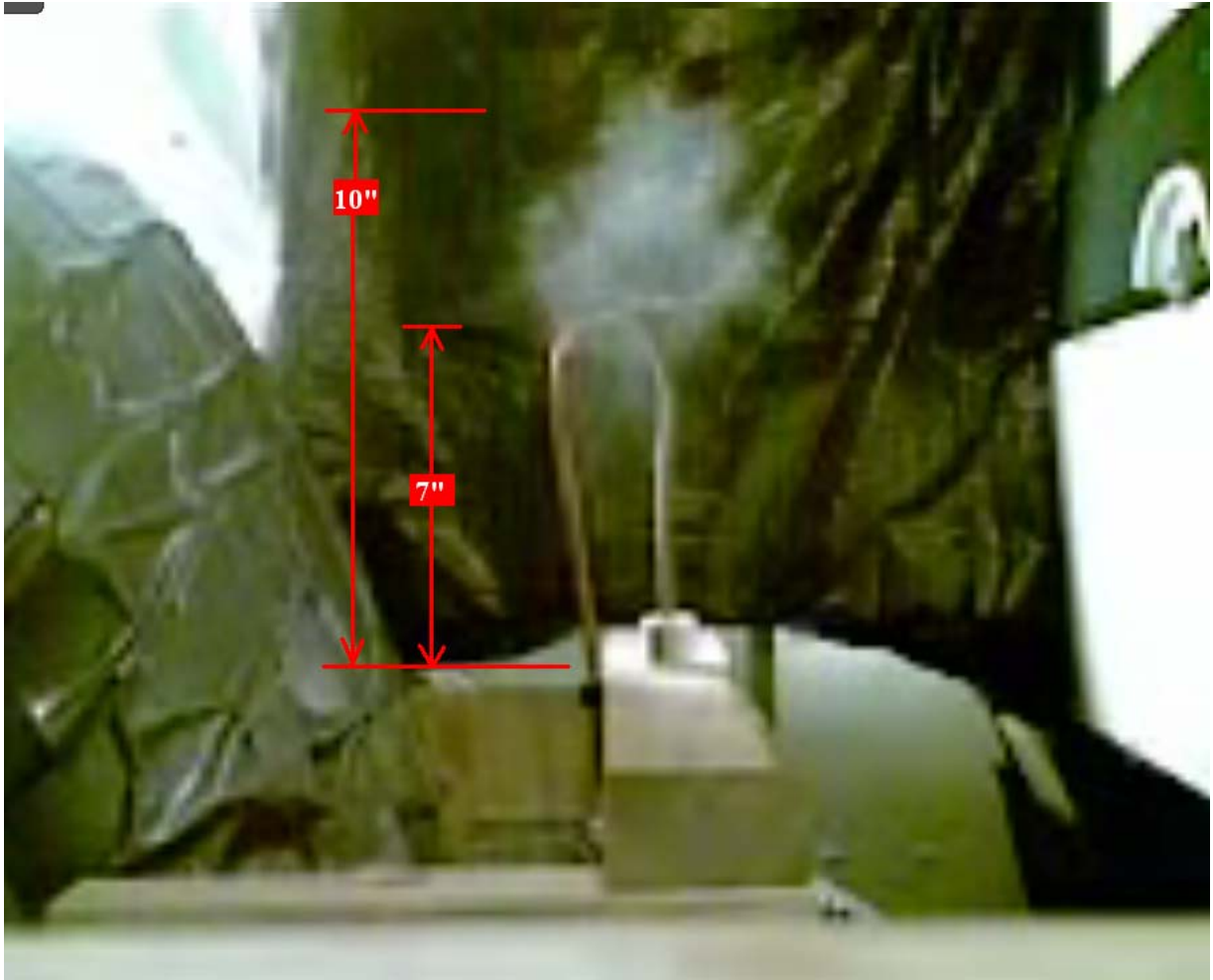


**Figure 6-11 Powder Cloud Height**

The variability of the system was checked by conducting tests similar to those described in section 3.3 where powder was released in each seat of row 2 separately, but the particles were collected in seat D of Row 3 at a height of 48 inches, as shown in Figure 6-12. The total number of particles collected during each test are plotted in Figure 6-13.

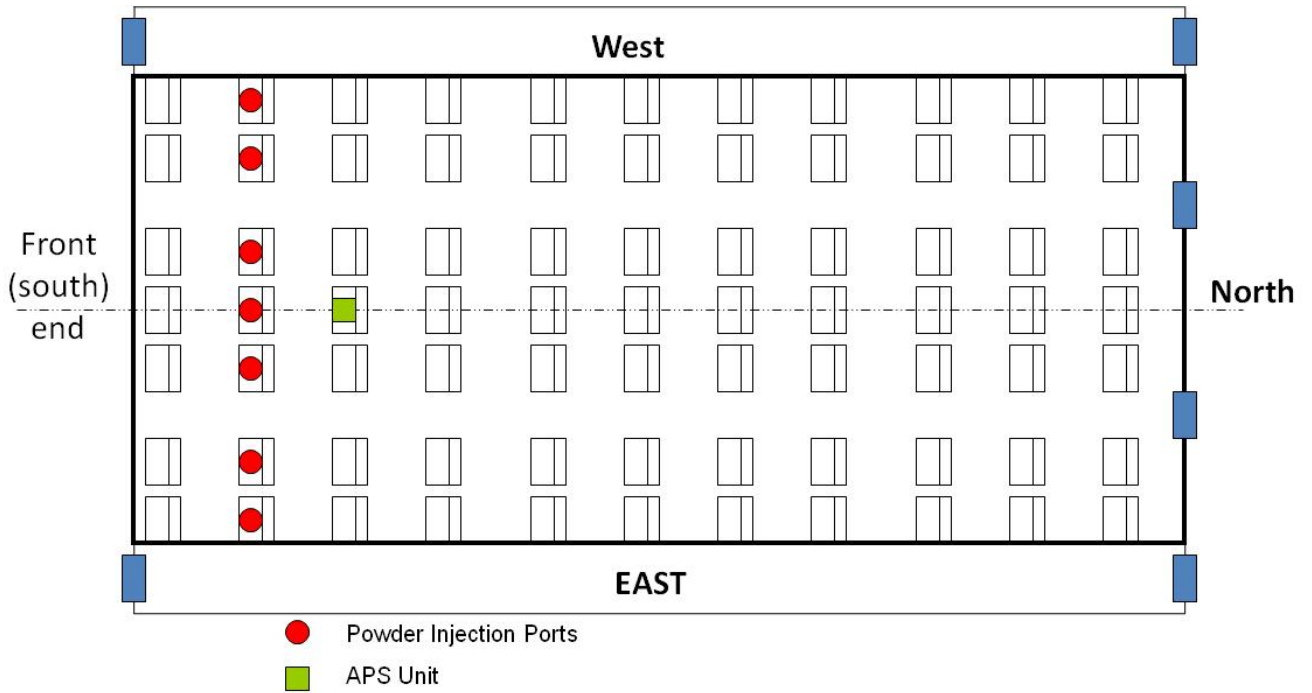


**Figure 6-12 Powder Injection System Verification - Data Collection Location**

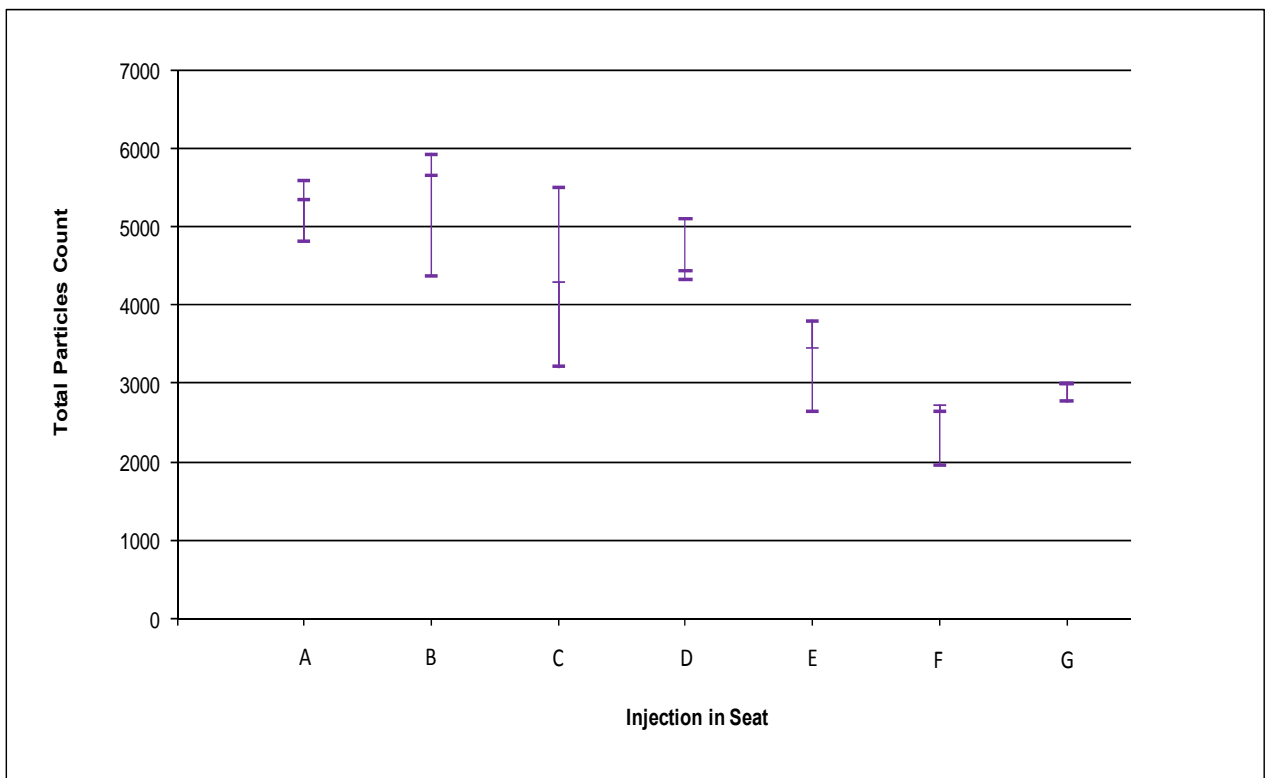


**Figure 6-13 Powder Injection Verification - Collected Data**

The total standard deviation of the above results was calculated by determining the standard deviations of seats A, B, C, ..., G and combining them using equation (5.2)

$$\sigma_T = \sqrt{\sigma_A^2 + \sigma_B^2 + \sigma_C^2 + \sigma_D^2 + \sigma_E^2 + \sigma_F^2 + \sigma_G^2}$$

Using equation (5.1), the standard error of the collected data was calculated with N=21. Equation (5.3) was finally used to estimate the relative uncertainty of the collected data. Its value was found to be  $u_i = \pm 0.19$ .

Combining this value with the uncertainty of the powder samples, which was calculated in "section 5.3.3" and whose value was found to be  $\pm 0.054$ , gives the uncertainty of the variables associated with the injection system and the data collection system. To find the total uncertainty of the system, the bias uncertainty of the APS unit which is  $\pm 10\%$  is combined with the uncertainty of the powder samples and with that of the injection system calculated above.

Therefore the total relative uncertainty is :

$$\begin{aligned} u_T &= \sqrt{u_i^2 + u_{ii}^2 + u_{APS}^2} \\ &= \sqrt{0.19^2 + 0.054^2 + 0.1^2} \\ &= \pm 0.22 \\ &= \pm 22\% \end{aligned}$$

where  $u_i$  is the uncertainty of the data collected and  $u_{ii}$  is the uncertainty of the powder samples.

With a  $\pm 10\%$  uncertainty from the manufacturer as the APS bias, the relative uncertainty of the powder injection system was found to be  $\pm 22\%$ .

### **6.3 Mockup Cabin Verification**

All of the tests were conducted in the Boeing 767 mockup cabin housed within the Airliner Cabin Environment Research Laboratory. The geometric shape and the dimensions of the mockup cabin are the same as an actual 767 aircraft. "Section 3.1" shows the details of the cabin with the seat locations and dimensions and "section 3.2" shows the air supply system that was used to provide the cabin with air.

In the results section, it was noticed that there is a swirl inside the mockup cabin and its rotational direction depends on the location inside the cabin, whether it is in the front section or in the middle section although the geometry of the structure is symmetrical and the air diffusers are identical. In order to check whether the obtained asymmetrical results inside the mockup cabin were due to an error in the geometry of the cabin or due to the assembly of the diffusers, several tests were conducted. The main idea was to test the cabin under normal operating conditions and then to make some changes and repeat the tests. After conducting the normal and the modified tests, the results showed that the asymmetry in the data collected, for the same location, was changed. This led us to conclude that the geometry of the mockup cabin or the diffusers or some other physical factors were not affecting the results and that the mockup cabin is a good representation of an aircraft cabin.

Two types of tests were conducted during the verification process, but the main procedures of the tests were the same. Powder was used in the first type, while smoke was used in the second type. In both types, the measurements were taken under three different conditions. These conditions were:

- Normal operating conditions – Exhaust Fans were ON – Doors 1, 2, 3, and 4 were closed. (For more details about the doors numbering, refer to Figure 6-14).
- Exhaust Fans were OFF – Doors 1 and 4 were opened – Doors 2 and 3 were closed.

- Exhaust Fans were OFF – Doors 2 and 3 were opened – Doors 1 and 4 were closed.

### 6.3.1 Mockup Cabin Verification using Powder

Talcum powder was released separately in each seat of Row 2 and the particles were collected, using the APS unit, at the following co-ordinates inside the cabin:

- 33 inches from the South Wall.
- In the middle (Center Line) of the cabin.
- 9 inches above the cabin floor.

The 3 different conditions were followed by turning the exhaust fans off and opening each set of doors. Figure 6-15 shows the exhaust fans and Figure 6-16 shows the results.

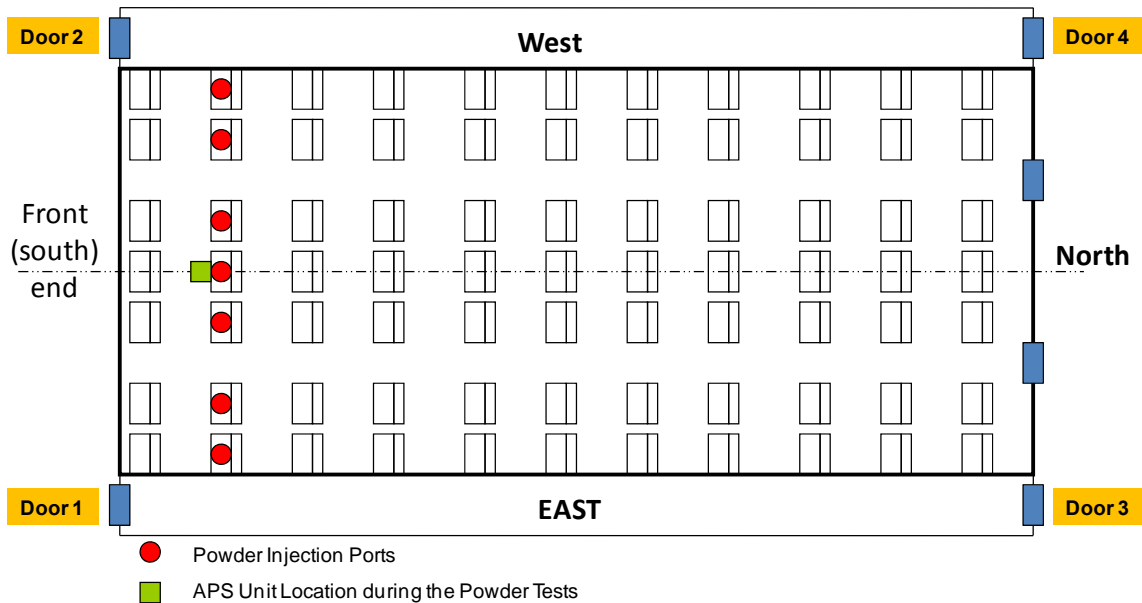


**Figure 6-14 Schematic of the Mockup Cabin Verification using Powder**



**Figure 6-15 Exhaust Fans of the Cabin**

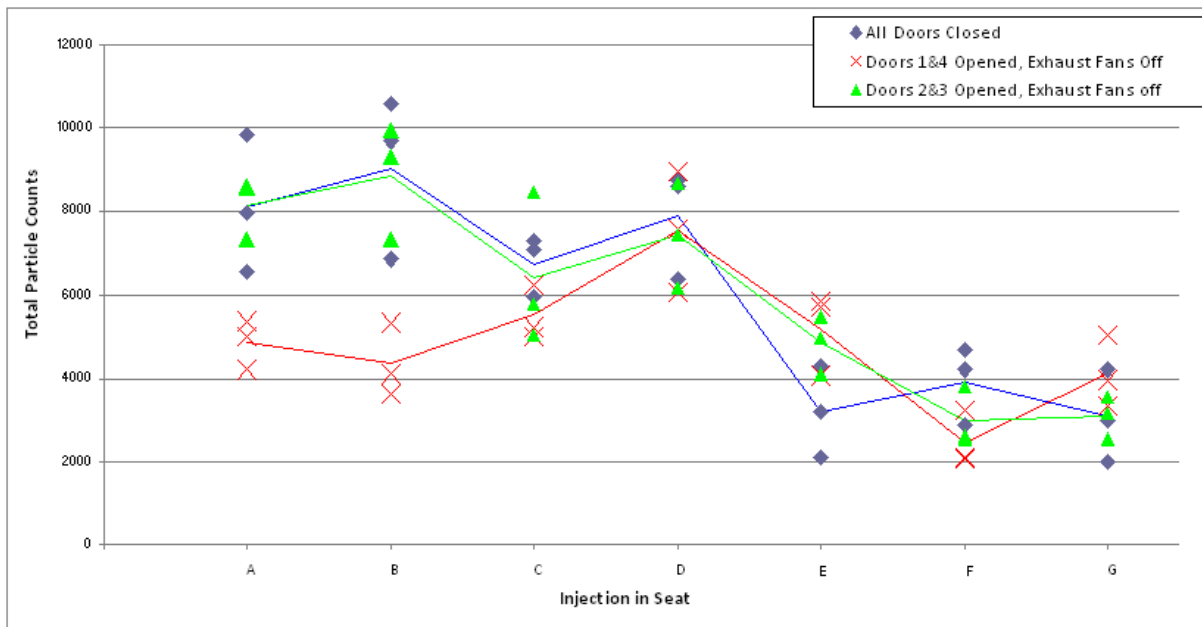


**Figure 6-16 Mockup Cabin Verification Results using Powder**

### 6.3.2 Mockup Cabin Verification using Smoke

The same procedures of changing the cabin environment were followed as in the powder injection tests, but in this section smoke was released in 6 seats of Row 3 and the particles were collected in two different locations using two APS units as shown in Figure 6-17. The first APS unit was placed in Row 4-seat D, while the second one was moved along the seats of Row 5. Three tests were run and the ratio of the total number of particles collected in each seat of Row 5 to that collected in seat 4D, during the same test, is plotted in Figure 6-19.

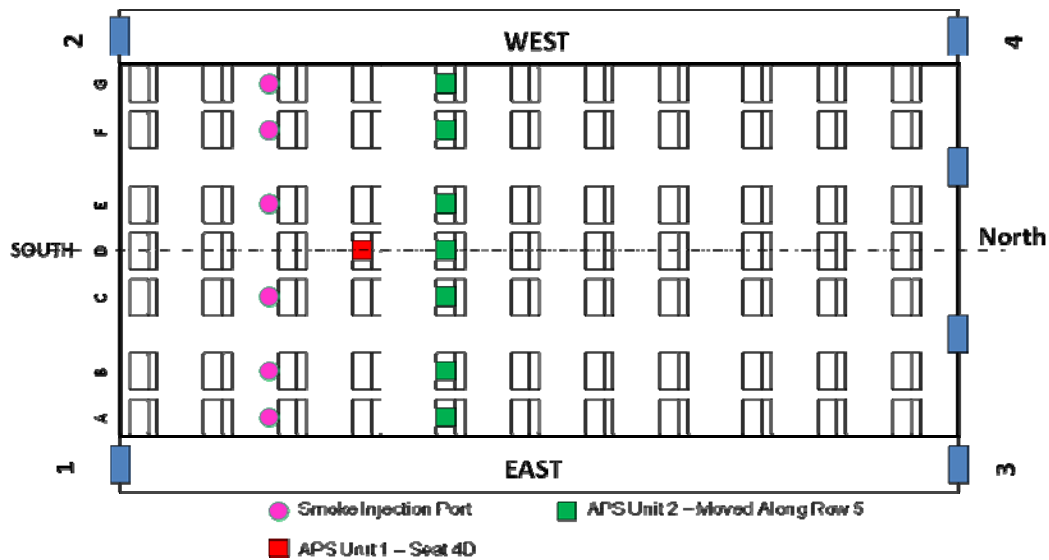


**Figure 6-17 Smoke Injection Setup for Cabin Verification**

The smoke system setup is shown in Figure 6-18, where

- 1: is an Air Compressor (15 gallons, 150 psi, 1.5 HP)
- 2: is a Wooden Box that contains a smoke generator machine
- 3: is a Plastic Barrel
- 4: represents equal length tubes that connect between the barrel and the outlet tube nozzles in the cabin

The air compressor directs air into the wooden box which contains the smoke generator. Once the smoke generator is activated, it will fill the box with smoke. As the air

enters the box, it will force the smoke out in its way through the only outlet as shown in Figure 6-18.

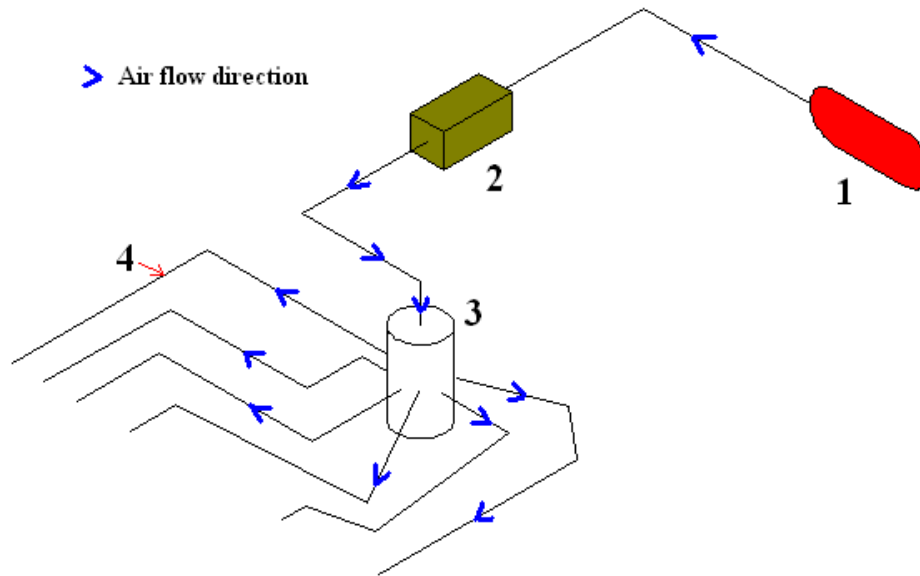


**Figure 6-18 Smoke System Setup**

Exiting the wooden box, the smoke moves into the plastic barrel and then out through equal length tubes into the outlet tubes inside the cabin. The barrel and the equal length tubes are used to provide equally distributed smoke flow throughout all outlet ports.

Adjusting the air compressor to provide a specific flow, it was found that smoke takes around 20 seconds to reach to the outlet nozzles inside the cabin, after the injection of air into the smoke box. For that, the air was injected into the box 25 seconds prior to each test starting time to make sure that all conducted tests have approximately the same amount of smoke. (Note that the duration time of the air supply is only 25 seconds; i.e. when the test started, the air supply was cut off).

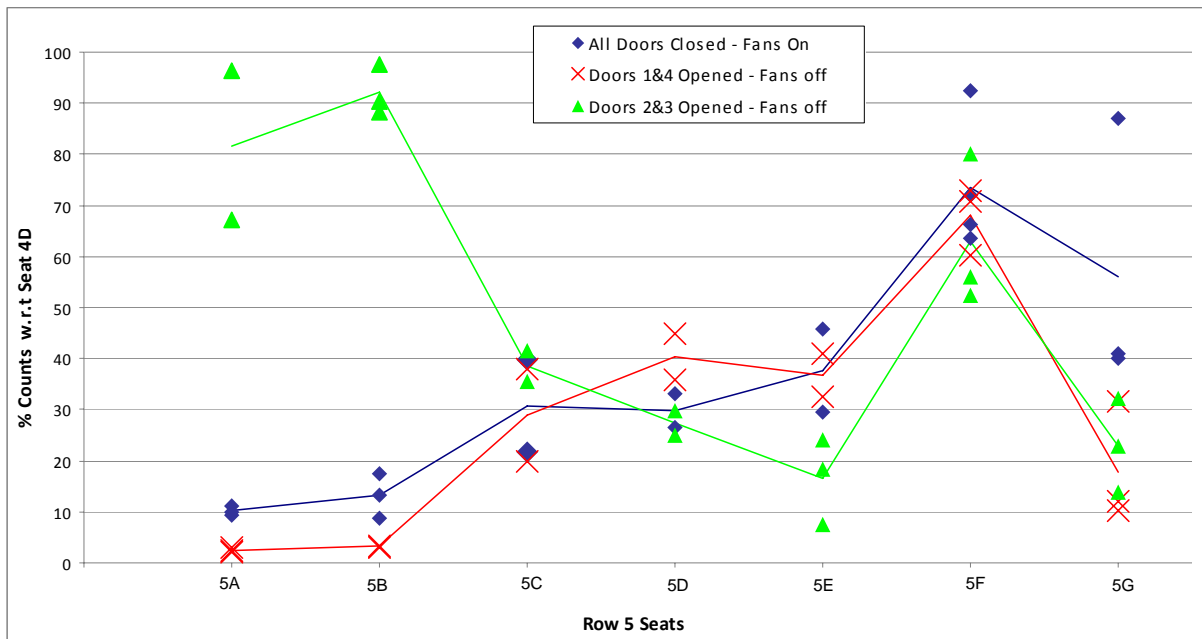


**Figure 6-19 Cabin Verification – Smoke Results**

Figure 6-16 shows that when doors 1 and 4 were opened the results were changed from the other two cases. Figure 6-19 shows the data when doors 2 and 3 were opened as compared to other test conditions. Either of the two types of tests, which depend on the location where the data were collected, shows that the results obtained were not affected by the geometry of the mockup, but rather on the mixing phenomenon occurring inside the cabin and on the conditions controlling the cabin environment.

## CHAPTER 7 - Summary

An experimental analysis of the best location for placing a particulates detecting sensor in the lateral direction and the optimum separating distance between two consecutive sensor locations in the longitudinal direction, to accurately track air quality incidents within a cabin, were described in the preceding chapters. The objective of the project was to collect powder particles at several locations inside an 11-row mockup aircraft cabin, representative of a Boeing 767 aircraft cabin in order to determine the optimum location for placement of a particle detecting sensor based on the total number of particles collected and the fastest detection time.

Multiple steps and procedures were taken in order to meet the project objectives. First, fine powder was released in each seat of the second row of the mockup cabin and an aerodynamic particle sizer (APS) was used to collect the particles in several locations in the lateral direction of row 2.

Several tests were performed to verify that the measuring devices and the testing environment were providing accurate results. It was found that the APS unit matched with another unit of the same manufacturer borrowed from another department, but didn't match with a newly calibrated unit. It was found that the newly calibrated unit underestimates the number of particles collected. Several checks were undertaken to identify the error of the third unit. It was found that the inner collecting nozzle of the APS was blocked with some particulates. The mockup aircraft cabin was tested and checked by changing the normal operating conditions of the cabin and it was shown that the geometry of the cabin or the diffusers did not affect the results obtained. Depending on that, it can be concluded that the mockup cabin is a representative cabin of a actual aircraft cabin.

The powder injection system accuracy and functionality were tested by conducting several tests inside the mockup cabin. A relative uncertainty of  $\pm 22\%$  was obtained which is acceptable as the APS bias was approximately  $\pm 10\%$ .

Of the six locations examined, two locations were selected as acceptable locations in the lateral direction, but one of the two locations appeared more suitable for sensor placement and selected as a representative location for the lateral direction if only one sensor per row was to be used. This location was on the centerline near the cabin floor. An uncertainty analysis was performed to check the variability of the measurements and it showed qualitatively that there was no major differences in the measured uncertainty for the above two locations. The total uncertainty for all locations considered in the lateral direction ranged between  $\pm 26\%$  to  $\pm 48\%$ .

After selecting the best location in the lateral direction of row 2, fine particles were released in two different rows during the longitudinal tests. The front and the middle regions of the cabin showed that particulates could be detected faithfully by a sensor if they were released in the same row as the sensor location, a row in front, and a row in back of the release. The uncertainty of the measurements taken in the middle of the cabin was approximately  $\pm 56\%$  as compared to about  $\pm 42\%$  in the front part of the cabin.

As a result, a total of four sensors was recommended to monitor particle releases in the 11 row mockup cabin. The locations of these sensors were on the center line near the cabin floor in each of row 2, 5, 8, and 11.

## **CHAPTER 8 - Recommendations**

More tests are recommended to reduce the uncertainty in the measurements. The relative uncertainties of the tests were relatively high due to the small sample size considered and due to the high level of disturbance inside the mockup cabin.

Since it was shown in the lateral direction analysis that both locations, II and III, are recommended in the lateral cross section of the cabin, more tests should be carried out in the longitudinal direction, but with the particles collected in location III.

Considering the comparison done in the longitudinal investigation between different sections of the cabin, a more detailed investigation should be conducted to understand the nature of the air motion and turbulence at different regions of the cabin. There might be different circulated eddies clockwise and counterclockwise directed.

The results of the study can be used to determine the source of the particulates release point by combining the results collected at different locations. For example, if we have several sensors inside the cabin and one of them yields "4000 particles for 15 seconds", where as another sensor yields "1000 particles for 40 seconds", we can use these data through a computer program to compare it with the results obtained for the longitudinal investigation and determine probable regions of the release. Note that further investigation is required to determine the average number of particles release by a sneeze and the average particle diameter, as well.

## References

- Berglund, L. (August 1998). Comfort and Humidity. *ASHRAE Journal* , 35-41.
- Cox., J. E. and Miro, C. R. (April 1997). AirCraft Cabin Air Quality. *ASHRAE Journal*, 22.
- Beneke, J. (In Progress). Small Diameter Particle Distribution in a Commercial Airliner Cabin. Kansas State University, Manhattan, KS.
- Draft Final Technical Report, Contaminant Transport in Airliner Cabins Project (2009), Institute for Environmental Research. Kansas State University, Manhattan, KS.
- Federal Aviation Administration (1989). Code of Federal Regulations. Aeronautics and Space. Washington, D.C.
- Gibbons R. D. and Coleman D. D. (2001). Statistical Methods for Detection and Quantification of Environmental Contamination. John Wiley & Sons, Canada.
- Hocking, M. B. (2005). Air Quality in Airplane Cabins and Similar Enclosed Spaces, *The Handbook of Environmental Chemistry*. Springer, Berlin, Germany.
- Hocking, M. B. (2003). Passenger Aircraft Cabin Air Quality - Trends, Effect, Societal Costs, Proposals. *Environmental Science and Pollution Research (ESPR)* , 3 (7), 173-174.
- Hoffman, F. O. and Gardner, R. H. (1983). Evaluation of Uncertainties in Radiological Assessment Models. Chapter 11 of Radiological Assessment: A textbook on Environmental Dose Analysis. Edited by Till, J. E. and Meyer, H. R. NRC Office of Nuclear Reactor Regulation, Washington, D.C.

HVAC Applications. *ASHRAE Handbook (2003)*.

Jennison, M. W. (1942). *Aerobiology Proceedings of a Symposium of the American Association for the Advancement of Science, 17*, 106-127.

Lebbin, P. (2006). *Experimental and Numerical Analysis of Air, Tracer Gas, and Particulate Movement in a Large Eddy Simulation Chamber*. Kansas State University, Manhattan, KS.

Meyer, B. (1983). *Indoor Air Quality*. Addison-Wesley. Seattle, Washington: Department of Chemistry, University of Washington.

Niren, L. N. and Hodgson, M. (2001). Low Relative Humidity and Aircraft Cabin Air Quality. *Indoor Air, 11* , 200-214.

O'Donnell, A., Donnini, G., and Nguyen, V. H. (1991). Air Quality, Ventilation, Temperature and Humidity in Aircraft. *ASHRAE Journal* , 42-46.

Padilla, A. M. (2008). *Experimental Analysis of Particulate Movement in a Large Eddy Simulation Chamber*. Kansas State University, Manhattan, KS.

The National Academy Press, (2002). *The Airliner Cabin Environment and the Health of Passengers and Crew*. The National Academy Press, Washington, D.C.

Repace, J. L. and Lowery, A. H. (1982). Tobacco Smoke, Ventilation, and Indoor Air Quality. *ASHRAE Transactions 88 (1)* , pp. 895-914.

Space, D. R., Johnson, R. A., Rankin, W. L., and Nagda, N. L. (2000). The Air Plane Cabin Environment: Past, Present, and Future Research. *ASTM Special Technical Publication, 1393* , 189-214.

Steele, W. G. and Coleman, H. W. (1999). *Experimentation and Uncertainty Analysis for Engineers*. (Second Edition). John Wiley & Sons. Canada.

Thibeault, C. (2002). Airliner Cabin Air Quality. *Occupational Medicine*, 17 (2) , 279-292.

Ventilation of Acceptable Air Quality. *ASHRAE Standard 62 (1999)*.

[www.ash.org/nosmokair.html](http://www.ash.org/nosmokair.html). (2003). Retrieved from ASH (Action on Smoking and Health).

Zhang, T., Chen, Q., and Lin, C. H. (2007) Optimal Sensor Placement for Airborne Contaminant Detection in an Commercial Aircraft Cabins. *HVAC&R Reseach*, 13(5), 683-696.

Zhang, Y., Sun, Y., et. al., (2005). Experimental Characterization of Airflow in Aircraft Cabins, Part I and Part II. *ASHRAE Transactions 111 (2)* , 45-59.

## **Appendix A - Supply Air Temperature Control System**

In order for the tests to be reliable and comparable, a controlled environment was maintained inside the mockup cabin. One of the parameters that was used to control the environment was the temperature of the air supplied into the main air supply duct of the cabin. The system described in "section 3.2" was controlled by a Lab-View software. Using the software, the supply temperature was controlled by controlling the chilled water flow rate out of the chiller and the hot water flow out of the hot water system.

Figure A-1 shows the main variables and parameters included in the software. Figure A-2 is a continuation of the software main window. The most important features in Figure A-2 are the two keys located below "Water Heater" and "Chiller Valve" columns, and the temperature plot figure. The temperature plot figure is a plot of the air supply temperature into the upstream of the main duct which was set at 60°F (15.5 C). The plot shows how the temperature was accurately maintained at 60°F with a variation of  $\pm 0.5^\circ\text{F}$ . The two keys, located below the water heater column and the chiller valve column are used to switch from automatic control to manual control. As shown in Figure A-2, the second key is switched up allowing us to control the chiller outlet flow manually. Figure A-3 shows the flow meter connected to the chiller. As the chiller valve is switched up and down, the flow out of the chiller can be monitored using this flow meter.

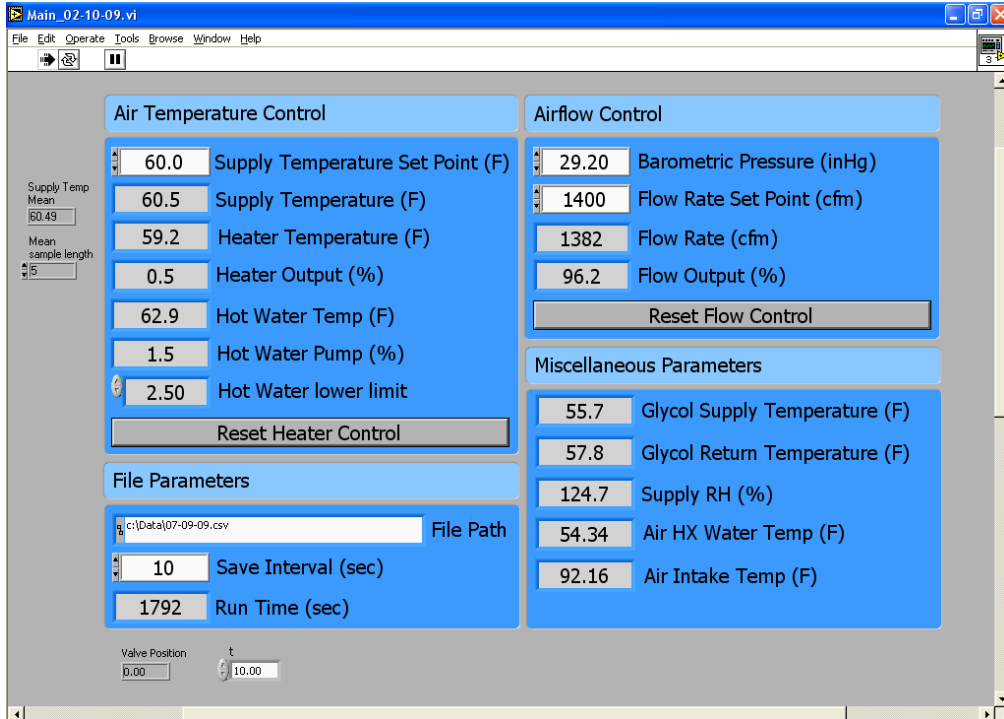


Figure A-1 Supply Air Temperature Lab View Control Software

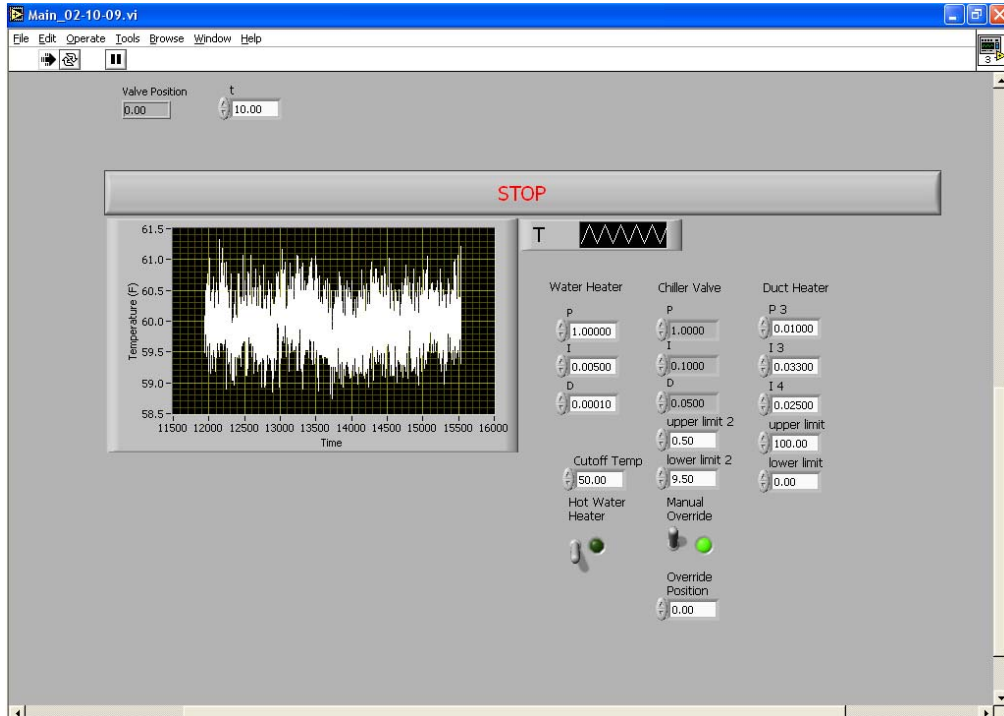


Figure A-2 Controlling Keys & Supply Temperature Plot



**Figure A-3 Chiller Flow Meter**

## Appendix B - Controlling the Powder Injection System

Another Lab View program was implemented to control the time of release of the powder, the time for charging the air tank, and all other parameters of the injection system parts described in "section 6.2". Figure B-1 shows the main window of the software. As shown in the figure, all parameters are easily controlled like the air tank charging time, the discharge time which is the time during which the discharge valve is kept opened, the time between charging and discharging, and the number of times to repeat the whole process.

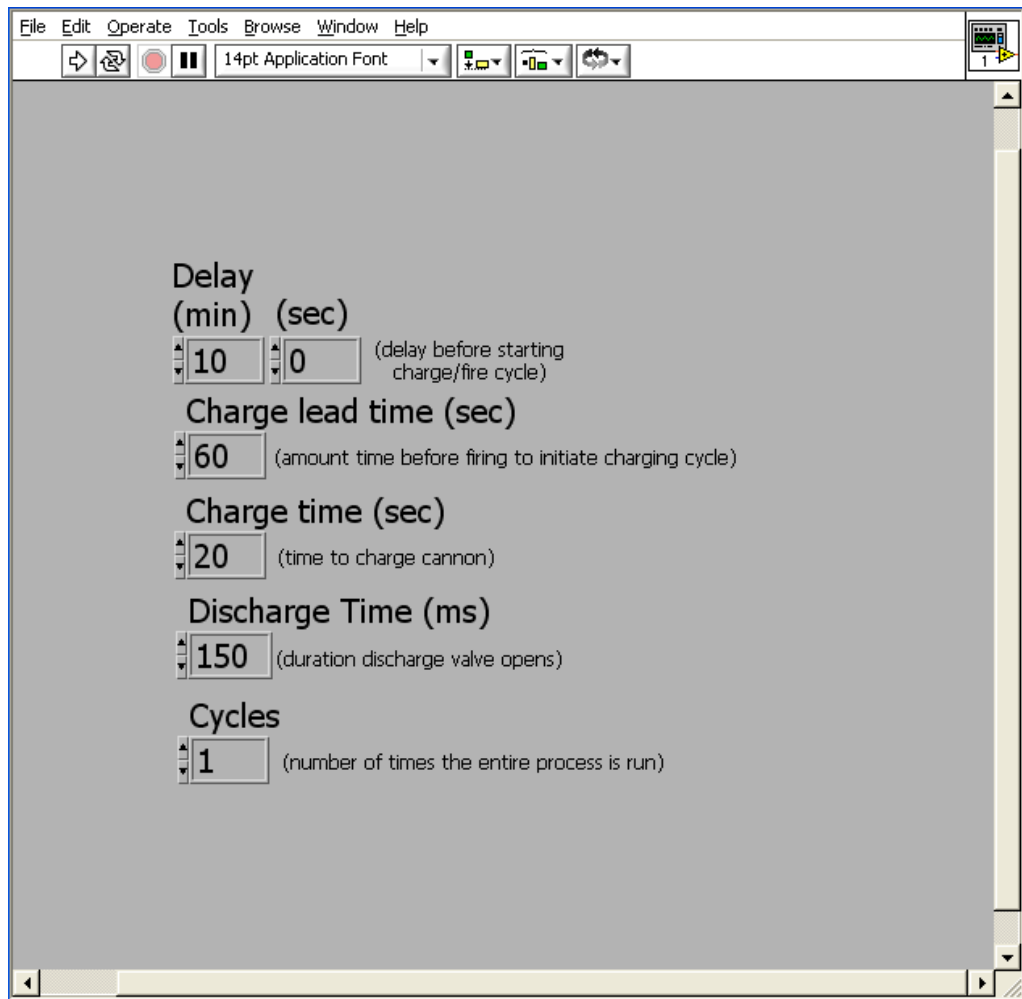


Figure B-1 Lab View Main Window Controlling the Powder Injection System

## **Appendix C - Aerodynamic Particle Sizer Control System**

The Aerosol Instrument Manager (AIM) software was used with the APS unit to classify and store all results collected during the tests. These files were converted easily into other user friendly files such as Excel and Notepad. Figure C-1 shows the main output screen of the AIM and it contains 4 main windows. The "Samples List" window, in the bottom left of the figure contains all the samples collected during each test. By selecting any sample, the plotted figure and the window beside it will show the number of particles collected at that time. The particles are classified based on their diameter size. Finally, the window in the bottom right of the figure is used for statistical analysis as it shows the mean and the median of the particles collected.

Adding up all the particles, shown in either the plot or in the up-right table, yields the total number of particles collected by the APS at that time. By performing this step for all the samples included in a test, a transient curve showing the particle distribution over the whole period of the test can be generated as shown in Figure C-2. The total number of particles collected during a test is the area under the curve.

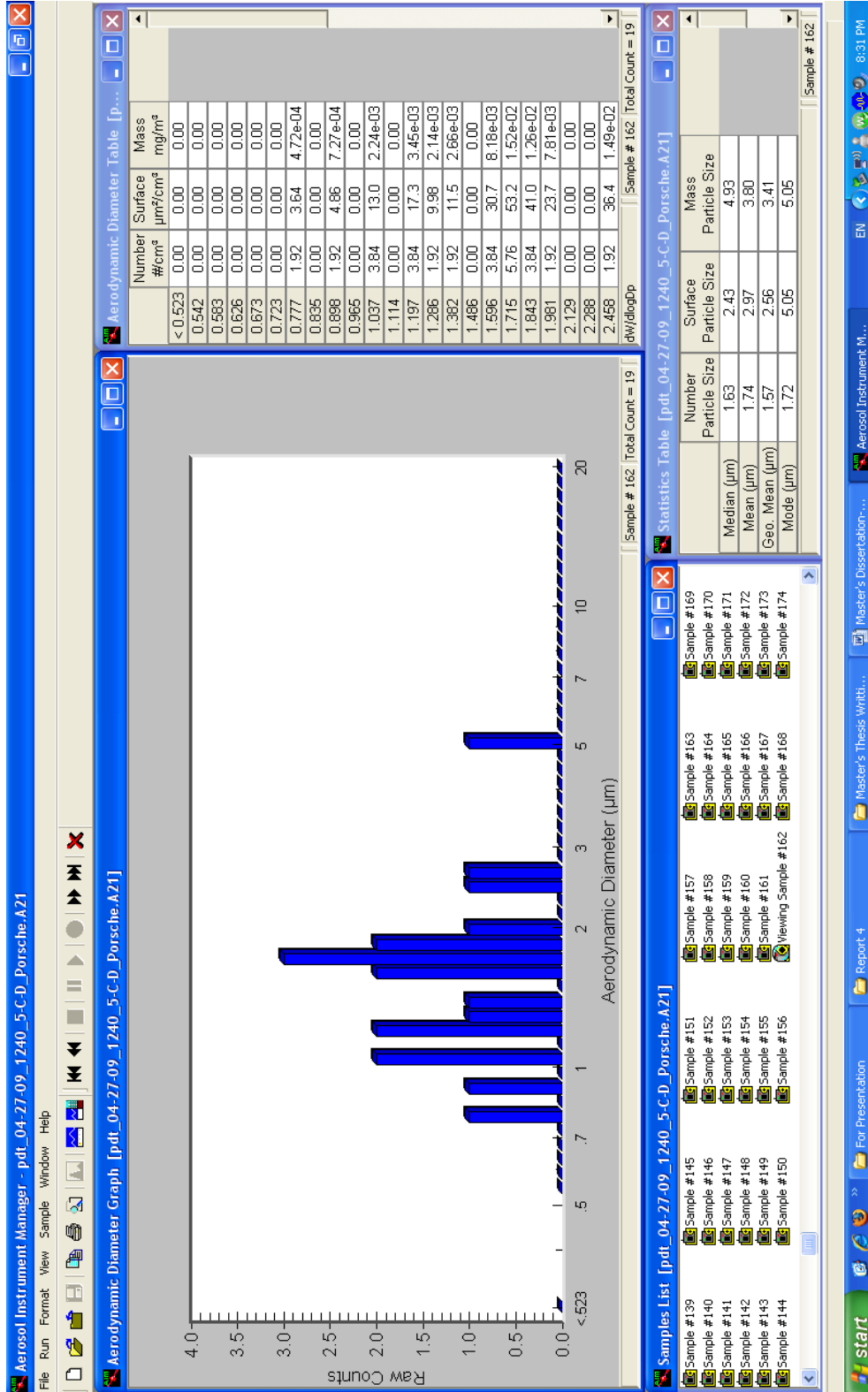
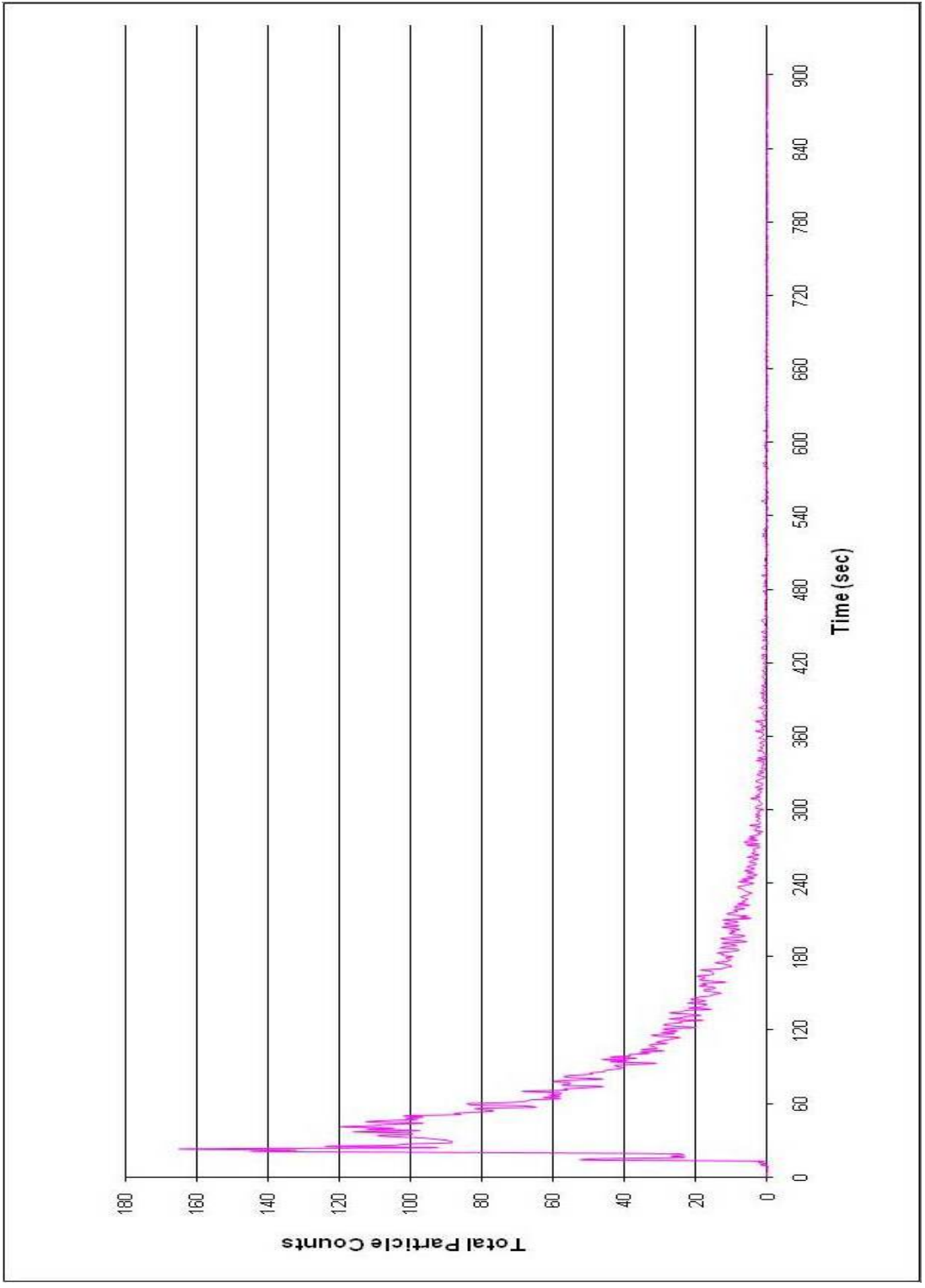
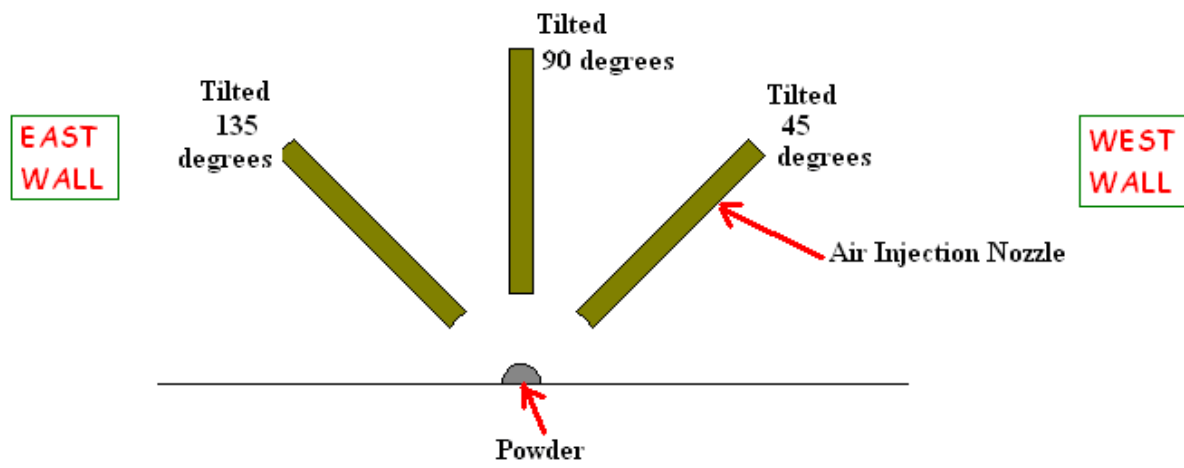


Figure C-1 AIM Software Windows



**Figure C-2 Transient Particle Distribution Example**

## Appendix D - Effect of the Air Injection Nozzle Tilting Angle for Seat G Injection



**Figure D-1 Injection Air Nozzle Tilting Angles Considered**

It was mentioned earlier in "Sec. 5.1" that the results obtained due to the injection in seat G are dependent on the direction of the powder release. This section provides a reference for the effect of the powder release direction.

To meet the above objective, the nozzle that directs the air into the powder was tilted into three different positions as shown in Figure D-1. The particles were collected in Location II and in Location III whose locations inside the mockup cabin are shown in Figure 3-29. Note that the angles are determined as if you were sitting in seat G, your face directed forward, and the injection tube was tilted from your right hand side towards the left hand side. For example, when the injection tube is in the 45° position, the back of the tube is toward the cabin wall and the air comes out into the cabin.

The detection times and the normalized particle counts obtained at both locations are shown in Figure D-2 and in Figure D-3, respectively.

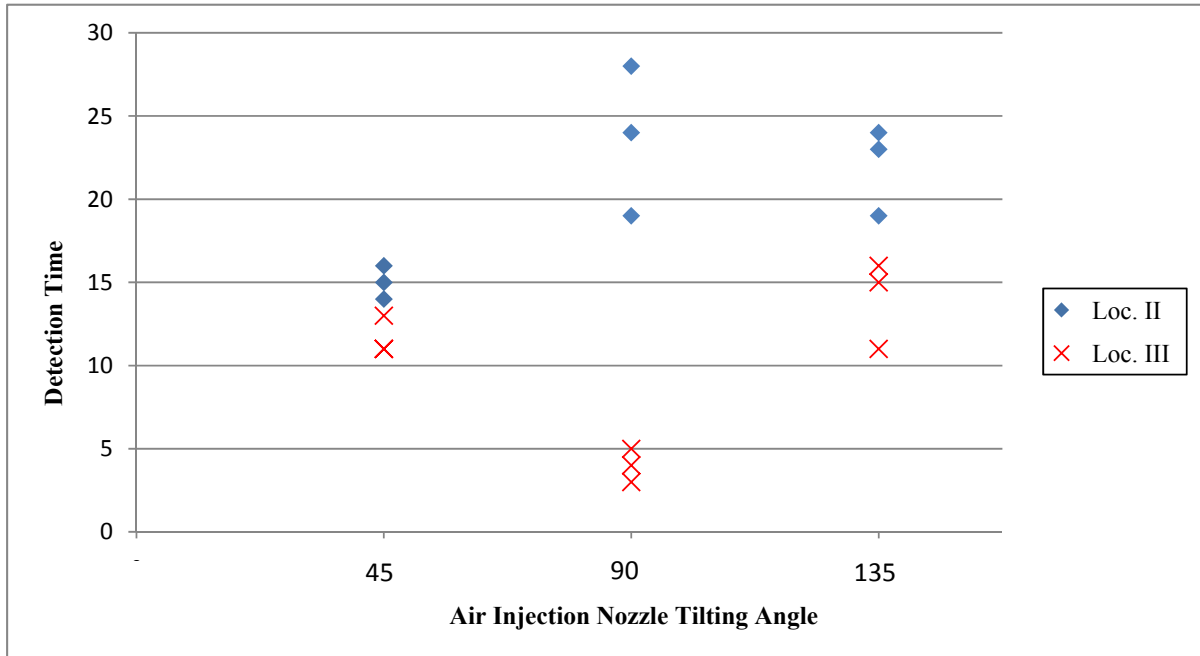


**Figure D-2 Comparison Between the Results Collected in Location II and in Location III with Different Powder Release Angles (Detection Time Results)**

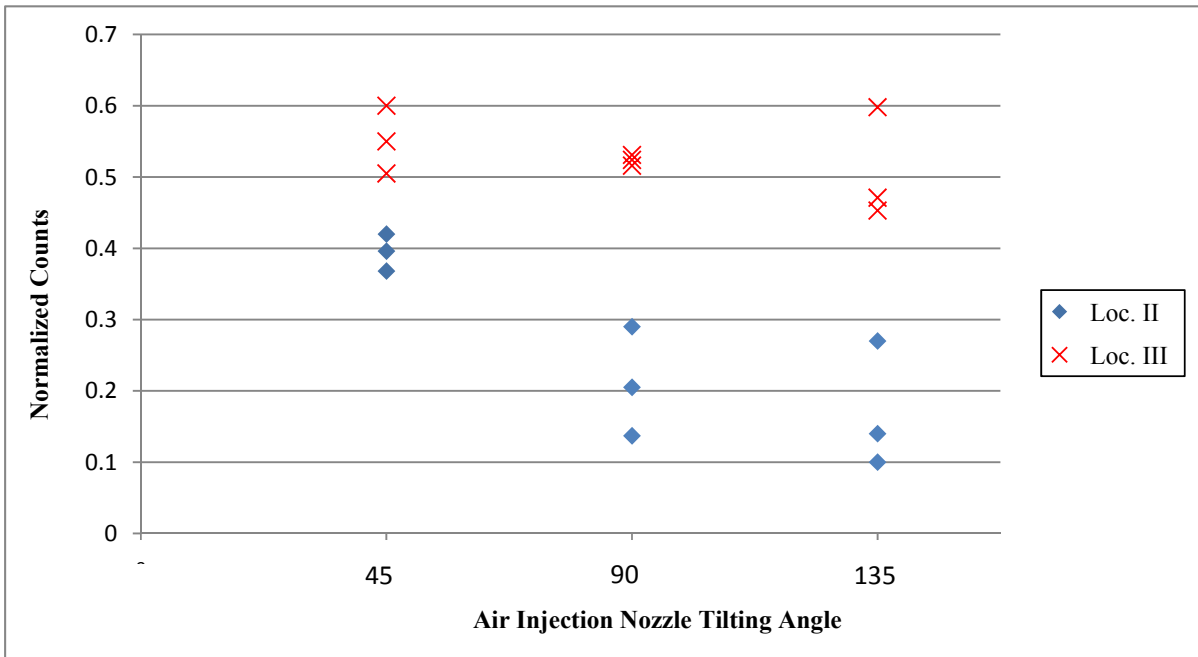


**Figure D-3 Comparison Between the Results Collected in Location II and in Location III with Different Powder Release Angles ( Normalized Particle Counts Results )**

Figure D-2 shows that there is a change in the detection time from one tilting angle to another. On the other hand, Figure D-3 shows that the total number of particles is less affected by the tilting angle since it represents the total number of particles collected during the whole period of the test. However, it should be mentioned that for Location II, under the 45° case, the detection time is less than the other considered cases (90 and 135 degrees) and the total number of particles is higher. This is due to the fact of the 45° case alignment. As was mentioned, for this case the air will move out from the tube into the entire space of the cabin. Thus, it will cause more powder to move towards Location II in a lower duration of time when compared to the other two cases. (for the 135° case, the powder will be directed toward the wall of the cabin, which will make a big difference).

Therefore, the tilting angle or the direction of the powder release affects the detection time results mainly and the total number of particles collected, as well.

## Appendix E - Powder Particles Settling Velocity

The settling velocity of a single particle can be predicted by using Stoke's law which is defined as:

$$V = \frac{g \cdot d^2 \cdot (\rho_p - \rho_f)}{18 \cdot \mu} \quad (E.1)$$

- where
- V: is the settling velocity
  - g : is the gravitational acceleration
  - d : is the particle diameter
  - $\rho_p$ : is the particle density
  - $\rho_f$ : is the fluid density (air)
  - $\mu$ : is the dynamic viscosity at the chamber temperature (300 K)

The gravitational acceleration "g", the air density and viscosity, and the particle diameter are all known. In order to determine the settling velocity, we need to determine the density of the talcum powder. Some references provide a value of 0.88 g/cc as a representative value of the talcum powder. To be more accurate and sure, the volume and weight of 5 different powder samples were measured and are shown in Table E.1. From this table, the average density of the talcum powder is found to be 0.949 g/cc.

**Table E-1 Talcum Powder Samlpe Properties**

Sample #	Volume (ml)	Powder Mass (g)	Density ( g/c.c )
1	15	13.627	0.908
2	15	13.32	0.888
3	15	13.782	0.919
4	25	25.032	1.001
5	25	25.715	1.029
Average Density =			0.949

After determining the powder density, the settling velocity was calculated for various diameters. Table E.2 along with Figure E-1 shows the settling velocity versus the powder particles diameter.

**Table E-2 Settling Velocity versus Particle Diameter**

Diameter ( $\mu\text{m}$ )	V(settling) (mm/sec)
0.5	0.0070
0.75	0.0158
1	0.0281
1.25	0.0439
1.5	0.0632
1.75	0.0860
2	0.1123
2.25	0.1421
2.5	0.1755
2.75	0.2123
3	0.2527
3.25	0.2965
3.5	0.3439
3.75	0.3948
4	0.4492
4.25	0.5071
4.5	0.5685
4.75	0.6334
5	0.7018

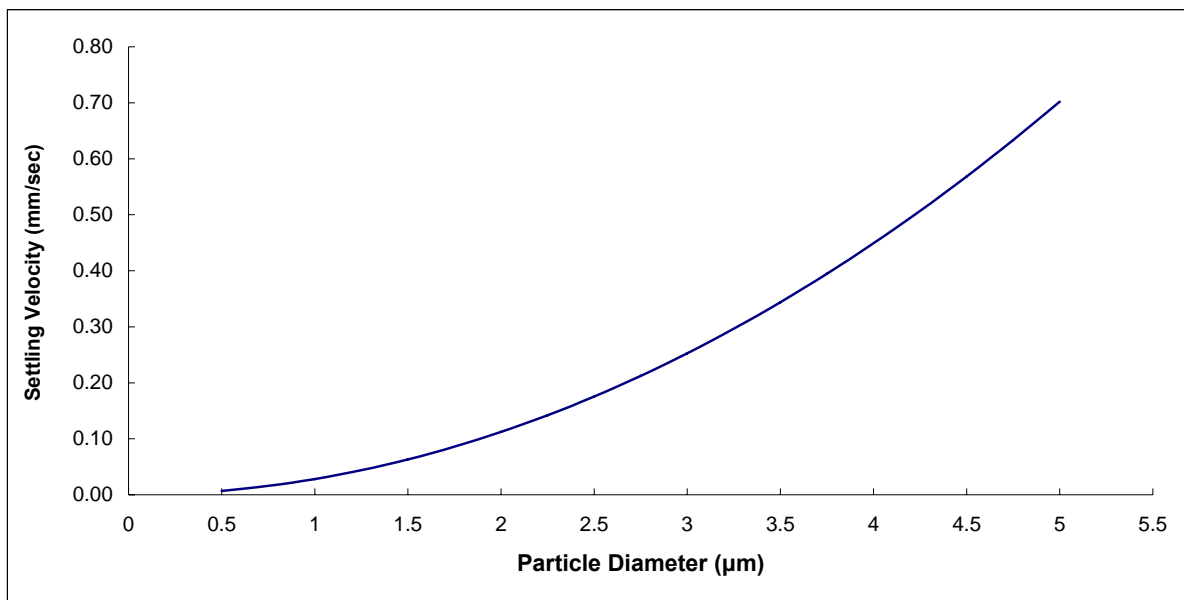


**Figure E-1 Settling Velocity vs. Powder Particle Diameter**